8-5-86

Robust Detection, Isolation, and Accommodation for Sensor Failures

R-0
8-11

Abbas Emami-Naeini, Muhammad M. Akhter, and Stephen M. Rock

Systems Control Technology, Inc.
Palo Alto, California

July 1986

Prepared for
Lewis Research Center
Under Contract NAS3-24079

NASA
National Aeronautics and Space Administration

1. Report No.	2. Government Accession No.	3. Recipient's Catalog No.
NASA CR-174825		

4. Title and Subtitle	5. Report Date
Robust Detection, Isolation, and Accommodation for Sensor Failures	July 1986
	6. Performing Organization Code

7. Author(s)	8. Performing Organization Report No.
Abbas Emami-Naeini, Muhammad M. Akhter, and Stephen M. Rock	SCT-85-5449
	10. Work Unit No.

9. Performing Organization Name and Address	11. Contract or Grant No.
Systems Control Technology, Inc. 1801 Page Mill Rd.; P.O. Box 10180 Palo Alto, California 94303	NAS3-24079
	13. Type of Report and Period Covered
	Contractor Report

12. Sponsoring Agency Name and Address	14. Sponsoring Agency Code
National Aeronautics and Space Administration Washington, D.C. 20546	505-34-02

15. Supplementary Notes

Final report. Project Manager, Walter C. Merrill, Instrumentation and Control Technology Office, NASA Lewis Research Center, Cleveland, Ohio 44135

16. Abstract

The objective of this research program is to extend the recent advances in robust control system design of multivariable systems to sensor failure detection, isolation, and accommodation (DIA), and estimator design. This effort provides analysis tools to quantify the trade-off between performance robustness and DIA sensitivity, which are to be used to achieve higher levels of performance robustness for given levels of DIA sensitivity. An innovations-based DIA scheme is used. Estimators, which depend upon a model of the process and process inputs and outputs, are used to generate these innovations. Thresholds used to determine failure detection are computed based on bounds on modeling errors, noise properties, and the class of failures. The applicability of the newly developed tools are demonstrated on a multivariable aircraft turbojet engine example. A new concept called the threshold selector was developed under this program. It represents a significant and innovative tool for the analysis and synthesis of DIA algorithms. Analytical results were obtained for the SISO case to compute optimal thresholds and to determine the size of minimum detectable failures, and a computer-aided technique was developed for the multivariable case. The estimators were made robust by introduction of an internal model and by frequency shaping. The internal model provides asymptotically unbiased filter estimates. The incorporation of frequency shaping of the LQG cost functional modifies the estimator design to make it suitable for sensor failure DIA. The results are compared with previous studies which used thresholds that were selected empirically. Comparison of these two techniques on a nonlinear dynamic engine simulation shows improved performance of the new method compared to previous techniques.

17. Key Words (Suggested by Author(s))	18. Distribution Statement
Analytical redundancy; Robust detection; Sensor failure; Jet engines	Unclassified - unlimited STAR Category 07

19. Security Classif. (of this report)	20. Security Classif. (of this page)	21. No. of pages	22. Price*
Unclassified	Unclassified	159	A08

*For sale by the National Technical Information Service, Springfield, Virginia 22161

SUMMARY

The objective of this research program is to extend the recent advances in robust control system design of multivariable systems to sensor failure detection, isolation, and accommodation (DIA), and estimator design. This effort provides analysis tools to quantify the trade-off between performance robustness and DIA sensitivity, which are to be used to achieve higher levels of performance robustness for given levels of DIA sensitivity. An innovations-based DIA scheme is used. Estimators, which depend upon a model of the process and process inputs and outputs, are used to generate these innovations. Thresholds used to determine failure detection are computed based on bounds on modeling errors, noise properties, and the class of failures. The applicability of the newly developed tools are demonstrated on a multivariable aircraft turbojet engine example.

A new concept called the threshold selector was developed under this program. It represents a significant and innovative tool for the analysis and synthesis of DIA algorithms. Analytical results were obtained for the SISO case to compute optimal thresholds and to determine the size of minimum detectable failures, and a computer-aided technique was developed for the multivariable case.

The estimators were made robust by introduction of an internal model and by frequency shaping. The internal model provides asymptotically unbiased filter estimates. The incorporation of frequency shaping of the LQG cost functional modifies the estimator design to make it suitable for sensor failure DIA.

The results are compared with previous studies which used thresholds that were selected empirically. Comparison of these two techniques on a nonlinear dynamic engine simulation shows improved performance of the new method compared to previous techniques.

TABLE OF CONTENTS

TABLE OF CONTENTS (Continued)

I. INTRODUCTION

The use of analytical redundancy (as opposed to hardware redundancy) for actuator/sensor failure detection, isolation, and accommodation (DIA) has been an active area of research during the last decade. Failure detection is the process of determining if a malfunction has occurred in a system. Failures in a system are detectable if the outputs following the failure are statistically different from the outputs prior to the failure. Failure detection implies that a no-failure condition can be differentiated from a failure condition. It does not imply that in the case of a failure, various failures can be differentiated from each other. Failure isolation is the process of differentiating between various failures which may occur in a system. Any two failures may be differentiated from each other if the outputs following them are statistically different. In general, more complex data processing is required for isolation than for detection. Failure accommodation refers to the substitution of a synthesized value for the faulty sensor's output.

The various techniques that have been developed for DIA can generally be thought of as belonging to three categories: failure-sensitive filters, multiple-hypothesis filter detectors, and innovations-based detection systems. A survey of various techniques up to 1975 can be found in Ref. 1 and references to the more recent work is contained in Refs. 2, 3, and 27. In Ref. 1, the issue of robustness of various techniques was pointed out as an open area for research. However, little has been done in the way of robustness analysis for various failure detection schemes. This study seems to be the first to address this important issue directly. It presents a systematic solution based on recent robustness analysis and design techniques [14] developed for multivariable systems. For example, Clark [2] points out the importance of robustness but his schemes have no guaranteed robustness properties. Leininger [4] addresses the problem of parameter uncertainty (D.C. mismatch), but does not come up with a remedy to guarantee robustness. The use of adaptivity for failure detection was discussed in a recent report [5]. However, these techniques are known to have undesirable robustness properties unless high-frequency unmodeled dynamics are taken into account.

This report addresses the important issue of robustness of sensor failure detection, isolation, and accommodation (DIA) techniques. The approach is based on extensions of robust control and estimation techniques and unifies various DIA methods. It is important to note that the method has been made practical so as to make an immediate impact on applied technology.

1.1 PROBLEM STATEMENT

The overall problem addressed in this report is the design of a robust, multivariable control system for a jet engine. A typical block diagram of such a system is shown in Figure 1.1. The blocks in the forward loop -- the actuators, plant dynamics, and sensors -- constitute the system. The blocks in the feedback system -- the control law, DIA logic, and the state estimator contain the subsystems which are to be designed. The design objective, ideally, is to select the proper configuration of these feedback subsystems such that the closed-loop system exhibits performance robustness with respect to system uncertainties and sensor failures.

In this study, the control law obtained from Refs. 6 and 7 was used and only the DIA subsystem was designed. In general, a comprehensive design technique would also consider the design of the control law as well.

Performance robustness requirements can be stated as tolerances on:

(P1) asymptotic behavior, e.g., steady-state command following and disturbance rejection; and

(P2) transient behavior, e.g., speed of response, damping, overshoot, etc.

(P3) detection and isolation sensitivity, e.g. ability and speed of correctly detecting a sensor failure.

Uncertainties in the system are caused by:

(U1) uncertain parameter values in the models of the actuators, plant dynamics, and sensors;

(U2) unmodeled dynamics, e.g., the effect of neglecting high-frequency phenomena, neglecting nonlinearities, and intentional reduced-order modeling;

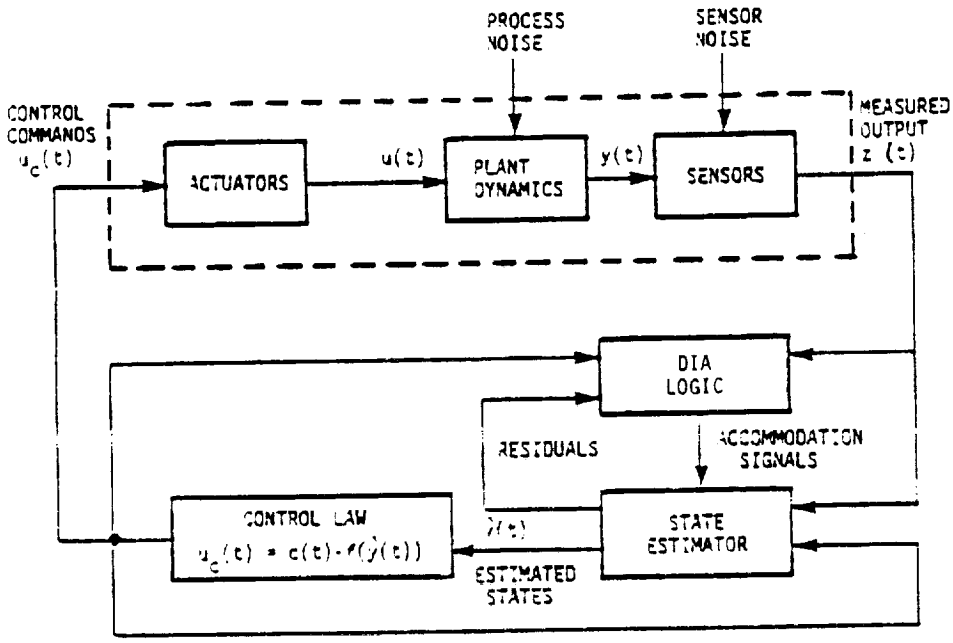

Figure 1.1 Generalized Block Diagram of a System with Sensor DIA

(U3) sensor failures of a known type, e.g., slow drift in a sensor bias;

(U4) DIA reconfiguration of the estimator and/or control law when the DIA presumes a sensor failure; and

(U5) uncertain external signals, e.g., sensor noise and disturbances.

Model uncertainties of the type in (U1) affect the steady-state (asymptotic) behavior and are the predominant cause of estimator bias and steady-state regulation errors. Those of the type in (U2) typically have a greater effect at higher frequencies and show up in the transient response as (possibly) undesirable behavior. A primary goal of this effort is to quantify the effect of these uncertainties (U1-U5) on DIA system performance and provide a design approach for improving DIA performance (P1-P3).

1.2 CONTRIBUTIONS

The general contribution of this research has been the extension of recent advances in robust control system design to sensor DIA and estimator design. The specific contributions are:

- analysis tools with which to quantify the trade-off between performance robustness and DIA sensitivity;
- design methods which allow higher levels of performance robustness to be achieved for given levels of DIA sensitivity;
- demonstration of the applicability of these tools using an aircraft turbine jet engine multivariable control example.

The requirement for these goals is explained with the aid of Figure 1.2. Plotted (conceptually) are levels of performance robustness against DIA sensitivity. A trade-off is indicated. As a design becomes more robust, it becomes less sensitive. Alternately, for a given level of DIA sensitivity, there is a maximum level of performance robustness achievable within the estimator and DIA logic design being applied. There are three curves in Figure 1.2. The one labeled "current" refers to the current state of the art DIA algorithms. The curve labeled "robust" refers to the idea of making the DIA robust. This is the subject of the present study and will result in

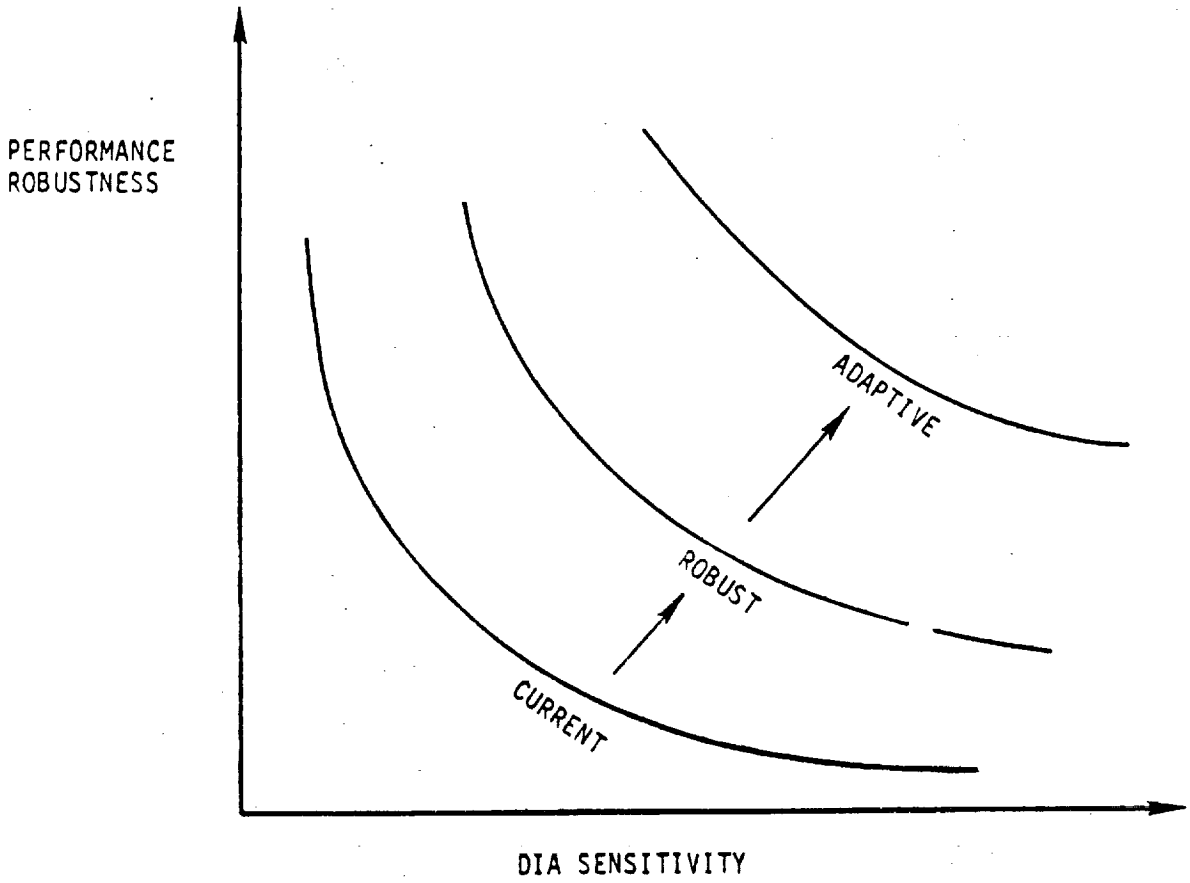

Figure 1.2 Performance Robustness vs. DIA Sensitivity

higher levels of performance robustness. The curve labeled "adaptive" points to the fact that even further improvements in performance may be achievable by an adaptive scheme. This requires basic research and would be the subject of future studies.

Curves such as those indicated in Figure 1.2, and more specifically in Figure 1.3, constitute a powerful design aid. The quantities in these figures will be defined precisely in the body of the report and these figures are presented here only to provide a flavor of the results to be discussed. Figure 1.3(a) shows the threshold, J_{th}, in an innovations-based DIA scheme as a function of a moving detection window, τ. This threshold is a fixed level against which some measure of the innovations signal is being compared. A failure is declared if the measure exceeds the threshold. Figure 1.3(b) shows the minimum detectable level of failure which is possible for a given DIA technique. These curves are functions of model error bounds, R.M.S. noise, and the class of failure signals. Figure 1.3(b) shows that the effect of different estimator speeds can also be evaluated. The ability to generate these curves is a powerful synthesis tool.

Plots such as shown in Figure 1.3 provide the means by which to evaluate design modifications made in search of the proper balance of robustness and DIA sensitivity. Furthermore, they provide information applicable to optimizing the search. The sensitivities of the system performance to design changes are calculated and the effects of critical parameters are identified.

This research has developed the analysis tools required to construct these curves. In particular:

- a "threshold selector" has been created which quantifies the effects of uncertainty on DIA performance;
- measures have been derived to quantify the uncertainty and the performance robustness.

This study has also provided advances to robust estimator design to achieve higher levels of performance robustness. Specifically, the accomplishments are:

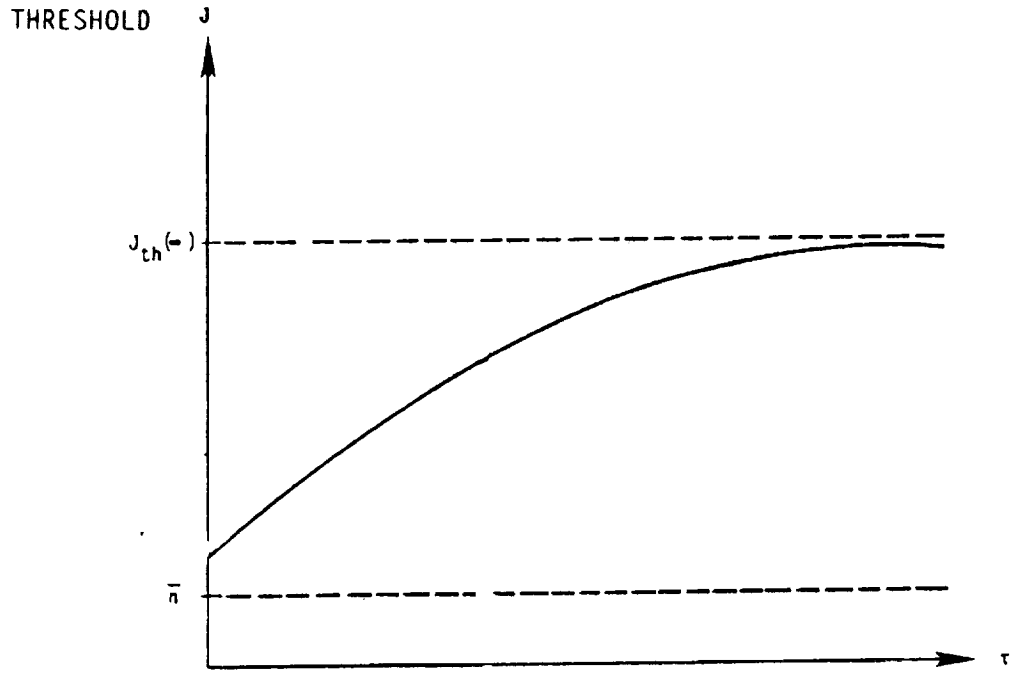

J: Threshold

J_{th}: Threshold for large detection window

$\bar{n}$: RMS noise

τ: length of moving detection window

Figure 1.3a Threshold vs. Detection Window

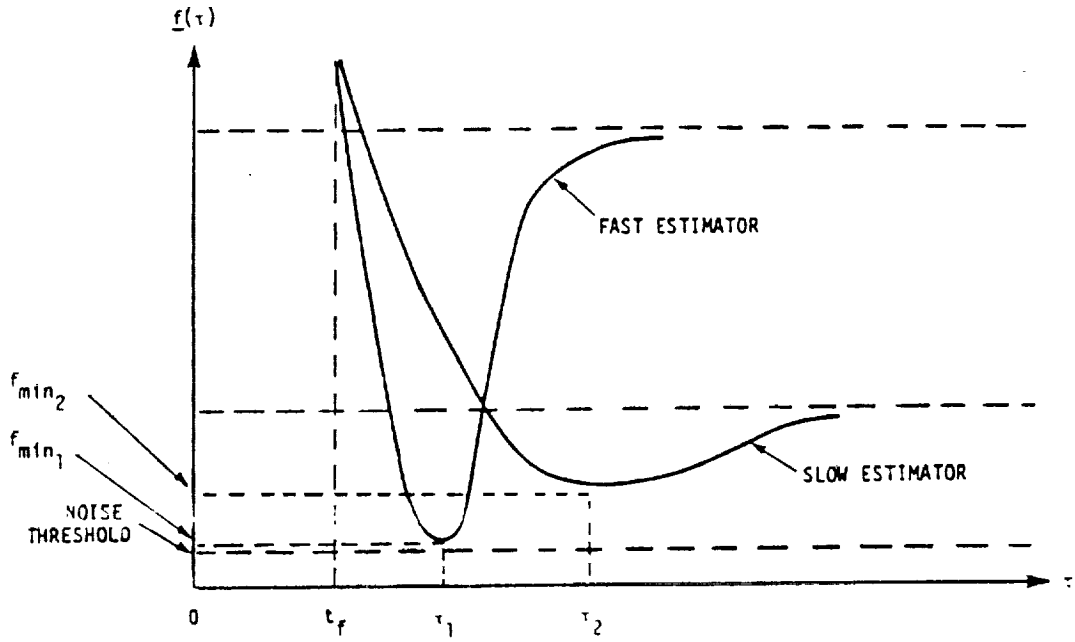

$\underline{f}(\tau)$: smallest size of detectable failure

t_f: time failure occurs

τ: length of detection window

Figure 1.3b Minimum Detectable Bias Shift vs. Detection Window

- the development of estimators using the "internal model principle" to achieve asymptotic convergence despite model error;

- the incorporation of frequency weighting in an LQG cost functional to modify an estimator design to be suitable for sensor failure DIA.

1.3 BACKGROUND

1.3.1 Previous Programs

Under subcontract to Pratt & Whitney Aircraft (PWA), Systems Control Technology, Inc. (SCT) conducted two previous studies in the area of sensor DIA under NASA contracts NAS3-22481, "Sensor Failure Detection System" and NAS3-23282, "Sensor Failure Detection for Jet Engines." The present program is an extension of these studies. The ultimate objective of all these programs is to provide sensor fail operational control capability while minimizing the required sensor hardware redundancy.

"Sensor Failure Detection System," NAS3-22481 [8])

The objective of this study was to develop an advanced concept for the DIA of sensor failures in gas turbine engine control systems. Five concepts were formulated from advanced techniques for sensor DIA. These concepts were evaluated by application to a turbofan engine and multivariable control system simulation. A simplified version of the simulation was used in the preliminary screening process to select one of the DIA concepts. This simplified model was also used for the filter designs in the various DIA concepts.

A functional diagram of the selected advanced concept is shown in Figure 1.4. A normal mode filter, i.e., a filter designed to use all sensor inputs with no failures assumed on those inputs, was used to generate the filter residuals and the estimated measurements. The DIA concept used innovations from the filter to detect hard failures and used the weighted sum-squared residuals (WSSR) technique to detect soft failures. Isolation of soft

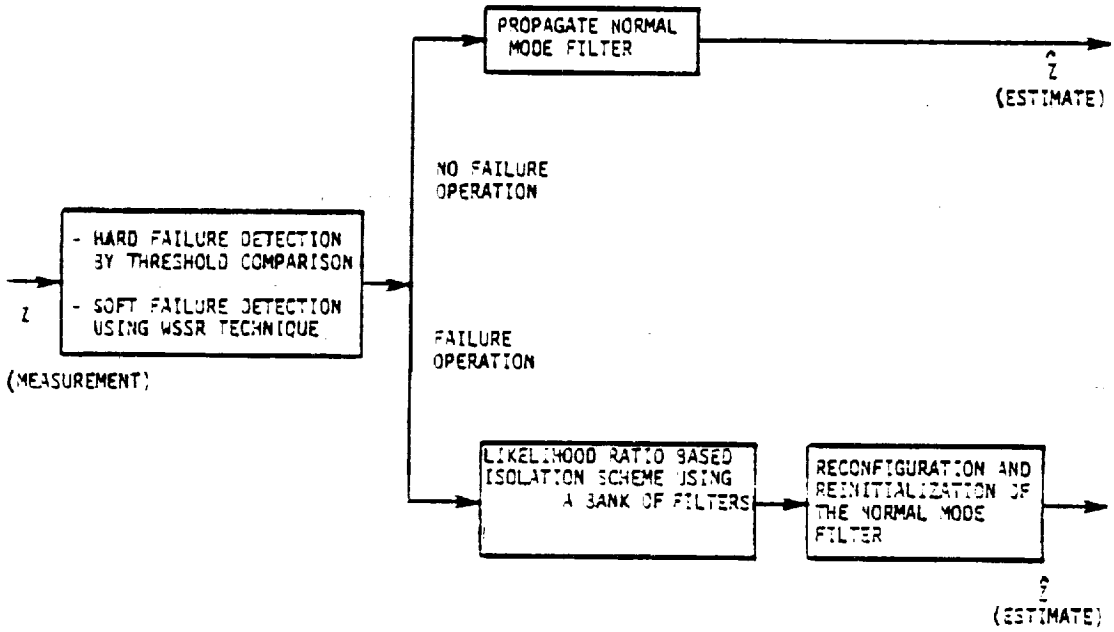

Figure 1.4 Detection, Isolation, and Accommodation (DIA) Concept [8]

failures was accomplished by likelihood ratio (LR) based testing of innovations from a bank of Kalman filters, each designed with the assumption of one failed input. Accommodation was accomplished by reconfiguring the normal mode filter to eliminate the failed sensor from the inputs to the filter. The DIA concept is summarized in Table 1.1. The DIA concept selected was compared against a baseline DIA concept based on the conventional techniques of parameter synthesis.

Table 1.1

Advanced Concept for Detecting, Isolating, and Accommodating Sensor Failures

Detection	-	Innovations testing based on WSSR technique for soft failure. Innovations testing against thresholds for hard failures.
Isolation	-	On-line isolation of hard failures using innovations testing; off-line isolation of soft failures using LR technique. Both structures employ bank of Kalman filters.
Accommodation	-	Reconfiguration and reinitialization of normal mode filter.

The configuration of the multivariable control and the components of the DIA logic used in conjunction with the engine simulation is shown in Figure 1.5. The form of the control law is given by

$$u = u_b + C_p(\hat{z}_p - z_{Pb}) + C_I \int (\hat{z}_I - z_{Ib})\ dt \qquad (1.1)$$

where u is the input vector $[WF\ AH\ CIVV\ RCVV\ BLC]^T$, $\hat{z}_p$ is the estimate of the output vector, $[N1\ N2\ PT4\ PT6\ FTIT]^T$, and $\hat{z}_I$ is a subset of the vector $\hat{z}_p$. $\hat{}$ denotes the estimates. u_b, z_{Pb}, and z_{Ib} are the base point vectors and C_p and C_I are proportional and integral control gain matrices. The proportional part of the control law provides regulation and the integral part provides trim for the fan speed (N1) and augmentor pressure (PT6). Note that the control law uses the estimates for both the proportional and integral portions.

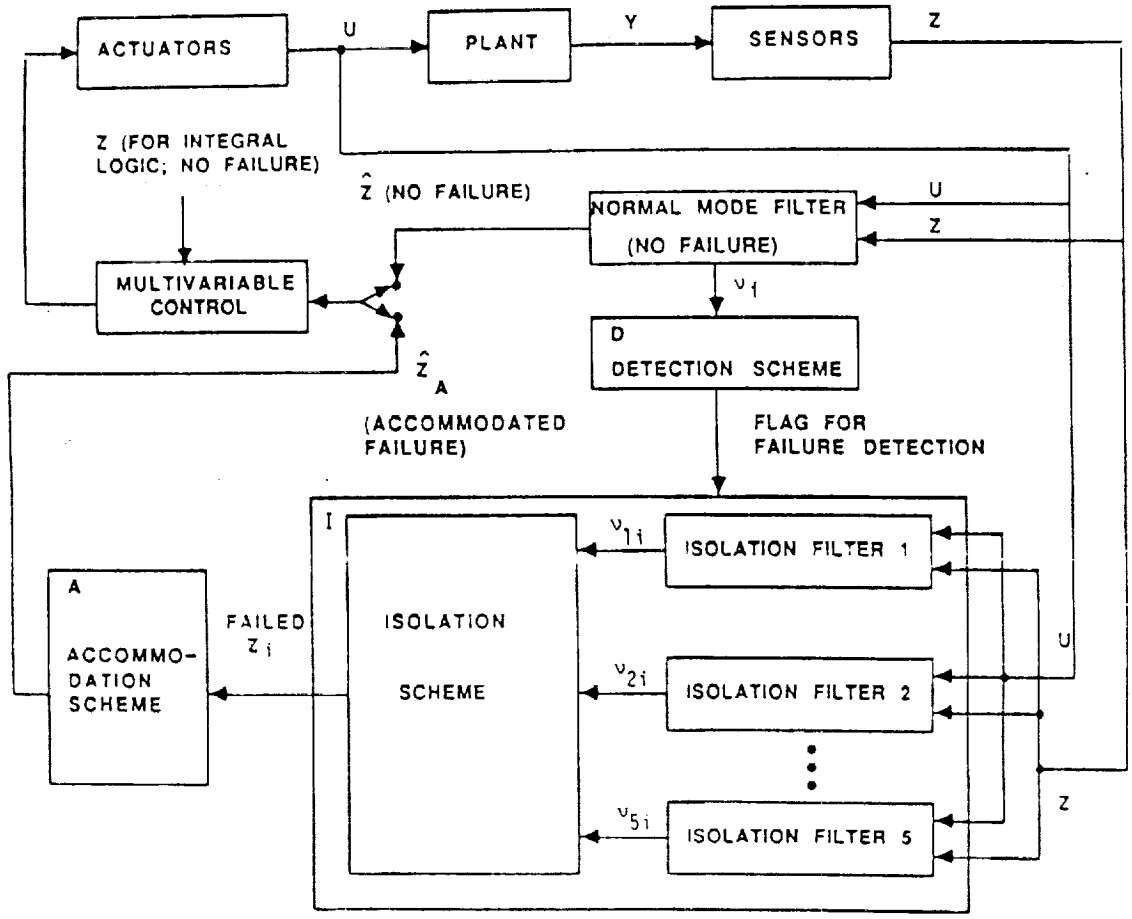

Figure 1.5 Detailed Block Diagram of DIA Concept [8]

As a result of this program, the advanced DIA concept was shown to be a viable DIA technique for application to gas turbine engines. While the performance of the advanced concept was generally good and its feasibility was demonstrated, several problem areas were identified. These included:

- steady-state and dynamic mismatch of the simplified nonlinear model;
- steady-state estimate errors with no failures induced;
- instabilities when accommodating failures;
- accommodation inaccuracies;
- missed detections and false alarms; and
- limited coverage on the flight envelope.

The models used in the no-failure filter and the isolation filters contained modeling errors which contributed to the above problems. The hard and soft failure-detection thresholds and the soft failure-isolation threshold were chosen empirically. They encompassed an estimate of model errors, and estimates of sensor noise and bias errors, and a built-in safety factor. Since the model errors were large, the thresholds were large and contributed to missed detections and false alarms and the overall poor detection performance for very slow drift failures.

"Sensor Failure Detection for Jet Engines," NAS3-23282 [9]

The objective of this program was to develop refinements to the sensor failure DIA algorithm (Figure 1.4) developed under NASA Contract NAS3-22481. These refinements included:

- improvement of the steady-state accuracy of the simplified model of the engine;
- improvement of the dynamic characteristics of the simplified model to be comparable with the nonlinear thermodynamic simulation;
- refinements to the DIA algorithm to be compatible with the improved model;

- elimination of the steady-state errors with no sensor failures caused by biased filter estimates;
- accommodation inaccuracies in case of failure detection and isolation;
- missed failure detections and false alarms.

Three revisions were developed and evaluated to address the above improvements. A detailed, nonlinear thermodynamic simulation was used to evaluate each revision. As a result, one revision was chosen for detailed evaluation and full envelope operation. This DIA algorithm has been programmed on a real-time, microprocessor-based controls computer [10, 11] at NASA Lewis Research Center in preparation for testing as part of a closed-loop control of an engine in a test cell.

This DIA concept, referred to as Revision 2 in the previous contract [9], operated as follows. In the case of no sensor failures, the outputs of the normal mode filter were fed to the proportional control part and the sensed outputs (N1 and PT6 only) were fed to the integral control. This ensured that in steady state, the engine outputs were at the reference point, i.e., there were no steady-state hang-off errors. In the case of a failure, the synthesized value of the outputs were fed to both the proportional and integral controls. Note that if the failed sensor is N1 or PT6, the integral logic ensured that the estimates of these measurements were driven to the reference point. A detailed block diagram of the overall system is shown in Figure 1.6.

The form of the control law, as shown in Figure 1.6, is given by:

No Failure:

$$u = u_b + C_p(\hat{z}_p - z_{Pb}) + C_I \int (z_I - z_{Ib})\, dt \qquad (1.2)$$

Failure:

$$u = u_b + C_p(\hat{z}_p - z_{Pb}) + C_I \int (\hat{z}_I - z_{Ib})\, dt \qquad (1.3)$$

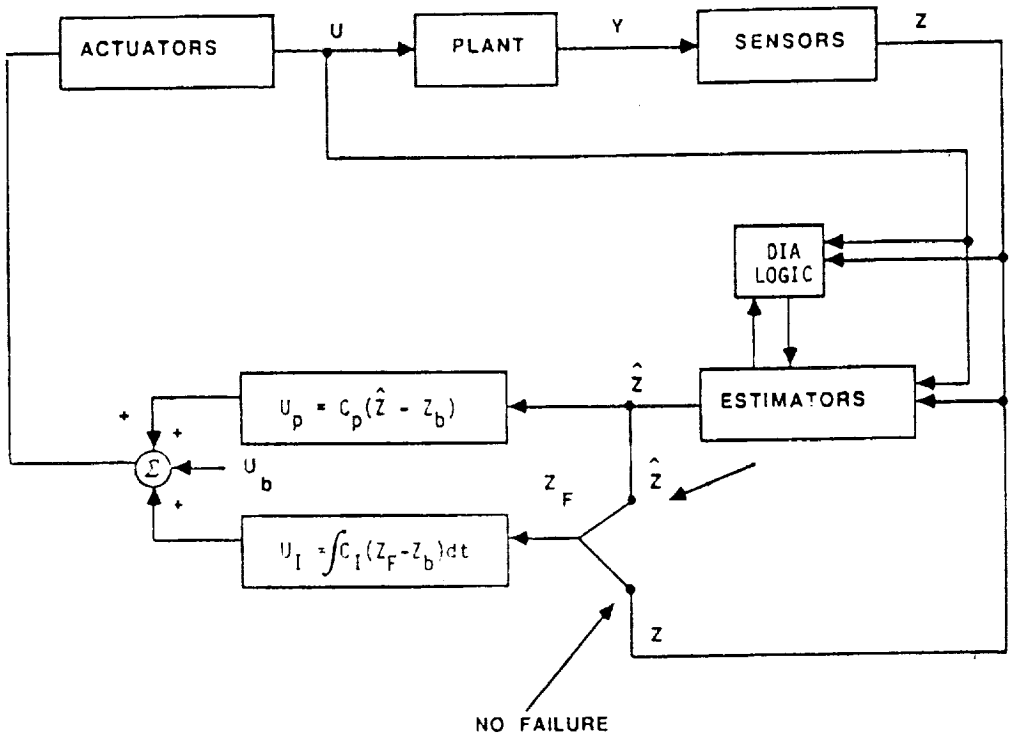

Figure 1.6 DIA Algorithm Revision 2 [9]

The symbols are the same as in (1.1). Note that the estimates are being used in the integral trim portion after failure isolation.

As part of the revision evaluation process, SCT:

(1) generated new gain matrices for both the normal and failure mode filters used in the DIA algorithm;

(2) defined a minimum complexity DIA algorithm;

(3) examined estimator gain sensitivity to flight condition; and

(4) developed the revisions for correcting the bias problem in the estimator outputs.

As a result of this study, the advanced DIA technique (Revision 2) was shown to have improved performance over the technique chosen in the first program. However, model errors limited the performance of the estimators and made determination of detection and isolation thresholds difficult. The present study attempts to alleviate these problems.

The scope of the present research effort is to develop an analytic understanding of the problems by applying the tools of robust multivariable control theory to accommodate modeling errors.

1.3.2 The Fundamental Issue: Model Uncertainty

The previous section has identified model uncertainty as the main source of problems in sensor DIA algorithm design. Model (system, plant) uncertainty refers to the uncertainty in the errors between the nominal model and the actual system. There are two generic uncertainty representations: structured and unstructured [13]. The former refers to model parameters which are uncertain. The latter refers to unmodeled dynamics which are also uncertain. Reduced-order modeling techniques, linearization about operating points, neglecting nonlinearities, etc., all result in contributions to either structured or unstructured uncertainty. Figure 1.7 illustrates how uncertainties can appear in a control system which includes sensor failure DIA

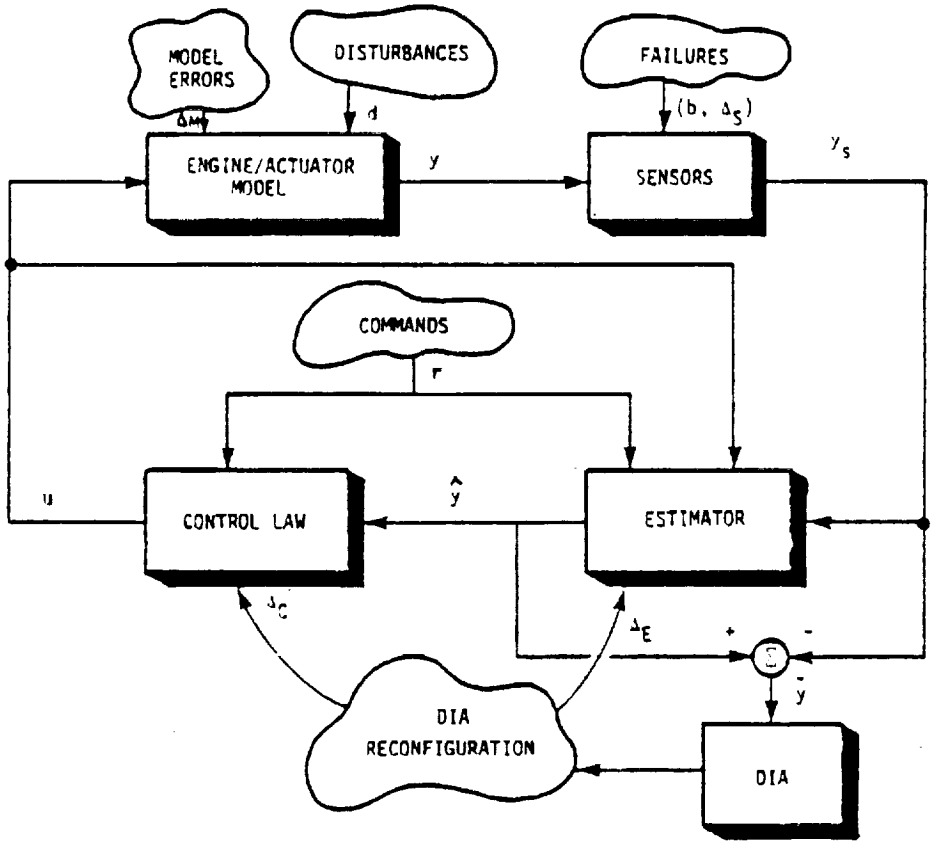

Figure 1.7 Block Diagram of Control System with Sensor Failure DIA Logic, Showing Sources of Uncertainty

logic. The "blocks" represent fixed devices or processors. The "clouds" represent the system uncertainty and can be broadly grouped into two classes:

(1) uncertain (external) inputs

r - reference commands

d - environmental disturbances

b - biases or drifts in a failed sensor

(2) uncertain (internal) dynamics, defined by the following transfer function matrices:

$\Delta_M(s)$ - plant model errors

$\Delta_S(s)$ - sensor failures

$\Delta_C(s)$, $\Delta_E(s)$ - control law and estimator reconfigurations from DIA

Since model uncertainty is the source of most difficulties, an approach is needed to deal with it in an effective manner. Robust DIA design provides a means to do this.

1.4 METHOD OF APPROACH

The method of approach developed in this report is to use robust control theory for threshold selector analysis and robust DIA filter design (as described in Section 1.2). This requires the isolation of uncertainties as shown in Figure 1.7. The approach establishes quantitative statements about the interrelation among performance, robustness, and system uncertainty. Figure 1.8 illustrates how all the uncertainties can be separately grouped for analysis. The external inputs, such as commands, disturbances, and failure biases, enter the system from the "outside." The dynamic uncertainties, such as model errors, sensor failures, and DIA reconfigurations, are "inside" the system and function as a feedback loop around the "interconnection" system. The interconnection system maps the external and internal uncertainties into the outputs, i.e. tracking error and filter residuals.

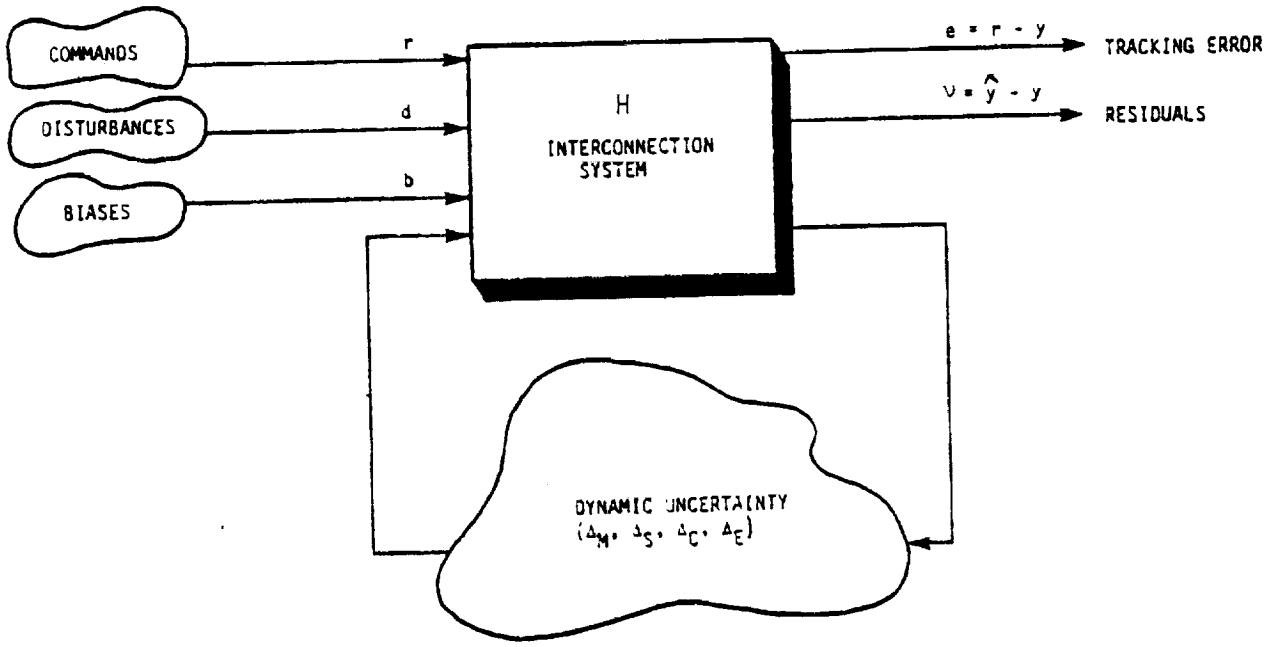

Figure 1.8 Fault-Tolerant System (with Separately Grouped Uncertainties)

Up until recent years, there has been no unified control design approach for such a system as shown in Figure 1.8. Research efforts [13-15], which are elaborations on the Small Gain Theorem [16,17] have established the mathematical framework for such an approach. Basically, the dynamic uncertainties (Δ_M, Δ_S, Δ_C, Δ_E) all propagate in a specific way so as to cause a quantifiable uncertainty about the map from the inputs (r,d,b) into the outputs (e,y), provided bounds can be found for the dynamic uncertainties. These bounds are obtainable from simple input/output system tests. Furthermore, if the nominal system model is linear, the bounds and subsequent input/output errors are fully representable in the frequency domain. For example, the effect of all dynamic uncertainties on the tracking error and the filter residuals can be represented by simple graphs. For good tracking with no sensor failures, the error response and the filter residuals should be small over all frequencies. On the other hand, if a failure occurs -- either a bias/drift b or structure change Δ_S -- then the filter residual frequency signature should be dramatically different from the normal (unfailed) mode. Otherwise, detection is not possible.

The approach utilizes the following recent advances [13-20] in control theory:

(1) Uncertainty Propagation [15]

The dynamic uncertainties, as shown in Figure 1.8, can be bounded in a sector in the frequency domain which then propagates through the interconnection system so that the system input/output map is also in a sector in the frequency domain. These sectors determine quantitatively the performance/robustness trade.

(2) Internal Model Principle [18]

The principle states that asymptotic tracking and disturbance rejection in the presence of plant uncertainty can only be achieved if the controlled system contains a replica (internal model) of the commands and disturbance signal generators. For example, tracking constant commands requires integrators in the loop.

These control design advances, together with methods for frequency-shaped LQG [26] allow for design of either the DIA logic or control/estimator directly in the frequency domain. Thus, if detection is desired for a particular failure, the compensation required can be seen in the frequency domain exactly. Simultaneously, one can determine the effect of the new compensation on tracking performance. A similar procedure can be used for adaptive design.

These ideas are illustrated in the flowchart of Figure 1.9, which shows how the tools generated from the method of approach can be used in a design process. Notice that the modeling errors combine with the sensor failures and the errors from DIA reconfigurations to form the system dynamic uncertainty. It is possible to determine a bound on this uncertainty. The control system (estimator/control law/DIA logic) is then evaluated in the frequency domain by propagating the dynamic uncertainty as outlined above. The evaluation process yields quantitative results which suggest how to modify or robustify the design. This is an iterative process.

Notice that there are three levels of design. Constant gain DIA filters provide a "first cut" design. Optimal thresholds for these filters can be determined as well as minimum size of detectable failures (Level 1). Note that these computations are a function of bound on model error, noise, and class of failures. If a higher level of performance is required, a robust DIA design can be carried out as shown in the flowchart (Level 2). Still better performance is possible by making the DIA filters adaptive (Level 3).

1.5 OUTLINE OF REPORT

This chapter has discussed the background and problem statement for this research effort. Current technology approaches were reviewed. The fundamental problem to be dealt with in DIA logic design, to achieve better performance, has been identified as model uncertainty. The proposed solution has been discussed at a high level. The rest of this report contains the technical details of the method of approach.

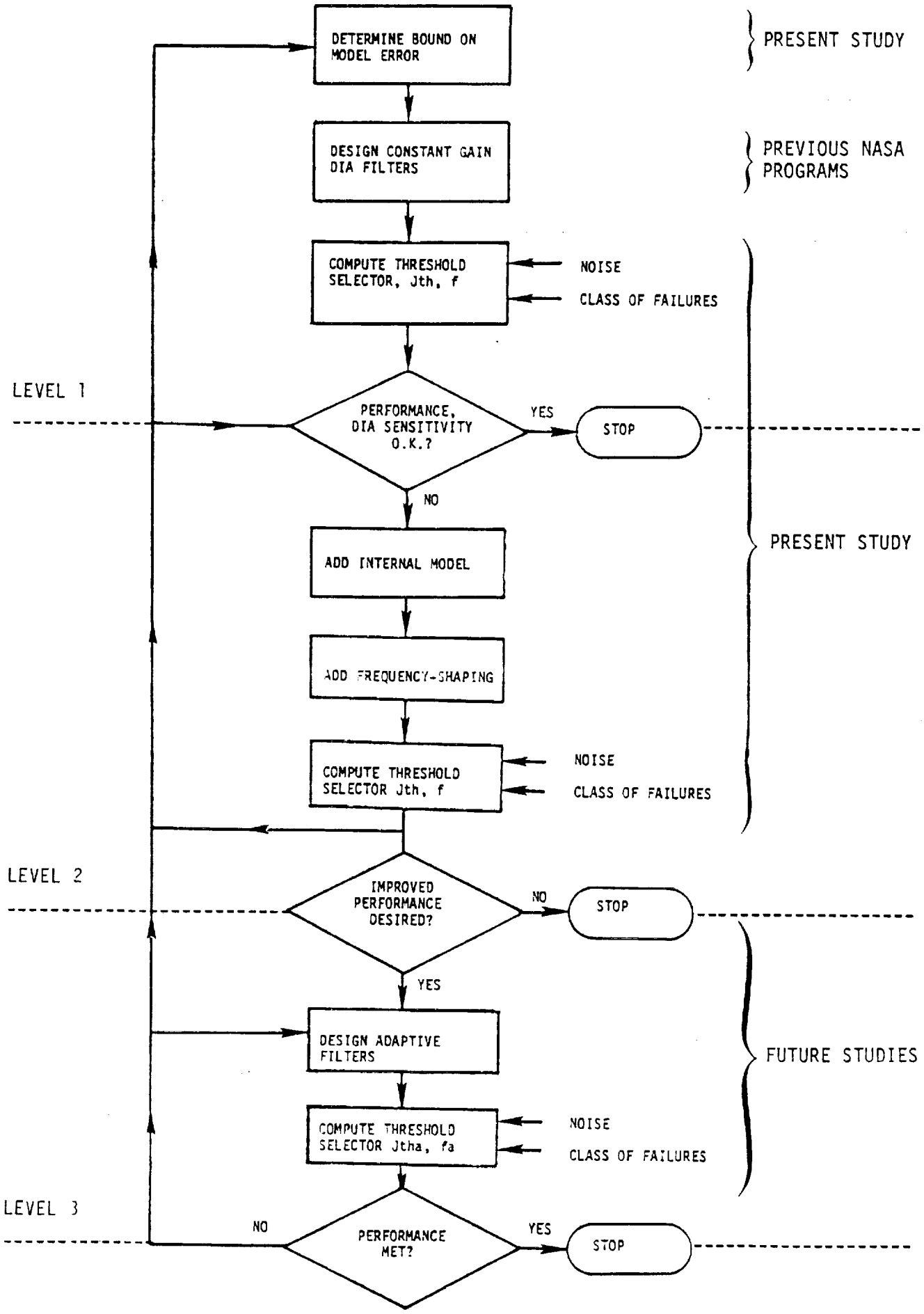

Figure 1.9 Design Approach

Chapter II discusses the effect of model uncertainty on stability and performance. Both stability and new performance robustness measures are developed. The performance robustness measures are with respect to tracking and disturbance rejection properties of the system. The effect of model uncertainty on asymptotic tracking capability is discussed. It is pointed out that for adequate asymptotic performance, an internal model is necessary. This creates certain so-called "structurally robust blocking zeros" to guarantee asymptotic performance.

Chapter III discusses the effect of model uncertainty on sensor failure DIA. The fundamental concept of the threshold selector is introduced. This represents a new, innovative tool for the analysis and synthesis of DIA algorithms. The threshold selector concept is illustrated both for a scalar example and for a model of a multivariable turbofan jet engine. A closed-form solution has been obtained for the scalar case, and a computer-aided design (CAD) approach was developed to solve the multivariable case.

Chapter IV discusses the design of robust filters for sensor failure DIA. The robustness of the filter is due to the presence of an internal model (as discussed in Chapter II) and due to the frequency-shaping of an LQG cost functional. The formulation and mathematical details of the frequency-shaped filters are discussed in this chapter. Results from an example using a dynamic simulation of a turbofan jet engine are presented.

Chapter V presents the results of an evaluation study comparing the performance of the proposed robust DIA scheme to one of the schemes developed in Ref. 9. It is found that the performance of the two techniques is similar for hard failures, but the proposed scheme shows considerable improvement in the case of soft failures.

Chapter VI provides some concluding remarks and directions for future research.

Appendix A discusses model uncertainty and contains a procedure along with results for generation of a bound on model error for a jet engine.

1.6 REMARKS ON NOTATION

Standard notation from control theory literature has been used whenever possible. For example, time domain quantities are usually denoted by lower case, whereas the same quantity in the frequency domain has been denoted by upper case. However, there are several exceptions. Lower case $b(t)$ is used to denote a bias in the time domain and $b(s)$ denotes the same quantity in the frequency, and similarly for $v(t)$ and $v(s)$. There are other exceptions that are generally clear from the context.

II. MODEL UNCERTAINTY AND ITS EFFECT ON STABILITY AND PERFORMANCE

Model uncertainty is the main problem in DIA algorithm design as discussed in Chapter I. How model uncertainty manifests itself affects what one can do to achieve a high performance DIA algorithm. Hence, its effects on stability and performance need to be studied before addressing its effects on detection and robust filter design (to be discussed in Chapters III and IV, respectively. This chapter discusses the sources of model uncertainty in dynamic systems. Both unstructured and parameter uncertainty are considered. Details on model uncertainty and a procedure for computation of its bound for a jet engine example are contained in Appendix A. This chapter concentrates on the effects of model uncertainty on stability and performance properties of the system. New measures are defined for performance robustness analysis which are similar to the well-known stability robustness measures [13]. The effect of model error on asymptotic tracking is explored. It is shown that an internal model is required in the DIA filter to eliminate the effect of the biases on the outputs of the system asymptotically. The inclusion of the internal model results in creation of certain structurally robust blocking transmission zeros to guarantee robustness.

2.1 MODEL UNCERTAINTY

A very natural way to determine model uncertainty is to perform an experiment which compares the model with data from the actual system (plant). If there is no error between the model and the plant, then one has perfect knowledge of the plant. Normally, this is not the situation -- the error is non-zero and represents how close the model is to the plant. For example, consider the simple experiment depicted in Figure 2.1(a), where e is the error between the perturbation output $\delta y_p = y - y_o$ from the actual plant and the corresponding output δy_m of the linearized model; δu is the perturbation input to both the plant and linearized model. $P_o(s)$ is a transfer function matrix description of the model.

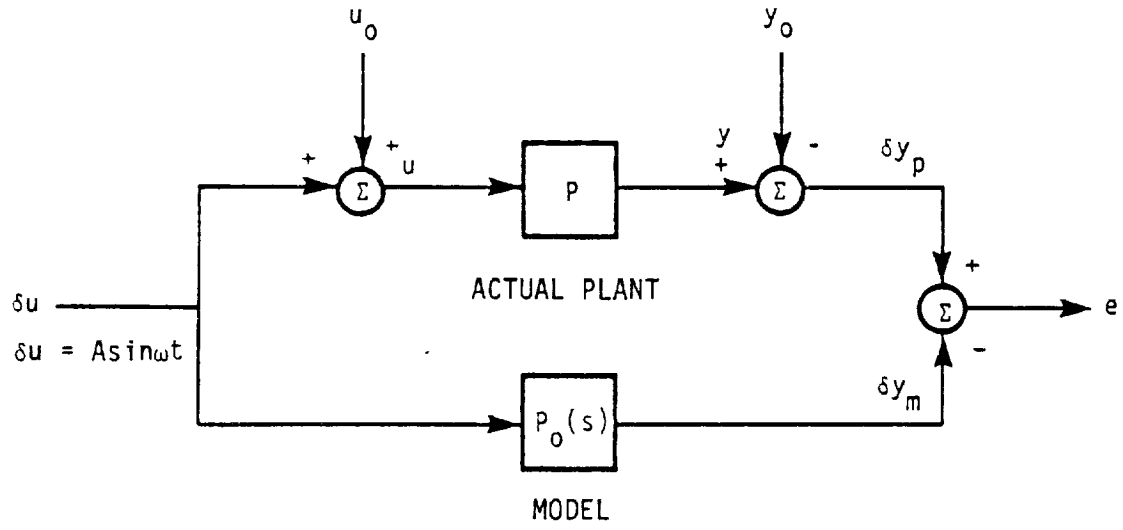

(a)

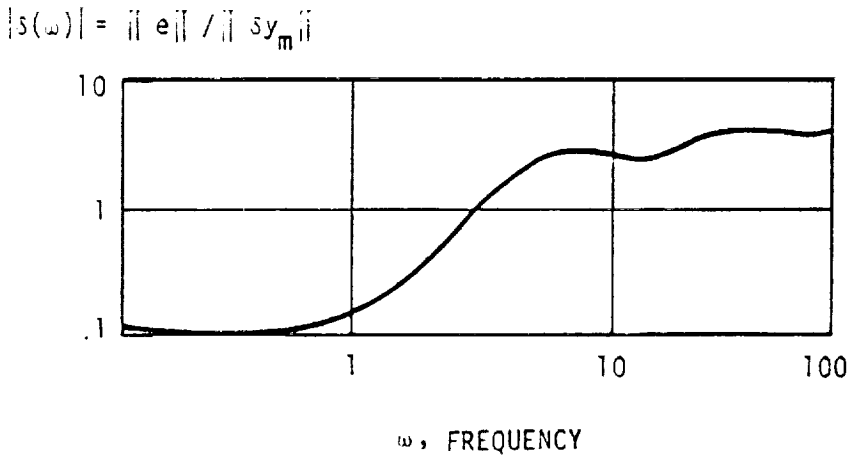

(b)

Figure 2.1 Experiment to Determine Model Uncertainty

By applying sinusoidal test inputs, one can experimentally obtain a frequency-dependent bound as shown in Figure 2.1(b). Often, a good model will be accurate at a certain frequency range, small $\delta(\omega)$*, and less accurate at other frequencies, large $\delta(\omega)$. Figure 2.1(b) is characteristic of unmodeled high-frequency phenomena, incorrectly modeled parameters, as well as some types of neglected nonlinearities. For jet engine models, the key problem is "DC mismatch," i.e. non-zero error at low frequency. This is the predominant cause of setpoint "hang-off" and estimator bias.

Sources of this type of uncertainty may be quite diverse. Slowly drifting parameters in an otherwise perfectly known linear time invariant (LTI) plant could yield the same uncertainty description as a plant with unknown nonlinearities approximated by an LTI model.** The key feature of this uncertainty is that, although it is bounded, one does not know the structure. Following Ref. 2, this is called the <u>unstructured</u> uncertainty of the model $P_o(s)$. Essentially, the unstructured uncertainty indicates the accuracy of the model in the neighborhood of the equilibrium. Equivalently, the plant input/output behavior in the neighborhood of the equilibrium can be described by the linearized uncertain model

$$P_m(s) = (I + \Delta(s))P_o(s) \tag{2.1}$$

where $\Delta(s)$ is the LTI unstructured output-multiplicative uncertainty operator with transfer function matrix $\Delta(s)$. All that is known about $\Delta(s)$ is that it is stable, causal, and bounded by

$$\bar{\sigma}[\Delta(j\omega)] \leq \delta(\omega), \quad \omega \geq 0 \tag{2.2}$$

where $\bar{\sigma}(\cdot)$ denotes the maximum (upper) singular value.

---

* $\delta(\omega)$ representing model error is not to be confused with perturbation quantities such as δY_p, δY_m, etc.

** To reflect parameter errors in $\delta(\omega)$ may require a very large number of experiments as shown in Figure 2.1(a).

In a general way, unstructured uncertainties account for all neglected dynamics, approximated nonlinearities, etc.

One further remark about the uncertain linearized model $P_m(s)$. For every input/output pair (u, y) which satisfies

$$Y(s) = P(s)\, U(s) \tag{2.3}$$

in the neighborhood of the equilibrium, there exists a $P_m(s)$ (equivalently, a $\Delta(s)$) such that $Y(s) = P(s)\, U(s)$. One way to view this is to imagine that $\Delta(s)$ contains a sufficiently large (theoretically infinite) number of adjustable parameters so that any input/output can be perfectly matched. The bound on $\Delta(s)$ in (2.2) conveys the worst case situation. Note that $\Delta(s)$ can be infinite dimensional, without loss of generality.

Parameter Uncertainty

Modeling of plant uncertainty by the description given in (2.1) and (2.2) will be used throughout. A state-space linear plant model is assumed to be given by

$$\dot{x} = A_o x + B_o u \tag{2.4}$$

$$y = C_o x + D_o u$$

with a corresponding model transfer function matrix

$$P_o(s) = C_o(sI - A_o)^{-1} B_o + D_o \tag{2.5}$$

This model is valid only for input/output behavior restricted to a neighborhood of the equilibrium point. A new equilibrium point will have a different nominal model, i.e., the parameters in $P_o(s)$ will change as a function of the equilibrium. This is easily seen in the definition of $P_o(s)$ given by (2.5). In a general way, one can consider the nominal model

to be a parametric model, where the parameters are adjusted to best fit the input/output data.

For example, let $P_\alpha(s)$ denote a parametric model of an uncertain plant $P(s)$, where α is a k-vector of parameters in the model. Standard parameter identification methods can be used to find the best $\alpha \in R^k$ to fit the data from the actual plant. For example, given plant input/output data (u, y) on the interval $t \in [0, T]$, a good parametric model is found from

$$\inf_{\alpha \in R^k} \| y - y_a \|_T \tag{2.6}$$

where inf denotes the greatest lower bound or infimum and $\|\cdot\|$ is a suitable norm, such as the L_2 norm

$$\|x\|_T = \left(\int_0^T x'(t)\, x(t)\, dt \right)^{1/2} \tag{2.7}$$

The perfect matching condition

$$Y_\alpha(s) = P_\alpha(s)\, U(s) \tag{2.8}$$

for some α and all (u, y) is never achieved for models of actual systems. The usual situation is the opposite. In fact, there is usually a range of α which solve (2.6).

The variations in α can be considered as uncertain parameters in the model. Since these parameters enter into the model in a definite manner, they can be referred to as the structured uncertainty of the model [13-15]. In a general way, unstructured uncertainties account for all neglected dynamics, approximated nonlinearities, etc. The structured uncertainty essentially yields the range of parameter variation in the model for a best fit of the data.

Parameter (or structured) uncertainties can also be viewed in a slightly different way. Consider the system

$$\dot{x} = (A_o + \delta A)x + (B_o + \delta B)u \qquad (2.9)$$

$$y = C_o x$$

where (A_o, B_o, C_o) are the nominal system matrices and $(\delta A, \delta B)$ represents a perturbation in the system parameters. Suppose further that $(\delta A, \delta B)$ are known to be bounded such that

$$\bar{\sigma}(\delta A) \leq a, \quad \bar{\sigma}(\delta B) \leq b \qquad (2.10)$$

Following the procedures developed in Refs. 4 and 5, one can construct bounds which include these parameter perturbations. Such a construction is useful when analyzing the effect of specific parameter uncertainties. Bounds on model error constructed in this way account for the type of uncertainties discussed by Leininger [4].

2.2 EFFECT OF UNCERTAINTY ON STABILITY AND PERFORMANCE

The model uncertainty discussed in the previous section has significant effects on both stability and performance of the system under feedback control. This section establishes quantitative trade-offs between uncertainty and stability, as well as performance. For this purpose, generic DIA configurations need to be considered for analysis and design purposes. In previous programs [8, 9], an estimator was designed as part of the DIA logic to provide synthesized estimates of system outputs. The estimator may operate both as part of the feedback loop or out of the feedback loop.

Consider the two generic candidate design schemes shown in Figures 2.2 and 2.3. The design in Figure 2.2, referred to as DIA 1, shows a feedback control system with an estimator running out of the control loop, i.e., "piggyback." The design in Figure 2.3, referred to as DIA 2, shows the estimator running in the loop. In both cases, the estimators contain the nominal plant model $P_o(s)$, which approximates the actual plant $P_m(s)$, and a dynamic filter gain $F(s)$, such that

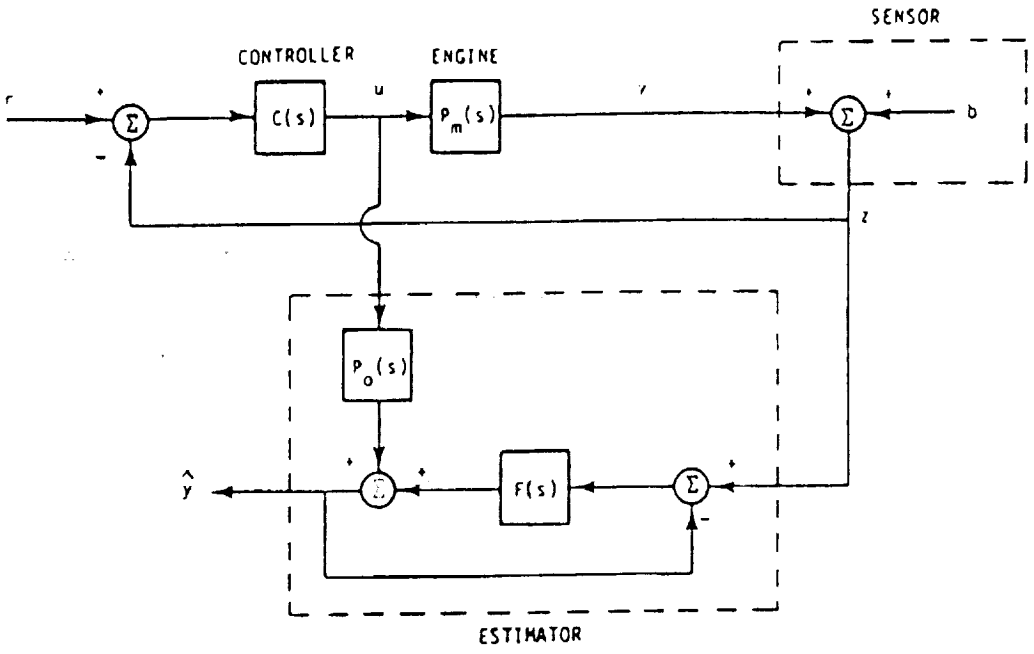

Figure 2.2 Estimator Out of Loop

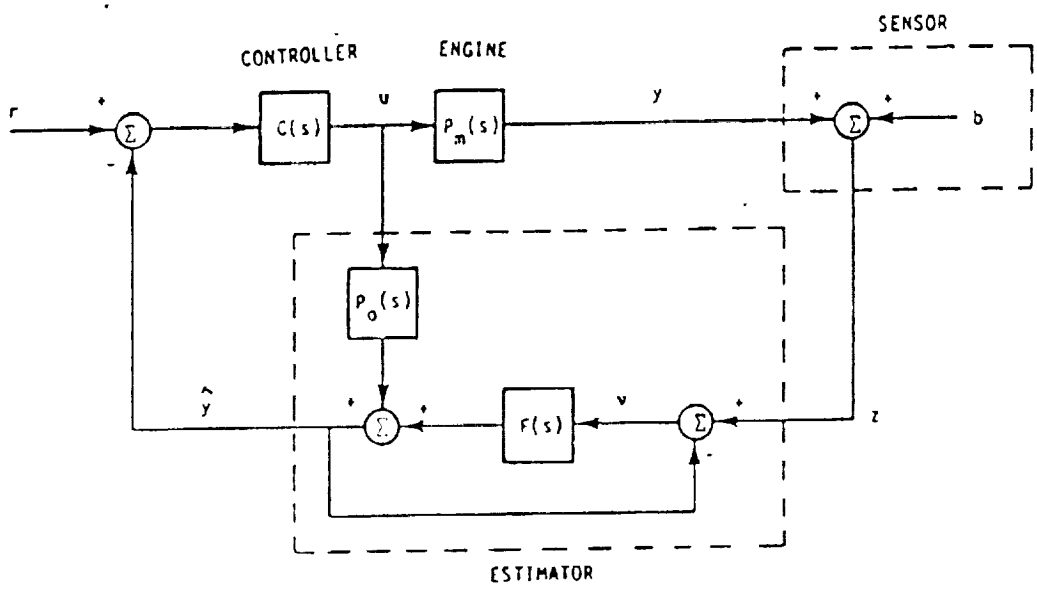

Figure 2.3 Estimator in the Loop

$$\hat{Y}(s) = P_o(s)U(s) + F(s)\nu(s) \tag{2.11}$$

$$\nu(t) = z(t) - \hat{y}(t) \tag{2.12}$$

$$z(t) = b(t) + y(t) \tag{2.13}$$

where $\hat{y}(t)$ is the estimate of the output $y(t)$, $\nu(t)$ is the innovations signal, and $z(t)$ is the sensor output, which is composed of the engine output y and a bias signal $b(t)$ which represents both sensor noise and a class of sensor failures. The estimator structure (2.11) is equivalent to the usual state space structure for estimators/observers, where

$$\dot{\hat{x}} = A\hat{x} + Bu + K\nu(t), \qquad \nu(t) = y(t) - \hat{y}(t) \tag{2.14}$$

$$\hat{y} = C\hat{x} + Du \tag{2.15}$$

In this case, the nominal plant model and filter are, respectively:

$$P_o(s) = C(sI - A)^{-1}B + D \tag{2.16}$$

$$F(s) = C(sI-A)^{-1}K \tag{2.17}$$

The control signal is given by

$$U(s) = \begin{cases} G_c(s)(R(s)-Z(s)), & \text{DIA 1} \quad (2.18) \\ G_c(s)(R(s)-Y(s)) & \text{DIA 2} \quad (2.19) \end{cases}$$

where R is the reference command and $G_c(s)$ is the controller transfer function.

Both of these designs capture the significant characteristics of current DIA schemes as well as being general enough to account for a large class of alternate DIA schemes. For example, DIA 1 is representative of either:

(1) a nominal (no failure) controller with DIA logic based on a "piggyback" estimator; or

(2) a reconfigured system where $G_c(s)$ is a controller/estimator combination with an estimator out of the loop for further DIA action.

Note that in (1) and (2) above, the out-of-loop estimator need not be the same. Similarly, DIA 2 is representative of either:

(3) a nominal (no failure) system where the DIA logic is based on an estimator in the loop; or

(4) a reconfigured system where the DIA logic is based on the estimator in the loop.

As in (1) and (2), the estimators in (3) and (4) need not be identical.

2.2.1 Effect of Model Error on Stability

In this section, tools are developed for determining the effect of uncertainty on stability of DIA 1 and DIA 2. It will be assumed here that the plant is represented by

$$P_m(s) = (I + \Delta(s))\, P_o(s) \tag{2.20}$$

with

$$\bar{\sigma}[\Delta(j\omega)] < \delta(\omega) \ , \quad \omega \geq 0 \tag{2.21}$$

where $P_o(s)$ is the nominal engine model obtained by linearization about an equilibrium and $\Delta(s)$ is the unstructured model uncertainty.

In order to analyze the systems, it is necessary to determine the transfer functions defined implicitly by,

$$E(s) = H_{er}R(s) + H_{eb}(s)b(s) \tag{2.22}$$

$$\nu(s) = H_{\nu r}(s)R(s) + H_{\nu b}(s)b(s) \tag{2.23}$$

The most convenient way to do this is via the "interconnection" structure where the uncertainty $\Delta(s)$ is isolated [15] as shown in Figure 2.4,

$$\begin{bmatrix} E(s) \\ \nu(s) \end{bmatrix} = \begin{bmatrix} H_{er} & H_{eb} \\ H_{\nu r} & H_{\nu b} \end{bmatrix} \begin{bmatrix} R(s) \\ b(s) \end{bmatrix} \tag{2.24}$$

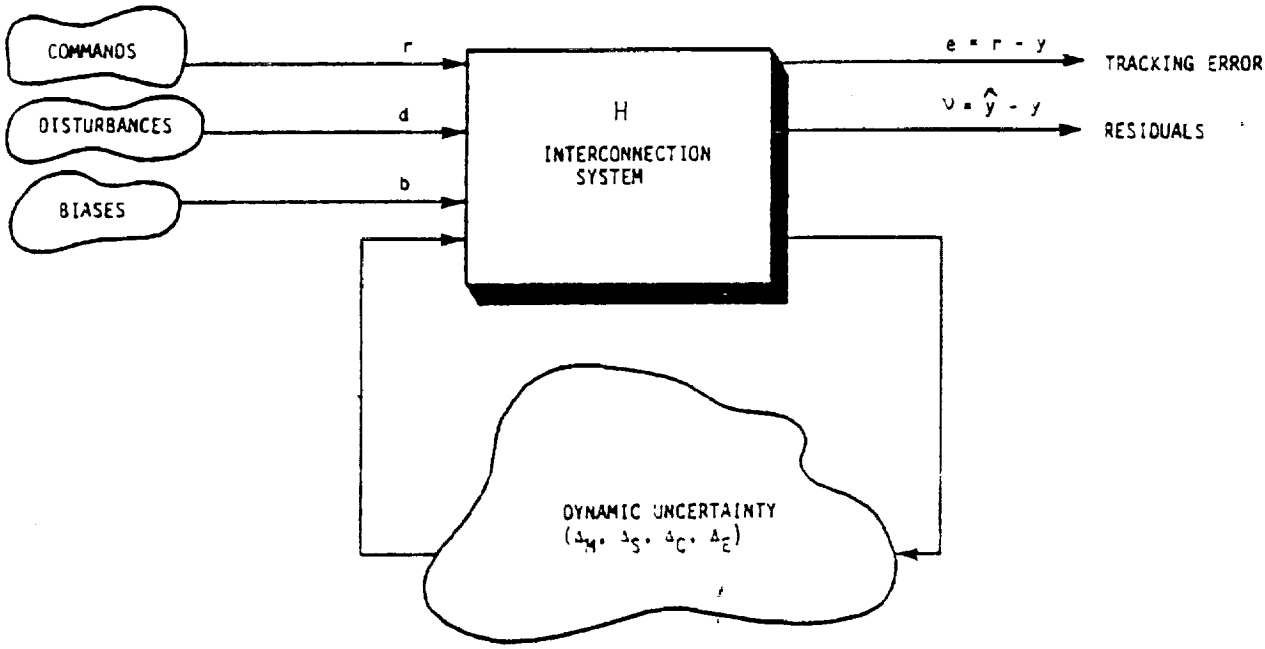

Figure 2.4 Fault-Tolerant System (with Separately Grouped Uncertainties)

A more detailed discussion of the interconnection system is provided in the next section. For DIA 1, one gets (suppress the 's' variable)

$$H_{er} = S(I + \Delta T)^{-1}$$

$$H_{eb} = T + S(I + \Delta T)^{-1}\Delta T \qquad (2.25)$$

$$H_{\nu r} = L(I + \Delta T)^{-1}\Delta T$$

$$H_{\nu b} = L(I + \Delta T)^{-1}$$

and likewise for DIA 2, one gets

$$H_{er} = S - S(I + GL)(I + \Delta TM)^{-1}\Delta T$$

$$H_{eb} = TM + S(I + GL)(I + \Delta TM)^{-1}\Delta TM \qquad (2.26)$$

$$H_{\nu r} = L(I + \Delta TM)^{-1}\Delta T$$

$$H_{\nu b} = L(I + \Delta TM)^{-1}$$

where

$$G = P_o G_c$$

$$S = (I + G)^{-1}, \quad T = (I + G)^{-1}G \qquad (2.27)$$

$$L = (I + F)^{-1}, \quad M = (I + F)^{-1}F$$

The transfer functions (2.25) and (2.26) are stable if

(1) S, T, M, and L are stable

(2) $\delta(\omega)\bar{\sigma}[T(j\omega)] < 1, \quad \omega \geq 0$ (2.28)

(3) $\delta(\omega)\bar{\sigma}[T(j\omega)M(j\omega)] < 1, \quad \omega \geq 0$

Consider the following scalar example, where

$$P_o(s) = \frac{a}{s+a}, \qquad G_c(s) = 1 + \frac{a}{s} \tag{2.29}$$

$$F(s) = \frac{k}{s+a} \tag{2.30}$$

and from (2.27),

$$G = \frac{a}{s}, \quad S = \frac{s}{s+a}, \quad T = \frac{a}{s+a} \tag{2.31}$$

$$L = \frac{s+a}{s+a+k}, \qquad M = \frac{k}{s+a+k}$$

Consequently, conditions (2) and (3) above yield the following model error bounds:

$$(2')\ \delta(\omega) < \left(1 + \left(\frac{\omega}{a}\right)^2\right)^{1/2}, \quad \omega \geq 0 \tag{2.32}$$

$$(3')\ \delta(\omega) < \left(1 + \left(\frac{\omega}{a}\right)^2\right)^{1/2}\left[\left(1 + \frac{a}{k}\right)^2 + \left(\frac{\omega}{k}\right)^2\right]^{1/2}, \quad \omega \geq 0$$

The above bounds can be interpreted as the maximum permissible bounds on model error for which the system (DIA 1 or DIA 2) remains stable. For example, if the actual model error is predominantly DC mismatch where the DC gain is known to within ± 10 percent, i.e., $\delta = .1$, then the above is certainly satisfied.

2.2.2 Effect of Model Error on Performance: Performance Robustness

Performance refers to the behavior of the system in relation to specified objectives, such as transient response, command following, and disturbance rejection. Performance robustness is the ability of the feedback system to maintain a performance specification despite plant uncertainty. In order to realize such robustness properties of feedback, it is necessary to establish quantitatively the trade-offs and relationships among performance, robustness, and plant uncertainty. Presented below is a method for directly analyzing performance robustness of uncertain multivariable systems.

2.2.3 Conic Sectors

Structured and unstructured uncertainties can both be viewed as belonging to an L_p-conic sector, defined as follows [15]:

Definition: A relation $(u, y) \in H$ is inside the L_p-conic sector, denoted $H \in L_p\text{-Cone}(C, R, S)$ if for some $p \in [1, \infty]$ there exists compatible operators C, R, and S such that $H - C$ is L_p-stable* and $\|S(y - Cu)\|_p \leq \|Ru\|_p$ for all $(u, y) \in L_p \times L_p$ with $y \in Hu$.

In the case of L_2-stable LTI operators R, S, and $H-C$ with transfer function matrices $R(s)$, $S(s)$, and $H(s)-C(s)$, respectively, the L_2-conic sector is equivalent to the frequency-domain condition,

$$\bar{\sigma}[S(j\omega)(H(j\omega)-C(j\omega))R^{-1}(j\omega)] \leq 1, \quad \forall\, \omega \tag{2.33}$$

Let $\Omega = \text{diag}\,(\alpha_1 \ldots \alpha_k)$ be a diagonal matrix containing all the structured uncertainties. Equivalent statements for plant uncertainty with the LTI model $P_m[\alpha]$ of P is that the structured uncertainty $\Omega \in L_2$-cone $(0, \beta, I)$, where $\beta = \text{diag}\,(\beta_1 \ldots \beta_k)$ and the unstructured uncertainty $\Gamma \in L_2$-cone $(0, I, I)$. Thus, conic sectors conveniently describe typical model (plant) uncertainty.

2.2.4 Plant Interconnection Model

It is convenient to represent the uncertain plant as shown in Figure 2.5, which is patterned after the uncertain system descriptions presented in Ref. 15. The operator

$$\Delta = \begin{pmatrix} \Omega & 0 \\ 0 & \Gamma \end{pmatrix} \tag{2.34}$$

---

* A relation H is said to be L_p-stable if for all $u \in L_p$, $y \in Hu \in L_p$, and there exists finite positive constant k such that $\|y\|_p \leq k\|u\|_p$.

contains all the uncertainties in the plant -- both structured and unstructured. The operator H is referred to as the plant interconnection system and serves to isolate all the uncertainties in Δ from the rest of the plant. Consequently, H is completely known. The governing plant equations are then

$$\begin{pmatrix} y \\ z \end{pmatrix} = H \begin{pmatrix} u \\ v \end{pmatrix} = \begin{pmatrix} H_{yu} & H_{yv} \\ H_{zu} & H_{zv} \end{pmatrix} \begin{pmatrix} u \\ v \end{pmatrix} \tag{2.35}$$

$$v = \Delta z \tag{2.36}$$

The plant input/output relation is given by

$$y = P[\Delta]u \tag{2.37}$$

with

$$P[\Delta] = P_o + H_{yv}(I - \Delta H_{zv})^{-1} \Delta H_{zu} \tag{2.38}$$

where P_o is the nominal plant defined by (2.39)

$$P_o = P[\Delta]_{\Delta=0} = H_{yu}$$

The uncertainty Δ can also be viewed as belonging to a conic sector, i.e. $\Delta \in L_2$-Cone $(0, R, I)$, $R = \text{diag}(\beta, I)$ which implies the conic sector descriptions of the uncertainties of Ω and Γ. The plant representation shown in Figure 2.5 is extremely useful in evaluating performance of the closed-loop system. With an LTI model, the conic-sector bound on Δ is equivalent to the frequency-domain condition,

$$\bar{\sigma}[\Delta(j\omega)R^{-1}(j\omega)] \leq 1, \qquad R(j\omega) = \text{diag}(\beta, \ell(\omega)I) \tag{2.40}$$

2.2.5 Normalization

The uncertainty and interconnection system can be normalized. Let ΔR^{-1} replace Δ, RH_{zv} replace H_{zv}, and RH_{zu} replace

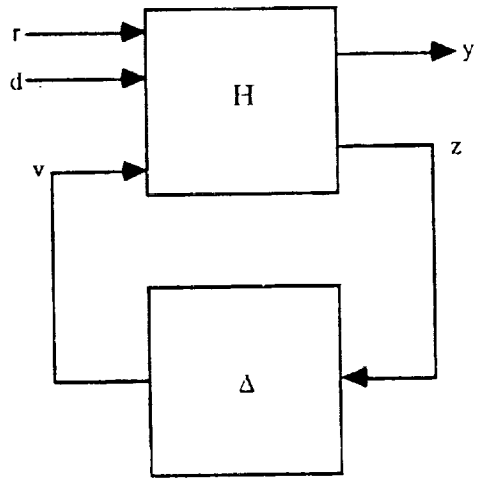

Figure 2.5 Control System as an Uncertain System

H_{zu}. $P[\Delta]$ now has the same form as before, but Δ is normalized so that

$$\Delta \in L_p\text{-cone } (0, I, I)$$

For convenience, assume that henceforth these replacements have been made and the plant interconnection system is normalized.

2.2.6 Performance Robustness Measures

Consider the feedback system shown in Figure 2.6. The plant has the transfer function

$$P(\Delta) = P_o(s)\ (I + \Delta(s)) \tag{2.41}$$

where $P_o(s)$ is the nominal plant transfer function and $\Delta(s)$ represents the unstructured input-multiplicative uncertainty. $P_o(s)$ expressed in terms of state variable matrices is

$$P_o(s) = C(sI-A)^{-1} B + D \tag{2.42}$$

The closed-loop interconnection system is

$$\begin{bmatrix} Y \\ Z \end{bmatrix} = \begin{bmatrix} H_{YR}(s) & H_{Yd}(s) & H_{YV}(s) \\ H_{ZR}(s) & H_{Zd}(s) & H_{ZV}(s) \end{bmatrix} \begin{bmatrix} R \\ d \\ V \end{bmatrix} \tag{2.43}$$

where for a unity feedback system ("suppressing" s)

$$H_{YR} = (I + P_o\ G_c)^{-1}\ P_o\ G_c \tag{2.44}$$

$$H_{YV} = (I + P_o\ G_c)^{-1}\ P_o \tag{2.45}$$

$$H_{ZV} = -\ (I + G_c\ P_o)^{-1}\ G_c\ P_o \tag{2.46}$$

$$H_{ZR} = (I + G_c\ P_o)^{-1}\ G_c \tag{2.47}$$

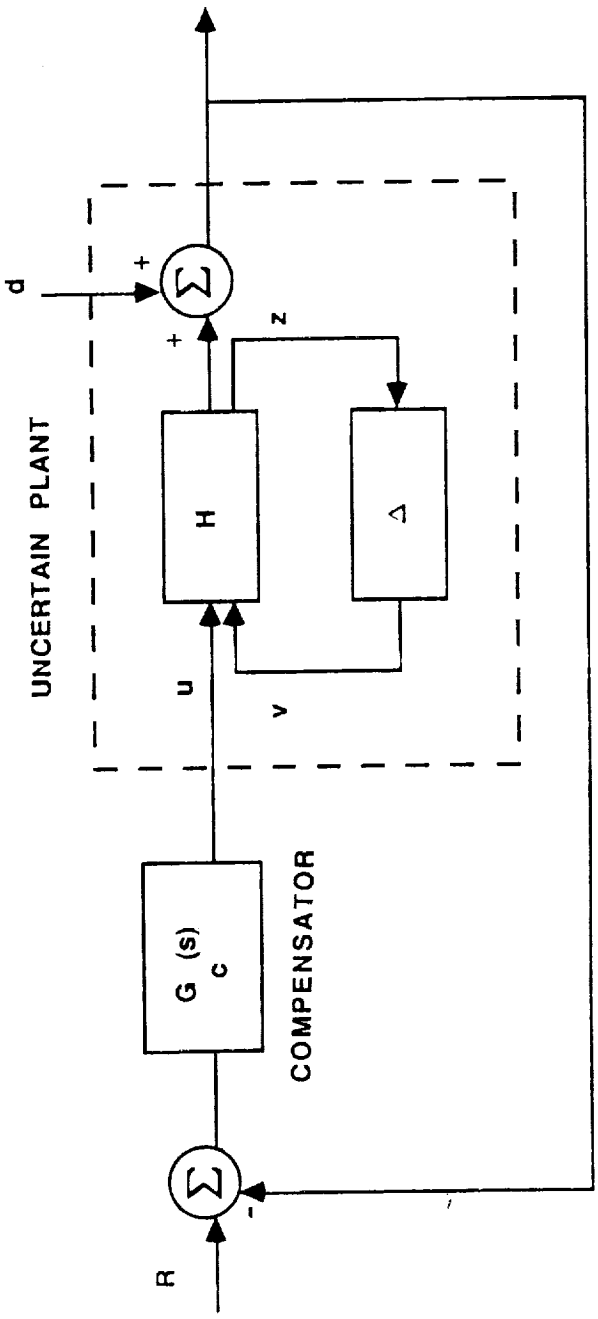

Figure 2.6 Control System with Uncertain Plant Feedback

Now assume that the tracking performance requirements are expressed in the frequency domain in terms of

$$\frac{\|H_{YR}(\Delta) - H_{YR}\|}{\|H_{YR}\|} < \rho(\omega) \qquad \omega \geq 0 \tag{2.48}$$

where H_{YR} is the nominal input-output transfer function, $H_{YR}(\Delta)$ is the perturbed input-output transfer function and $\rho(\omega)$ represents some given function of frequency which specifies tolerable tracking performance degradation. Furthermore, if $\delta(\omega)$ represents a bound on model uncertainty, i.e.

$$\|\Delta\| < \delta(\omega) \qquad \omega \geq 0 \tag{2.49}$$

then the tracking performance robustness properties of the system is described by the following theorem.

Theorem 2.1: Assume that the tracking performance requirements are expressed by (2.48) and the closed-loop interconnection system is stable. Then tracking performance requirements are guaranteed if

$$\delta_{PR_T}(\omega) > \delta(\omega) \qquad \omega \geq 0 \tag{2.50}$$

where

$$\delta_{PR_T}(\omega) = \frac{\rho(\omega)\ \bar{\sigma}(H_{YR})}{\sigma(\bar{H}_{ZV})\sigma(\bar{H}_{YR})\rho(\omega) + \sigma(\bar{H}_{YV})\sigma(\bar{H}_{ZR})} \tag{2.51}$$

is the tracking performance robustness measure.

Proof: Assuming $d = 0$, from Eqs. (2.38) and (2.43), it follows that

$$H_{YR}(\Delta) = H_{YR} + H_{YV}(I - \Delta H_{ZV})^{-1}\ \Delta\ H_{ZR} \tag{2.52}$$

Substituting (2.52) into (2.48), one obtains

$$\|H_{YV}(I - \Delta H_{ZV})^{-1}\ \Delta\ H_{ZR}\| \leq \rho(\omega)\ \|H_{YR}\| \tag{2.53}$$

Using the matrix inequalities

$$\bar{\sigma}(AB) \geq \bar{\sigma}(A)\ \underline{\sigma}(B) \tag{2.54}$$

$$\underline{\sigma}(I - C) \geq 1 - \bar{\sigma}(C) \quad \text{if} \quad \bar{\sigma}(C) < 1 \tag{2.55}$$

$$\underline{\sigma}(A) = \frac{1}{\bar{\sigma}(A^{-1})} \tag{2.56}$$

then it follows from (2.53) that

$$\frac{\bar{\sigma}(H_{YV})\ \delta\ \bar{\sigma}(H_{ZR})}{1 - \delta\ \bar{\sigma}(H_{ZV})} \leq \rho(\omega)\ \bar{\sigma}(H_{YR}) \tag{2.57}$$

Solving for the worst-case value of δ in (2.57) and naming the particular value satisfying (2.57) δ_{PR_T} we have

$$\delta_{PR_T} = \frac{\rho(\omega)\ \bar{\sigma}(H_{YR})}{\bar{\sigma}(H_{ZV})\bar{\sigma}(H_{YR})\rho(\omega) + \bar{\sigma}(H_{YV})\bar{\sigma}(H_{ZR})} \tag{2.58}$$

Therefore, so long as

$$\delta < \delta_{PR_T} \tag{2.59}$$

then (2.57) is satisfied and the tracking performance robustness is guaranteed. Q.E.D.

Suppose that the disturbance rejection performance robustness is expressed as

$$\|Y\| \leq \beta(\omega) \qquad \omega \geq 0 \tag{2.60}$$

where $\beta(\omega)$ describes the allowable disturbance rejection performance degradation. The following theorem describes the performance robustness properties of the system.

Theorem 2.2: Assume that the disturbance rejection requirements are expressed by (2.60) and the closed-loop interconnection system is stable. Then the disturbance rejection performance robustness is guaranteed if

$$\delta_{PR_D}(\omega) > \delta(\omega) \qquad \omega \geq 0 \tag{2.61}$$

where

$$\delta_{PR_D}(\omega) = \frac{\beta - \bar{\sigma}(H_{Yd})}{\bar{\sigma}(H_{ZV})(\beta - \bar{\sigma}(H_{Yd})) + \bar{\sigma}(H_{YV})\bar{\sigma}(H_{Zd})} \tag{2.62}$$

is the disturbance rejection performance measure.

Proof: Assuming $R = 0$, from (2.36) and (2.43) it follows that

$$H_{Yd}(\Delta) = H_{Yd} + H_{YV}\Delta(I - H_{ZV}\Delta)^{-1} H_{Zd} \tag{2.63}$$

and

$$\| H_{Yd} + H_{YV}\Delta(I - H_{ZV}\Delta)^{-1} H_{Zd} \| \leq \beta \tag{2.64}$$

Using the matrix inequalities (2.54) through (2.56), the above equation can be written as

$$\frac{\bar{\sigma}(H_{Yd})(1 - \bar{\sigma}(H_{ZV})\,\delta) + \bar{\sigma}(H_{YV})\,\delta\,\bar{\sigma}(H_{Zd})}{1 - \delta\,\bar{\sigma}(H_{ZV})} \leq \beta \tag{2.65}$$

Solving for the worst-case value of δ from (2.65) and naming it $\delta_{PR_D}(\omega)$ we obtain

$$\delta_{PR_D}(\omega) = \frac{\beta - \bar{\sigma}(H_{Yd})}{\bar{\sigma}(H_{ZV})(\beta - \bar{\sigma}(H_{Yd})) + \bar{\sigma}(H_{YV})\bar{\sigma}(H_{Zd})} \tag{2.66}$$

Then, so long as

$$\delta < \delta_{PR_D} \tag{2.67}$$

(2.65) is satisfied and the disturbance rejection performance robustness is guaranteed. Q.E.D.

The stability robustness measure for the system is given by [13]:

$$\delta_{SR}(\omega) = \frac{1}{\bar{\sigma}(H_{ZV})} \tag{2.68}$$

and the system is stable provided that

$$\delta_{SR}(\omega) > \delta(\omega) \tag{2.69}$$

It is easy to see that

$$\delta_{PR_T}(\omega) < \delta_{SR}(\omega) \qquad \omega \geq 0 \tag{2.70}$$

$$\delta_{PR_D}(\omega) < \delta_{SR}(\omega) \qquad \omega \geq 0 \tag{2.71}$$

Figure 2.7 shows the stability and performance robustness measures for a fifth-order multivariable system for 5% performance degradation from nominal. These measures then establish how accurate the plant model has to be for specified performance as a function of frequency. Note that various controller designs can be evaluated on the basis of these measures.

2.2.7 Effect of Model Error on Asymptotic Tracking

The discussion to follow will illustrate the internal model principle [18], namely that, design of robust filters (and controllers) to achieve asymptotic tracking and disturbance rejection, despite model error, can only be accomplished if a model of the command and disturbance is incorporated in the filter (controller). It is shown that the inclusion of the internal model creates appropriate structurally robust blocking zeros.

The critical performance measure for engine control is the ability to achieve asymptotic tracking despite model error at DC. This section highlights some of the main issues associated with this problem.

In order to evaluate the effect of model error on asymptotic tracking, assume that the following conditions hold:

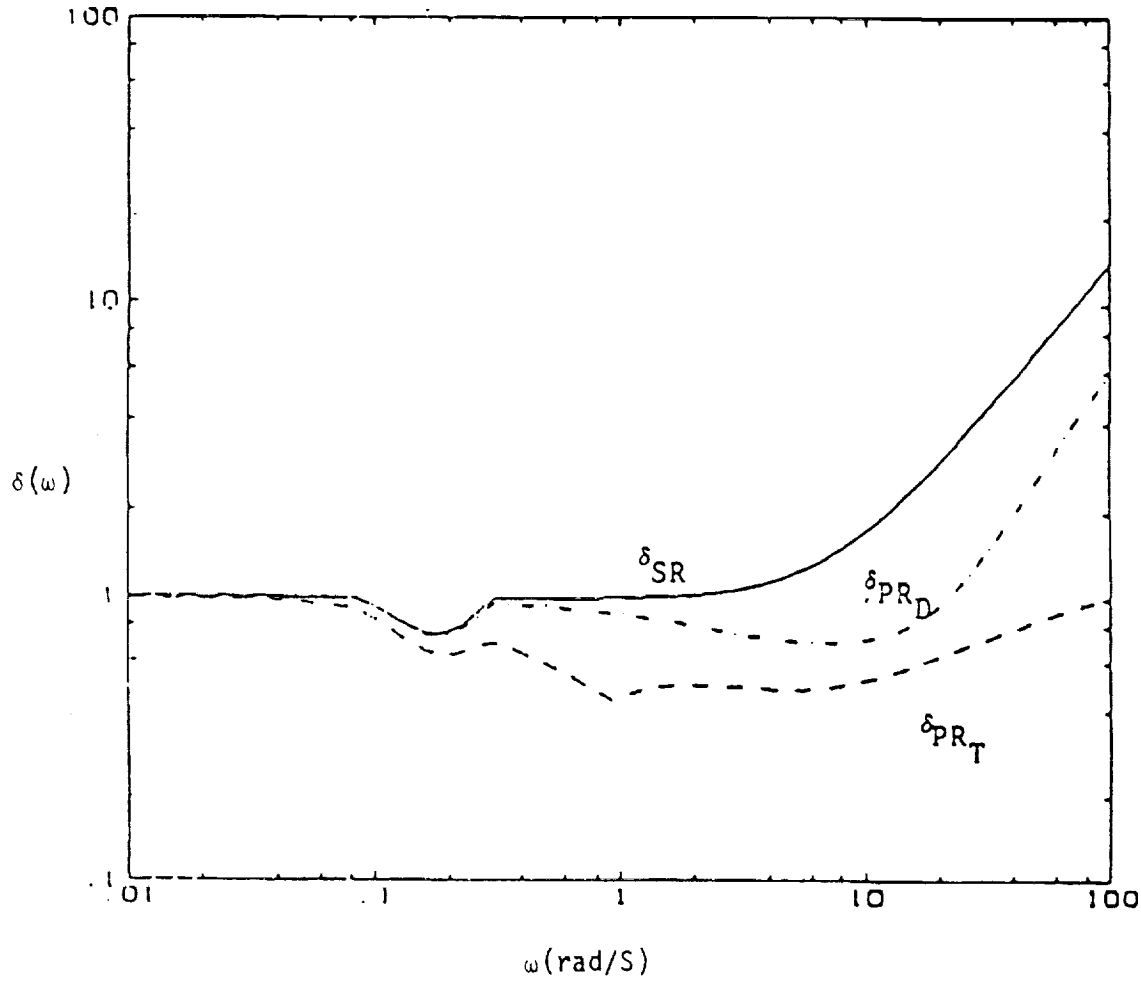

Figure 2.7 Performance (δ_{PR_T}, δ_{PR_D}) and Stability Robustness (δ_{SR}) Measures as a Function of Frequency

(1) The model error satisfies (2.28), i.e., the system is stable.

(2) The reference $r(t) \to r_{ss}$ (constant) as $t \to \infty$.

(3) There is no sensor failure, i.e., $b = 0$.

These conditions, together with (2.31), yield the following steady-state signals for DIA 1 (estimator out of loop):

$$e_{ss} = 0 \tag{2.72}$$

$$H_{\nu r} = L(I+\Delta T)^{-1}\Delta T$$

$$= \frac{s+a}{s+a+k}\left(1 + \Delta \frac{a}{s+a}\right)^{-1} \Delta \frac{a}{s+a} \tag{2.73}$$

$$\nu(s) = H_{\nu r}(s)\, R(s) \tag{2.74}$$

$$\nu_{ss}(s) = \frac{a\Delta(0)}{(a+k)(1+\Delta(0))} R_{ss}(s) \tag{2.75}$$

Similarly, for DIA 2 (estimator in the loop)

$$\nu(s) = H_{\nu r}(s)R(s) \tag{2.76}$$

$$H_{\nu r} = L(I+\Delta TM)^{-1}\Delta T \tag{2.77}$$

$$e_{ss} = -\nu_{ss} = -\frac{a\Delta(0)}{a+k+k\Delta(0)} r_{ss} \tag{2.78}$$

This latter result exhibits the undesirable "hang-off" when the estimator is in the loop, e.g., DIA 2. This problem can be eliminated if the filter in DIA 2 contains an integrator, e.g., if F(s) in (2.30) has the form,

$$F(s) = \frac{f_1 s + f_2}{s(s+f_3)} \tag{2.79}$$

To see this, consider the plant and controller of (2.29) with F(s) as in (2.79), then

$$G = \frac{a}{s}, \qquad T = \frac{a}{s+a} \tag{2.80}$$

$$L = (I+F)^{-1} = \frac{s(s+f_3)}{s(s+f_3) + f_1 s + f_2} \tag{2.81}$$

$$M = LF = \frac{f_1 s + f_2}{s(s+f_3) + f_1 s + f_2} \tag{2.82}$$

For DIA 2

$$H_{vr} = L(I + \Delta TM)^{-1} \Delta T \tag{2.83}$$

and

$$\lim_{s \to 0} H_{vr} = 0 \tag{2.84}$$

It then follows that $e_{ss} = 0$.

Internal Model Principle and Structurally Robust Blocking Zeros:

The internal model principle states that asymptotic tracking and disturbance rejection in the presence of plant uncertainty can only be achieved if the controlled system contains a replica (internal model) of the commands and disturbance signal generators [18-20]. For example, tracking constant commands and rejection of constant disturbances requires integrators in the loop. The presence of the internal model creates zeros of transmission in certain transfer functions. For instance, for command following, transmission zeros are created between the reference input and the tracking error at the frequencies of the commanded signal. These zeros referred to as "blocking" zeros, are also structurally robust, i.e., the locations of the zeros are unaffected by parameter variations.

For sensor failure DIA systems, if the plant's steady-state output is to be unaffected by a failure (represented by the bias b), then the transfer function from b to u (and therefore y) must contain a structurally robust blocking zero. This would happen if an internal model is present in the filter. The following examples illustrates this.

Example 2.1 SISO System with Unknown Measurement Bias:

Consider the SISO plant

$$P_o(s) = \frac{a}{s+a} \tag{2.85}$$

with the filter containing the internal model

Plant:

$$\begin{aligned} \dot{x} &= -ax + au \\ y &= x \\ z &= y + b \end{aligned} \tag{2.86}$$

Filter:

$$\begin{aligned} \dot{\hat{x}} &= -a\hat{x} + K_1(z - \hat{z}) + au \\ \dot{\hat{b}} &= K_2(z - \hat{z}) \\ \hat{z} &= \hat{x} + \hat{b} \end{aligned} \tag{2.87}$$

Control law:

$$u = -K_o\hat{x} \tag{2.88}$$

Then substitution of the control law in the system equations results in the overall system equations from the bias to the control

$$\begin{bmatrix} \dot{\hat{x}} \\ \dot{\hat{b}} \\ \dot{x} \end{bmatrix} = \begin{bmatrix} -a-K_1-aK_o & -K_1 & K_1 \\ -K_2 & -K_2 & K_2 \\ -aK_o & 0 & -a \end{bmatrix} \begin{bmatrix} \hat{x} \\ \hat{b} \\ x \end{bmatrix} + \begin{bmatrix} K_1 \\ K_2 \\ 0 \end{bmatrix} b$$

$$u = -[K_o \quad 0 \quad 0] \begin{bmatrix} \hat{x} \\ \hat{b} \\ x \end{bmatrix} \tag{2.89}$$

For a linear time-invariant system of the form

$$\begin{aligned} \dot{x} &= Ax + Bu \\ y &= Cx + Du \end{aligned} \tag{2.90}$$

the transmission zeros are defined as those frequencies at which the system matrix (pencil)

$$Y_Z(s) = \left[\begin{array}{c|c} sI-A & B \\ \hline -C & -D \end{array}\right] \tag{2.91}$$

loses rank [22].

The zeros from b to u are given by

$$Y_Z(s) = \det \left[\begin{array}{ccc|c} s+a+K_1+aK_o & K_1 & -K_1 & K_1 \\ K_2 & s+K_2 & -K_2 & K_2 \\ aK_o & 0 & s+a & 0 \\ \hline K_o & 0 & 0 & 0 \end{array}\right] = 0$$

$$= -K_o K_1 s(s+a) \tag{2.92}$$

i.e., there is a zero at the origin. Furthermore, this zero is <u>structurally robust</u>, i.e., its location does not change in spite of the parameter errors in the system matrices. To see this, assume that the system matrices are modified such that

$$\tilde{P}_o(s) = \frac{a+\beta}{s+a+\varepsilon} \tag{2.93}$$

where ε and β represent plant parameter variations of any size so long as the closed-loop system remains stable.

The overall system equations from b to u are now given by

$$\begin{bmatrix} \dot{\hat{x}} \\ \dot{\hat{b}} \\ \dot{x} \end{bmatrix} = \begin{bmatrix} (-a-aK_o-K_1) & -K_1 & K_1 \\ -K_2 & -K_2 & K_2 \\ -(a+\beta)K_o & 0 & -(a+\varepsilon) \end{bmatrix} \begin{bmatrix} \hat{x} \\ \hat{b} \\ x \end{bmatrix} + \begin{bmatrix} K_1 \\ K_2 \\ 0 \end{bmatrix} b$$

$$u = [-K_o \quad 0 \quad 0] \begin{bmatrix} \hat{x} \\ \hat{b} \\ x \end{bmatrix} \tag{2.94}$$

The zeros are

$$\gamma_z(s) = \det \left[\begin{array}{ccc|c} s+a+aK_o+K_1 & K_1 & -K_1 & K_1 \\ K_2 & s+K_2 & -K_2 & K_2 \\ (a+\beta)K_o & 0 & s+a+\varepsilon & 0 \\ \hline K_o & 0 & 0 & 0 \end{array}\right] = 0$$

$$= -K_1K_2s(s-a-\varepsilon) \tag{2.95}$$

which confirms the fact that the zero at $s=0$ is unaffected by parameter variations hence the robustness property.

Example 2.2 Multivariable System with Unknown Constant Measurement Bias:

Consider the general square multivariable system

$$\text{Plant:} \quad \begin{aligned} \dot{x} &= Ax + Bu \\ y &= Cx \\ z &= y + b \end{aligned} \tag{2.96}$$

$$\text{Filter:} \quad \dot{\hat{x}} = A\hat{x} + Bu + K_1(z-\hat{z}), \qquad \hat{y} = C\hat{x} \tag{2.97}$$

$$\hat{z} = \hat{y} + \hat{b}$$

$$\dot{\hat{b}} = K_2(z-\hat{z}) \tag{2.98}$$

Control law: $u = -K_o \hat{x}$ (2.99)

The overall system equations are

$$\begin{bmatrix} \dot{x} \\ \dot{b} \\ \dot{x} \end{bmatrix} = \begin{bmatrix} A-BK_o-K_1C & -K_1 & K_1C \\ -K_2C & -K_2 & K_2C \\ -BK_o & 0 & A \end{bmatrix} \begin{bmatrix} \hat{x} \\ \hat{b} \\ x \end{bmatrix} + \begin{bmatrix} K_1 \\ K_2 \\ 0 \end{bmatrix} b$$

$$u = [-K_o \quad 0 \quad 0] \begin{bmatrix} \hat{x} \\ \hat{b} \\ x \end{bmatrix} \tag{2.100}$$

The transmission zeros of the system are given by

$$\gamma_z(s) = \det \left[\begin{array}{ccc|c} sI-A+BK_o+K_1C & K_1 & -K_1C & -K_1 \\ K_2C & sI+K_2 & -K_2C & -K_2 \\ -B K_o & 0 & sI-A & 0 \\ \hline -K_o & 0 & 0 & 0 \end{array}\right] = 0 \tag{2.101}$$

which after elementary row and column operations is equivalent to

$$\gamma_z(s) = \det \left[\begin{array}{cc|c|c} sI-A & -K_1 & & 0 \\ -K_o & 0 & 0 & 0 \\ \hline 0 & 0 & sI-A & 0 \\ \hline 0 & -K_2 & 0 & sI \end{array}\right] \tag{2.102}$$

which shows the presence of blocking zeros at the origin. To see that these transmission zeros are structurally robust, consider the parameter and controller perturbations

$$\tilde{A} = A + \delta A \tag{2.103}$$

$$\tilde{B} = B + \delta B \tag{2.104}$$

$$\tilde{K}_o = K_o + \delta K_o \tag{2.105}$$

$$\tilde{K}_1 = K_1 + \delta K_1 \tag{2.106}$$

$$\tilde{K}_2 = K_2 + \delta K_2 \tag{2.107}$$

The transmission zeros of the perturbed system are given by

$$\tilde{Y}_z(s) = \left[\begin{array}{cc|c|c} sI-\tilde{A} & -\tilde{K}_1 & 0 & 0 \\ -\tilde{K}_o & 0 & 0 & 0 \\ \hline 0 & 0 & sI-\tilde{A} & 0 \\ \hline 0 & -\tilde{K}_2 & 0 & sI \end{array}\right] \tag{2.108}$$

which confirms the fact that the transmission zeros at the origin are structurally robust as they are not affected by plant parameter variations.

The above development can also be carried out for systems with a non-zero direct transmission term ($D \neq 0$) and with more complicated dynamics for the bias b. The conclusions would be the same.

2.3 SUMMARY

In this chapter, we have discussed various sources of model uncertainty and its representation. The effects of model uncertainty on stability and performance was discussed for two generic configurations. New performance robustness measures were introduced to determine tracking and disturbance rejection performance robustness properties. The effects of modeling errors on asymptotic tracking were discussed. It was shown that an internal model is required in the filter to produce unbiased estimates.

III. EFFECT OF MODEL UNCERTAINTY ON FAILURE DETECTION: THE THRESHOLD SELECTOR

One of the most difficult problems in sensor failure DIA algorithm design is the ability to evaluate analytically the DIA algorithm in the presence of model error. In this section, for the first time, a unified framework which allows for this analysis is presented. A new concept is introduced, referred to as the threshold selector, which is a nonlinear inequality whose solution defines the set of detectable sensor failure signals. The threshold selector is consistent with the frequency domain model uncertainty description that has been emphasized in this study. What follows is a heuristic discussion of failure detection which leads to the notion of the threshold selector. For illustrative purposes, the focus will be on the innovations approach to failure detection. As will be seen, the methodology is quite general and not limited to just the innovations approach. The conventional technique of selecting thresholds in innovations-based DIA filters has been based on noise. In a previous study [9], constant thresholds were selected based on a measure of innovations size obtained from a no failure hypothesis filter. However, the current technique determines thresholds based on model error, sensor noise, and class of failures, as well as the speed of the DIA filters.

The threshold selector inequality to be presented here represents a new and innovative tool in the analysis and synthesis of DIA algorithms. In particular, good estimates for the minimum threshold set are obtained in the multivariable case. In this case, it is necessary to compute operator gains dependent upon the norm measure used in detection. DIA designs, more sophisticated than those illustrated here, can also be analyzed and synthesized using the threshold selector inequality.

3.1 INNOVATIONS APPROACH TO FAILURE DETECTION

Many sensor failure detection schemes (for example, see Refs. 1, 8 and 9) have been based on determining the characteristics, such as the RMS value, of

the innovations $\nu(t)$, over a given finite time interval $t \in [0, T]$. In this section, a framework will be presented within which it is possible to evaluate directly the effect of model uncertainty on the ability to detect a failure. The analysis presented also proves to be extremely valuable in the selection of the DIA estimator.

The problem formulation is as in Chapter II. From (2.24), the innovation sequence may be expressed as

$$\nu(s) = H_{\nu b}(s)b(s) + H_{\nu r}(s)R(s) \tag{3.1}$$

where $H_{\nu b}$ and $H_{\nu r}$ are dependent on the model uncertainty Δ, and from (2.25) and (2.26),

$$H_{\nu r}(s) = H_{\nu b}(s)\Delta(s)T(s) \tag{3.2}$$

Define the bias b as

$$b = n + f \tag{3.3}$$

where n is zero-mean sensor noise and f is a drift signal associated with a class of sensor failures. In practice, the situation is that a known class of failures is possible, and detection is limited by some bounded noise signal and bounded model error. Let Ω_n, Ω_f, and Ω_Δ denote, respectively, the bounded sets of noise signals n, failure signals f, and model errors Δ. Let $J(\tau)$ denote a measure of the innovation size on the interval $0 < t < \tau$, where $J(\tau)$ is given by

$$J(\tau) = \|\nu\|_\tau \tag{3.4}$$

The (truncated) norm operation $\|\cdot\|_\tau$ is based on an RMS measure of the innovations and will be defined precisely below. The norm in Eq. (3.4) may be evaluated either in the time domain or frequency domain using Parseval's theorem [28]. Hence, the notation

$$J(\tau) = \|\nu(s)\|_\tau \tag{3.5}$$

denotes evaluation in the frequency domain. Substituting (3.2) into (3.4) gives

$$J(\tau) = \|H_{\nu b}(s)(N(s) + F(s) + W(s)T(s)R(s))\|_{\tau} \tag{3.6}$$

With no model error, $\Delta = 0$ and

$$\nu(s) = H_{\nu b}(s)(N(s) + F(s)) \tag{3.7}$$

Thus, a non-zero bias due to sensor failure is detectable in y through the dynamics of $H_{\nu b}$ given by (2.26). Under mild constraints, it is possible to detect the presence of failure for relatively small bias. The only limit is due to noise levels in the sensor. However, the model error effectively raises the detection threshold (3.6). It was found in previous applications of sensor failure DIA logic to the turbofan engine problem [8, 9] that the model error considerably dominates any sensor noise level and is the primary cause of false alarms and misses. What is sought is a means to detect the presence of failure bias b despite model uncertainty Δ. More specifically, what are the conditions of the transfer function matrices $H_{\nu b}$ and $H_{\nu r}$ in (3.1) such that the ability to detect a failure is maximized? Further, what is the most sensitive detection scheme for a known class of failures?

3.1.1 False Alarm

A major requirement on detection is to reduce or prevent false alarms. Thus, in the absence of any failure signal, $J(\tau)$ should be less than a threshold value, J_{th}. Setting $f = 0$ in (3.6) gives*

$$J_{th}(\tau) = \sup_{x} \|H_{\nu b}(s)(N(s) + W(s)T(s)R(s))\|_{\tau} \tag{3.8}$$

---

* For the sake of brevity, the notation $\sup_{x}(\cdot)$ is used in place of $\sup_{x \in \Omega_x}(\cdot)$ for all $x = n, f, \Delta$. Likewise, $\sup_{x,y}(\cdot)$ means $\sup_{x \in \Omega_x, y \in \Omega_x}(\cdot)$

where $\sup(\cdot)$ denote the supremum or the least upper bound. Note that the threshold function is dependent upon the known reference command r as well as bounds on the noise and model errors. In fact, with no model errors, $\Delta = 0$ and the threshold is determined strictly by the worst-case noise level, i.e.,

$$J_{th}(\tau) = \sup_{n} \|H_{\nu b}(s)N(s)\|_{\tau} \tag{3.9}$$

3.1.2 The Threshold Selector

Setting a threshold to eliminate false alarms due to sensor noise and model error will cause the detector to miss certain failures. The question is: What is the minimum detectable failure? In other words, find the threshold failure set. Denote this set by $\underline{\Omega}_f$, which is defined as those $f \epsilon \Omega_f$ such that

$$\inf_{\Delta,n,f} J(\tau) > J_{th}(\tau) \tag{3.10}$$

where $\inf(\cdot)$ denotes the infinum or the greatest lower bound. Substituting (3.6) and (3.8) into the above gives

$$\inf_{\Delta,n,f} \|H_{\nu b}(s)(N(s) + F(s) + \Delta(s)T(s)R(s)\|_{\tau} > \sup_{\Delta,n} \|H_{\nu b}(s)(N(s) + \Delta(s)T(s)R(s)\|_{\tau} \tag{3.11}$$

If we decompose the innovations into components due to the noise, failure, and error model

$$\nu(s) = \nu_n(s) + \nu_f(s) + \nu_{\Delta}(s) \tag{3.12}$$

then (3.11) may be rewritten as

$$\inf_{\Delta,n,f} \|\nu_n + \nu_f + \nu_{\Delta}\|_{\tau} > \sup_{\Delta,n} \|\nu_n + \nu_{\Delta}\|_{\tau} \tag{3.13}$$

Since this inequality generates the minimum threshold set, it is referred to as the threshold selector. An estimate of the smallest size of failure f which is detectable can now be calculated.

Theorem 3.1: An estimate of the size of minimum detectable failure $|f|$ is given by

$$|f| \geq 2\, J_{th}(\tau)/\beta(\tau) \tag{3.14}$$

with the threshold as

$$J_{th}(\tau) \triangleq (\max_{\omega} \bar{\sigma}\,[L(j\omega)])\ \bar{n} + \delta|r|\bar{\sigma}\, L(Q_{\tau 1}\ LT)(\tau)] \tag{3.15}$$

and

$$\beta(t) \triangleq \bar{\sigma}[Q_{\tau 1} L(\tau - t_f)] \tag{3.16}$$

$|r| \triangleq$ norm of the reference input signal

$|f| \triangleq$ norm of the failure signal

$Q_{\tau k} \triangleq$ operator gains which are functions of type of failure and reference signals; $k = i, j$

$\delta \triangleq$ upper bound on model error (constant)

$t_f \triangleq$ failure time

$\tau \triangleq$ size of detection window

$\bar{n} \triangleq$ bound on RMS sensor noise

Proof: A conservative estimate of the threshold set can be found from the inequality:

$$\inf_{f,\Delta} \|v_f(s)\|_\tau > 2 \sup_{\Delta,n} \|v_n(s) + v_\Delta(s)\|_\tau \tag{3.17}$$

since (3.17) implies (3.13). This can be seen as follows. We may rewrite (3.17) as

$$\inf_{f,\Delta} \|\nu_f(s)\|_\tau - \sup_{\Delta,n} \|\nu_n(s) + \nu_\Delta(s)\| > \sup_{\Delta,n} \|\nu_n(s) + \nu_\Delta(s)\|_\tau \tag{3.18}$$

and since

$$\sup_{\Delta,n} \|\nu_n(s) + \nu_\Delta(s)\| > \inf_{f,\Delta} \|\nu_n(s) + \nu_\Delta(s)\|_\tau \tag{3.19}$$

(3.18) may be written as

$$\inf_{f,\Delta} \|\nu_f(s)\|_\tau - \inf_{\Delta,n} \|\nu_n(s) + \nu_\Delta(s)\|_\tau > \sup_{\Delta,n} \|\nu_n(s) + \nu_\Delta(s)\|_\tau \tag{3.20}$$

However,

$$\begin{aligned} \|\nu_f(s) + \nu_n(s) + \nu_\Delta(s)\|_\tau &> |\|\nu_f(s)\|_\tau - \|\nu_n(s) + \nu_\Delta(s)\|_\tau| \\ &= \|\nu_f(s)\|_\tau - \|\nu_n(s) + \nu_\Delta(s)\|_\tau \end{aligned} \tag{3.21}$$

as long as

$$\|\nu_f(s)\|_\tau > \|\nu_n(s) + \nu_\Delta(s)\|_\tau \tag{3.22}$$

Substituting (3.21) into (3.20), we have

$$\inf_{\Delta,n,f} \|\nu_n(s) + \nu_f(s) + \nu_\Delta(s)\|_\tau > \sup_{\Delta,n} \|\nu_n(s) + \nu_\Delta(s)\|_\tau \tag{3.23}$$

which is (3.13).

In order to utilize (3.13) or (3.14), it is necessary to specify the detection measure $\|\cdot\|_\tau$, and the sets Ω_f, Ω_n, and Ω_Δ. Suppose that detection is based on the root mean square (RMS) measure,

$$\|x\|_\tau = \left(\frac{1}{\tau}\int_0^\tau |x(t)|^2 dt\right)^{1/2} \tag{3.24}$$

where $|x(t)|$ is the Euclidean norm of $x(t)$, i.e.,

$$|x(t)| = (x'(t)x(t))^{1/2} \tag{3.25}$$

Furthermore, let

$$\Omega_f = \{f | f(t) = f_0 1(t - t_f),\ |f_0| \geq f,\ t_f \varepsilon [0, \tau]\}^* \tag{3.26}$$

$$\Omega_n = \{n |\ \|n\|_\tau \leq \bar{n}\ \} \tag{3.27}$$

$$\Omega_\Delta = \{\Delta | \bar{\sigma}[\Delta(j\omega)] \leq \delta(\omega),\ \ \omega \geq 0\} \tag{3.28}$$

In other words, the sensor failure signal f occurs at some time $t_f \varepsilon [0,\tau]$; and is represented by an abrupt shift in bias; the noise signal n is arbitrary, except that it is bounded in norm (3.27); and the model error Δ is bounded as described in (3.28). Note that by allowing the noise to be in the set Ω_n, it is not possible to distinguish at each instant of time $n \varepsilon \Omega_n$ from $f \varepsilon \Omega_f$. Therefore, it is necessary to view the innovations over a (moving) time window τ, e.g., as in (3.24). One can now calculate an estimate of the smallest f in (3.26) by evaluating (3.13) over (3.17). The mathematical machinery for this calculation is available [14-16], but requires the introduction of the following definitions.

Let H denote an operator with proper rational transfer function matrix $H(s)$. Let Γ_k denote the linear operator defined by

$$(\Gamma_k H)(t) = \begin{cases} \mathscr{L}^{-1}\ [H(s)], & k = 0 \\ \mathscr{L}^{-1}\ \left[\dfrac{(k-1)!}{s^k} H(s)\right], & k = 1,2,\ldots \end{cases} \tag{3.29}$$

where $\mathscr{L}^{-1}[\cdot]$ is the inverse Laplace transform operator. Thus, corresponding to $H(s)$, $(\Gamma_0 H)(t)$ is the impulse response matrix, $(\Gamma_1 H)(t)$ is the step response matrix, and so on. It is also convenient to define the matrix operator,

---

* $1(t)$ is the unit step function, i.e., $1(t) = 0$, $t < 0$; $1(t) = 1$, $t \geq 0$.

$$(Q_{\tau k}H)(\tau) = \left(\frac{1}{\tau} \int_0^{\tau} [(\Gamma_k H)(t)]'[(\Gamma_k H)(t)]dt \right)^{1/2} \tag{3.30}$$

With definitions (3.29) and (3.30), one can now calculate (3.17). In order to facilitate the presentation here, we make the simplifying assumption that the model error Δ is constant (e.g., DC model mismatch only) and is sufficiently small so that

$$(I + \Delta T)^{-1} \sim I, \quad (I + \Delta TM)^{-1} \sim I \tag{3.31}$$

or equivalently*

$$H_{vb}(s) = L(s) \tag{3.32}$$

From (3.17) it then follows that

$$\inf_{f,\Delta} \|L(s)F(s)\|_{\tau} > 2 \sup_{\Delta,n} \|L(s)N(s) + L(s)\Delta(s)T(s)R(s)\|_{\tau} \tag{3.33}$$

We will now evaluate the above norms in the time domain. Using the relations [28]

$$\|\alpha A\| = |\alpha| \|A\| \tag{3.34}$$

$$\|AB\| \leq \|A\| \|B\| \tag{3.35}$$

and the fact that

$$\underline{\sigma}(A) \leq \frac{\|Ax\|}{\|x\|} < \bar{\sigma}(A) \tag{3.36}$$

the left-hand side of (3.33) may be replaced by

$$|f| \, \underline{\sigma} \, [Q_{\tau 1}(L(\tau - t_f))] \tag{3.37}$$

where the $\inf(\cdot)$ has been replaced by the lower singular value from (3.36) and (3.26) was substituted for $f(t)$. We then have that

---

* Note that without this simplification, one has to deal with (3.17) directly which is rather awkward.

$$|f|\ \underline{\sigma}[Q_{\tau 1}(L(\tau-t_f))] > 2 \sup_{\Delta,n} \|L(s)N(s) + L(s)W(s)T(s)R(s)\|_\tau \tag{3.38}$$

Now if we ensure that

$$|f|\ \underline{\sigma}[Q_{\tau 1}(L(\tau-t_f)] > 2 \sup_{\Delta,n}(\|L(s)\|_\tau \|N(s)\|_\tau + \|\Delta(s)\|_\tau \|L(s)T(s)R(s)\|_\tau \tag{3.39}$$

then using (3.35) and the fact that

$$\|A+B\| \leq \|A\| + \|B\| \tag{3.40}$$

(3.37) follows from (3.38) since the right-hand side of (3.38) is smaller than (3.38). Furthermore, if we use the identity [28]

$$\|a\|_2 = \bar{\sigma}(a) = \max_\omega |A(j\omega)| \tag{3.41}$$

then the right-hand side of (3.39) may be written using (3.27), (3.41), (3.28), and (3.30) as

$$2(\max_\omega |L(j\omega)|\ \bar{n} + \delta|r|\bar{\sigma}[Q_{\tau 1}(LT)(\tau)]) \tag{3.42}$$

Substituting (3.42) for the right-hand side of (3.39) we now have

$$|f|\underline{\sigma}[Q_{\tau_1} L(\tau-t_f)] > 2\ (\max_\omega |L(j\omega)|\ \bar{n} + \delta|r|\bar{\sigma}[Q_{\tau 1}(LT)(\tau)]) \tag{3.43}$$

where we have used the assumption that

$$r(t) = r\ 1(t) \tag{3.44}$$

If we define the threshold as

$$J_{th}(\tau) \triangleq \max_\omega |L(j\omega)|\bar{n} + \delta|r|\ \bar{\sigma}[Q_{\tau 1}(LT)(\tau)] \tag{3.45}$$

and

$$\beta(\tau) \triangleq Q_{\tau 1}(L(\tau-t_f)) \tag{3.46}$$

then (3.43) may be written as

$$|f| \geq \frac{2J_{th}(\tau)}{\beta(\tau)} \tag{3.47}$$

which is the desired relation (3.14). Q.E.D.

Figure 3.1 shows a conceptual plot of $|f|$ vs. τ. Note that in the presence of noise, the detection window must be large enough to separate noise from the bias shift due to sensor failure. Further, there is a detection window τ, dependent on t_f, such that $|f|$ is a minimum. But, t_f is not known; consequently, one can only evaluate the effect of window selection. Figure 3.1 is also useful in evaluating the filter dynamics. If the dynamics of the filter are fast, there is a sharper, lower threshold than when the filter is slow. Figure 3.1 illustrates this critical trade-off in filter design, i.e., threshold vs. detection window. Figure 3.2 shows a typical plot of threshold J_{th} vs. τ. In Theorem 3.1, we assumed that the reference input signal was a step. However, other reference input signals may be used such as a ramp input signal, as done in the examples below.

Example 3.1: Consider the following scalar example, where

$$P_o(s) = \frac{a}{s+a}, \tag{3.48}$$

with proportional plus integral control

$$G_c(s) = 1 + \frac{a}{s} \tag{3.49}$$

and filter dynamics,

$$F(s) = \frac{k}{s+a} \tag{3.50}$$

then from (2.27),

$$G(s) = \frac{a}{s}, \; S(s) = \frac{s}{s+a}, \; T(s) = \frac{a}{s+a} \tag{3.51}$$

$$L(s) = \frac{s+a}{s+a+k}, \; M(s) = \frac{k}{s+a+k} \tag{3.52}$$

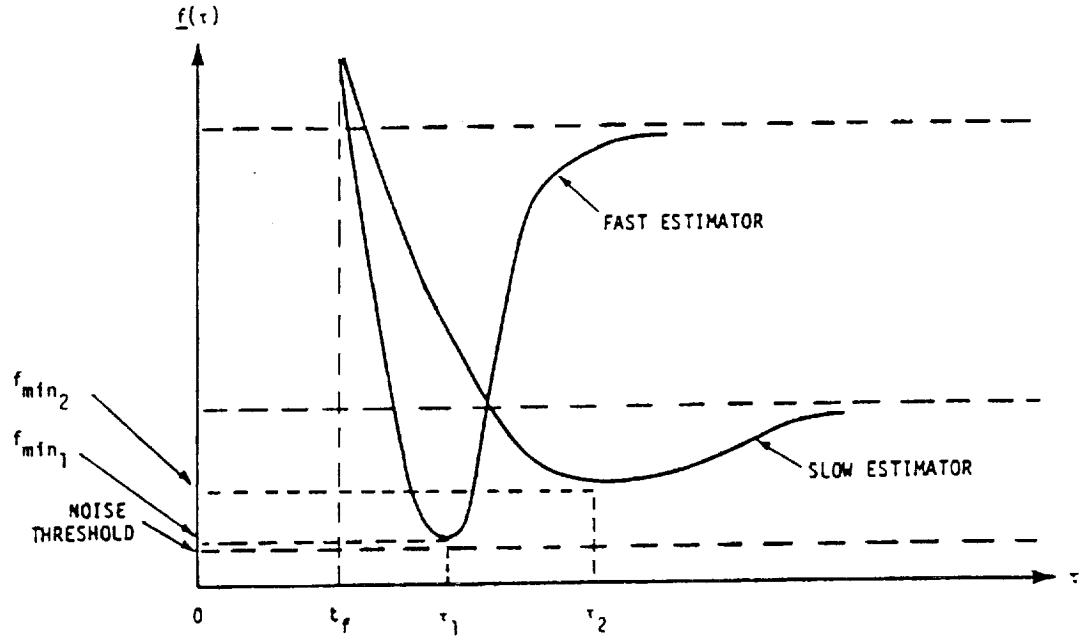

$\underline{f}(\tau)$: smallest size of detectable failure

t_f: time failure occurs

τ: length of detection window

Figure 3.1 Threshold Selector: Minimum Detectable Bias Shift (f) vs. Detection Window (τ)

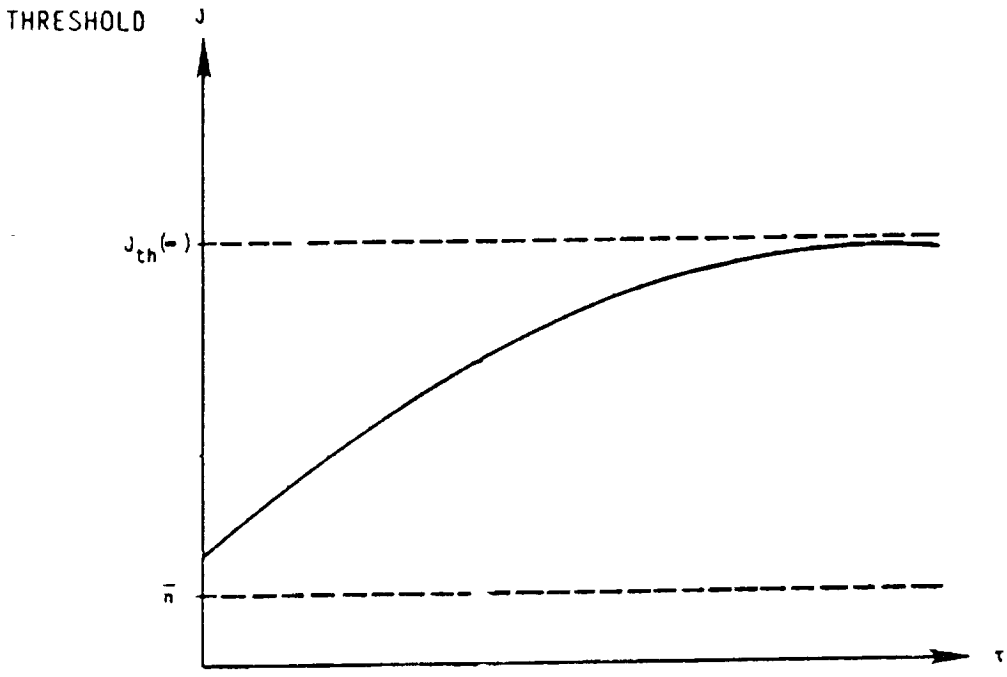

J: Threshold

J_{th}: Threshold for large detection window

$\bar{n}$: RMS noise

τ: length of moving detection window

Figure 3.2 Threshold vs. Detection Window

and

$$L(s)T(s) = \frac{a}{s+a+k} \tag{3.53}$$

Now

$$\Gamma_1\ LT(t) = \mathscr{L}^{-1}\left[\frac{a}{s(s+a+k)}\right]$$

$$= \frac{a}{a+k}\left(1 - e^{-(a+k)t}\right) \tag{3.54}$$

and

$$\Gamma_1\ L(t) = \mathscr{L}^{-1}\left[\frac{s+a}{s(s+a+k)}\right]$$

$$= \frac{a}{a+k} + \frac{k}{a+k}\, e^{-(a+k)t} \tag{3.55}$$

Therefore,

$$Q_{\tau 1}\ LT(\tau) = \left(\frac{1}{\tau}\int_0^{\tau}\left[\frac{a}{a+k}(1 - e^{-(a+k)t})\right]^2 dt\right)^{1/2} \tag{3.56}$$

$$Q_{\tau 1}\ L(\tau - t_f) = \left(\frac{1}{\tau}\int_0^{\tau-t_f}\left[\frac{a}{a+k} + \frac{K}{a+k}\, e^{-(a+k)t}\right]^2 dt\right)^{1/2} \tag{3.57}$$

and after the integrations have been performed, we obtain

$$Q_{\tau 1}\ LT(\tau) = \left[\frac{a^2}{2(a+k)^3\tau}\ [2(a+k)\tau - 3 - e^{-2(a+k)\tau} + 4e^{-(a+k)\tau}]\right]^{1/2} \tag{3.58}$$

$$Q_{\tau 1} L(\tau - t_f) = \left\{\frac{1}{2\tau(a+k)^3}\ [2a^2(a+k)(\tau-t_f) - k^2 e^{-2(a+k)(\tau-t_f)} - 4ake^{-(a+k)(\tau-t_f)} + k^2 + 4ak]\right\}^{1/2} \tag{3.59}$$

Since the singular value of a scalar quantity is simply its absolute value, then

$$\bar{\sigma}[(Q_{\tau 1}LT)(\tau)] = |(Q_{\tau 1}\ LT)(\tau)| \tag{3.60}$$

and

$$\underline{\sigma}[(Q_{\tau 1}\ L)\ (\tau - t_f)] = |(Q_{\tau 1}\ L)(\tau - t_f)| \tag{3.61}$$

Also we have that

$$\bar{\sigma}(L(j\omega)) = \sqrt{\frac{a^2 + \omega^2}{(a+k)^2 + \omega^2}} \tag{3.62}$$

and

$$\max_{\omega} \bar{\sigma}[L(j\omega)] = 1 \qquad \text{since} \quad a > 0 \text{ and } k > 0 \tag{3.63}$$

Finally, we obtain for the threshold

$$J_{th}(\tau) = \bar{n} + \delta|r|\ |(Q_{\tau 1}\ LT)(\tau)| \tag{3.64}$$

or

$$J_{th}(\tau) = \bar{n} + \delta|r| \cdot \left| \left[\frac{a^2}{2(a+k)^3 \tau} [2(a+k)\tau - 3 - e^{-2(a+k)\tau} + 4e^{-(a+k)\tau}] \right]^{1/2} \right| \tag{3.65}$$

and

$$\beta(\tau) = |(Q_{\tau 1}L)(\tau)| \tag{3.66}$$

or

$$\beta(\tau) = \left| \left\{ \frac{1}{2\tau(a+k)^3} \left[2a^2(a+k)(\tau-t_f) - K^2 e^{-2(a+k)(\tau-t_f)} \right. \right. \right.$$

$$\left. \left. \left. - 4aKe^{-(a+k)(\tau-t_f)} + K^2 + 4aK \right] \right\}^{1/2} \right| \qquad (3.67)$$

The closed-form solution of threshold as a function of the detection window is given by

$$f(\tau) = \frac{2\, J_{th}(\tau)}{\beta(\tau)} \qquad (3.68)$$

In the limit as $\tau \to \infty$

$$J_{th}(\infty) \to \bar{n} + \delta|r| \left| \frac{a}{(a+k)} \right| = \text{constant.} \qquad (3.69)$$

$$\beta(\infty) \to \left| \frac{a}{(a+k)} \right| \qquad (3.70)$$

and

$$f(\infty) \to 2\left[n \left| \frac{(a+k)}{a} \right| + \delta|r|\right] = \text{constant.} \qquad (3.71)$$

For the case of soft failures, one can derive similar closed-form expressions. For example, soft failures with a ramp reference input r

$$J_{th}(\tau) = \bar{n} + \delta|r| \left\{ \frac{1}{\tau} \left[-\frac{a^2}{2(a+k)^5} e^{-2(a+k)\tau} + \frac{a^2}{(a+k)^2}\frac{\tau^3}{3} + \frac{a^2}{(a+k)^4}\tau \right. \right.$$

$$+ \frac{2a^2}{(a+k)^5} e^{-(a+k)\tau} - \frac{a^2\tau^2}{(a+k)^3} - \frac{2a^2}{(a+k)^5}((a+k)\tau+1)\, e^{-(a+k)\tau}$$

$$\left. \left. + \frac{a^2}{2(a+k)^5} \right] \right\}^{1/2} \qquad (3.72)$$

$$\beta(\tau) = \left\{ \frac{1}{\tau} \left[\frac{a^2}{(a+k)^2} \frac{(\tau-t_f)}{3} - \frac{K^2}{2(a+k)^5} e^{-2(a+k)(\tau-t_f)} \right. \right.$$

$$+ \frac{K^2}{(a+k)^4} (\tau-t_f) + \frac{aK}{(a+k)^3} (\tau-t_f)^2 + \frac{2K^2}{(a+k)^5} e^{-(a+k)(\tau-t_f)}$$

$$+ \frac{2aK}{(a+k)^5} e^{-(a+k)(\tau-t_f)} ((a+k)(\tau-t_f) + 1)$$

$$\left. \left. - \frac{3K^2}{(2(a+k)^5} - \frac{2aK}{(a+k)^5} \right] \right\}^{1/2} \qquad (3.73)$$

Figure 3.3 shows the results for the hard failure with two different estimator speeds. The parameters being used are a=1, t_f=.001, $\bar{\varepsilon}$=.01, δ=.05, γ=1, K=2 (slow estimator), and K=10 (fast estimator). This shows that the threshold selector is also useful in evaluating the filter dynamics. If the dynamics of the filter are fast, there is a sharper minimum in f and generally lower thresholds than when the filter is slow.

The results for soft failures with the same parameters are shown in Figure 3.4. Note that the behavior is quite different from before. For hard failures, there is a single sharp minimum in f which corresponds to a very small detection window. For soft failures, f has a hyperbolic type behavior. There is not a unique minimum, and a larger detection window compared to the hard failure case needs to be selected. These results are quite reasonable as they agree with intuition.

3.1.3 A Computer-Aided Design Approach for Computing Optimal Thresholds

It was anticipated that a closed-form solution for the multivariable case was not possible hence a computer-aided design (CAD) approach was also developed for the threshold selector analysis. The basic operations involved in the computation of the thresholds are calculations of frequency response characteristics of L and transient response matrices of L and LT dynamic systems. Note that the expression for L is

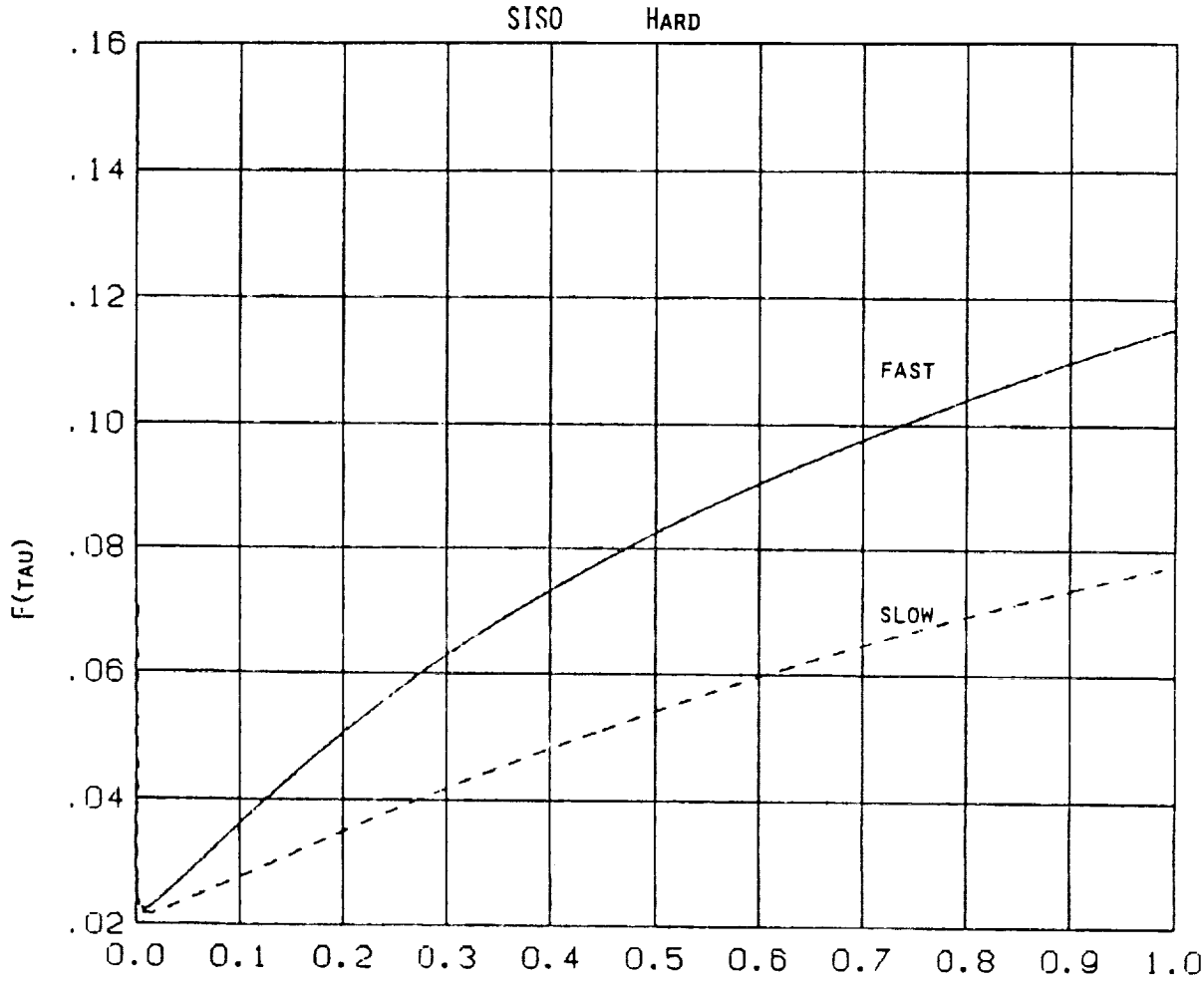

Figure 3.3a Minimum Detectable Failure vs. Detection Window (τ)

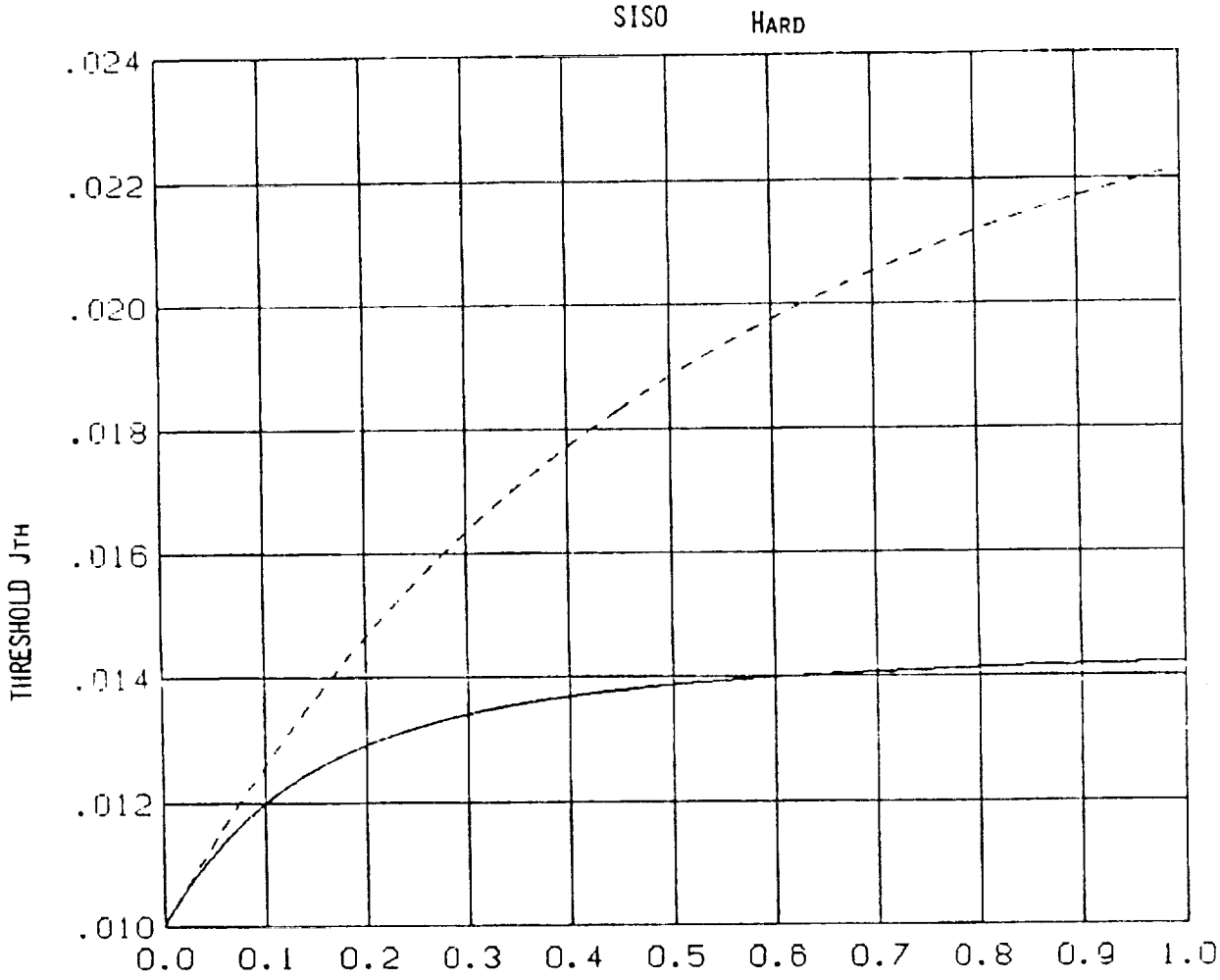

Figure 3.3b Minimum Detectable Failure vs. Detection Window (τ)

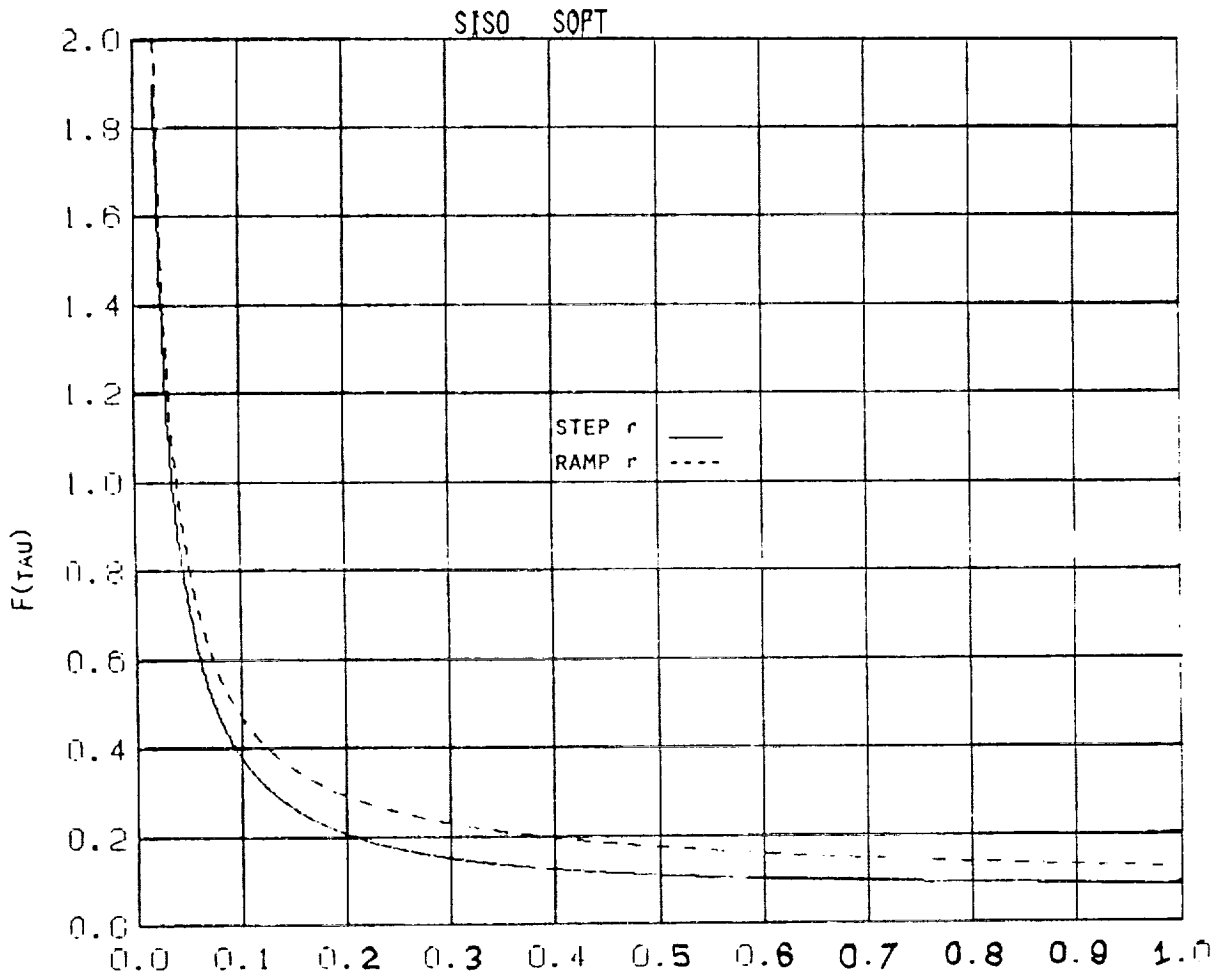

Figure 3.4a Minimum Detectable Failure vs. Detection Window (τ)

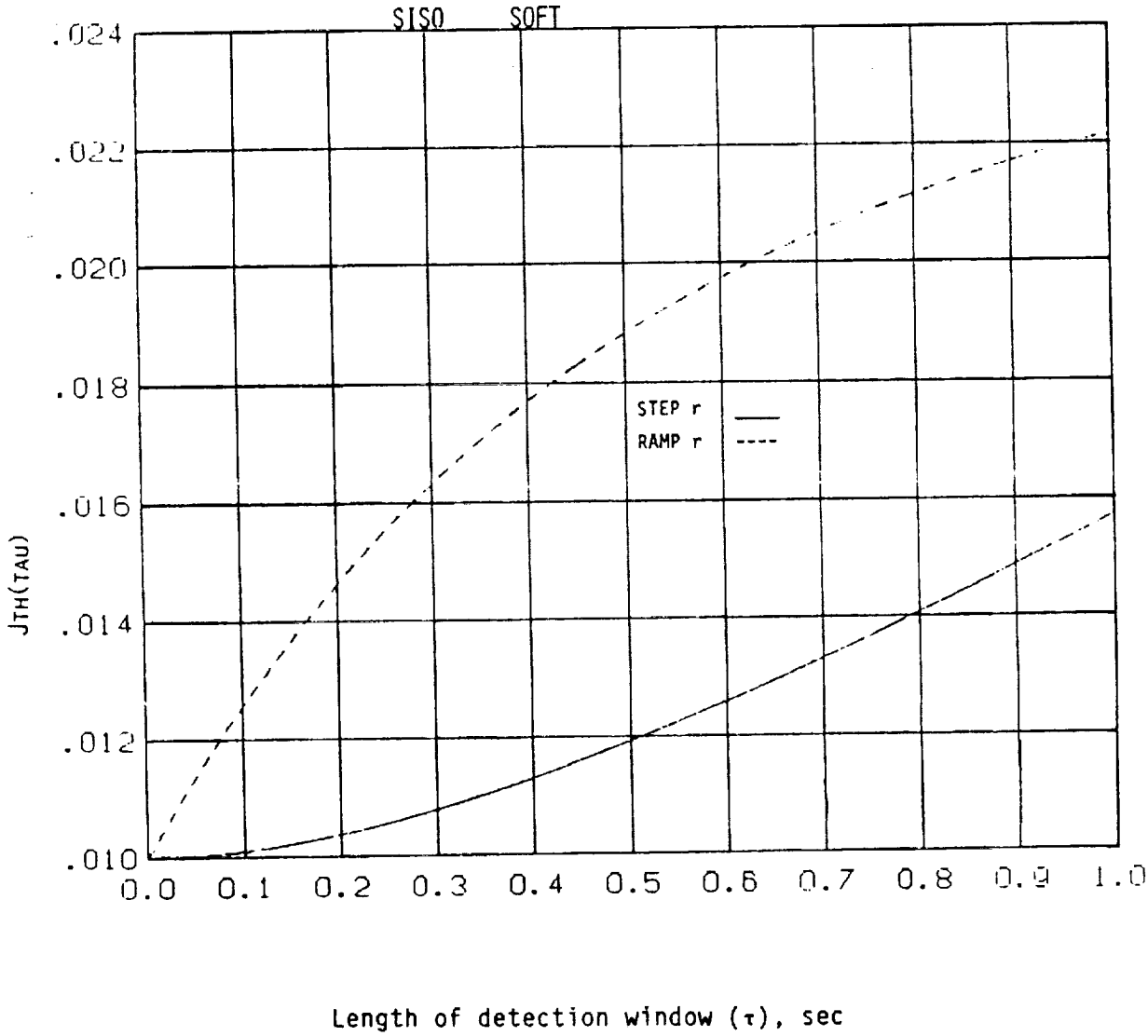

Figure 3.4b Minimum Detectable Failure vs. Detection Window (τ)

$$L(s) = (I + F(s))^{-1}$$

which is simply the inverse return difference matrix of the filter. To compute the transient response of systems with transfer functions $L(s)$ and $L(s)T(s)$, a (minimal) state-space realization of these systems is required. In the single-input/single-output (SISO) case, a minimal state-space realization for $L(s)$ denoted by $(A_{r\ell}, B_{r\ell}, C_{r\ell}, D_{r\ell})$ can be written down by inspection. Similarly, LT is a dynamic system whose transfer function involves products of certain inverse return matrices, etc. as shown in Figure 3.5. To obtain a minimal realization (A_r, B_r, C_r, D_r) for this system, the block diagram manipulation facility of CTRL-C [21] called INTERC was used. To use this tool, the different blocks in the system block diagram are numbered as shown in Figure 3.5. The various interconnections are then specified. The procedure yields a non-minimal realization for the system of order $n_s = 5$ in this case. The procedure MINREAL* is then utilized to obtain a minimal realization for the system which is of order $n_s = 1$ and agrees with hand calculations. Suppose $h(t)$ is the impulse response of $L(s)T(s)$ system corresponding to the state-space realization (A_r, B_r, C_r, D_r) and $h_1(t)$ is the impulse response of $L(s)$ system corresponding to the state-space realization $(A_{r\ell}, B_{r\ell}, C_{r\ell}, D_{r\ell})$. Then the threshold is given by

$$f = \frac{2(\bar{n} + \delta|r|\, Q_{\tau 1}(LT))}{Q_{\tau 1}(L(\tau - t_f))} \tag{3.74}$$

$$f = \frac{\bar{2}(n + \delta|r|(\frac{1}{\tau}\int_0^{\tau}[\int_0^{t} h(t_1)dt_1]'[\int_0^{t} h(t_2)dt_2]dt)^{1/2})}{(\frac{1}{\tau}\int_0^{\tau-t_f}[\int_0^{t} h_1(t_3)dt_3]'[\int_0^{t} h_1(t_4)dt_4]dt)^{1/2}} \tag{3.75}$$

*MINREAL uses the staircase algorithm to remove uncontrollable and/or unobservable modes.

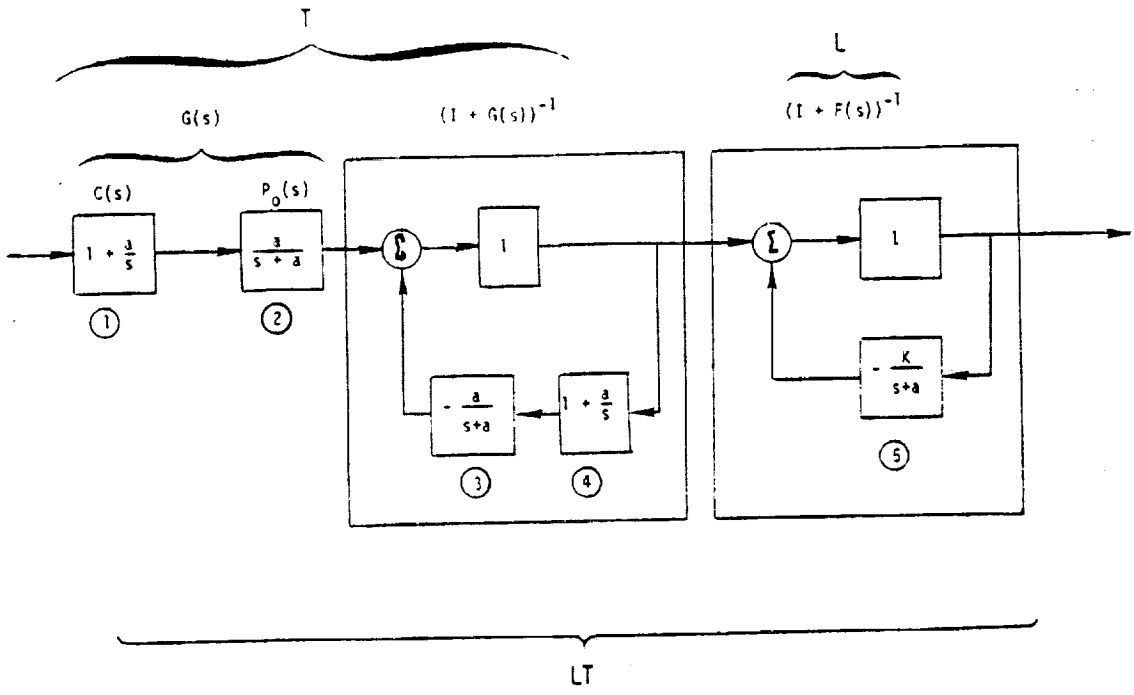

Figure 3.5 Block Diagram for SISO Case: CAD Method

where

$$\int_0^t h(\cdot)d(\cdot) = \text{step response of } (A_r, B_r, C_r, D_r) \tag{3.76}$$

and

$$\int_0^t h_1(\cdot)d(\cdot) = \text{step response of } (A_{r\ell}, B_{r\ell}, C_{r\ell}, D_{r\ell}) \tag{3.77}$$

A procedure was then written in CTRL-C to calculate the threshold curve for Example 3.1. Figure 3.6 shows the plots of the thresholds generated by CTRL-C both for the closed form and the CAD technique using the same values of parameters. The integration step for the CAD plot is .001 sec. The slight discrepancy in the two curves would disappear if smaller integration steps are used. Figure 3.7 shows the plots of threshold selector for a slow (a=1,k=1) and a fast (a=1,k=10) estimator.

Example 3.2: Multivariable Control of a Turbofan Engine

To illustrate the idea of threshold selector in the multivariable case, a model of a turbofan engine and its multivariable control at sea level static conditions with a power lever angle (PLA) of 36° was chosen [12].

The states of the system are

X_1 = Fan Speed, SNFAN (N_1) - rpm

X_2 = Compressor Speed, SNCOM (N_2) - rpm

X_3 = Burner Exit Slow Response Temperature, T_{t41o} - °R

X_4 = Fan Turbine Inlet Slow Response Temperature, $T_{t4.51o}$ - °R

The engine controls are:

U_1 = Main Burner Fuel Flow, WFMB - lb/hr

U_2 = Nozzle Jet Area, Aj - ft^2

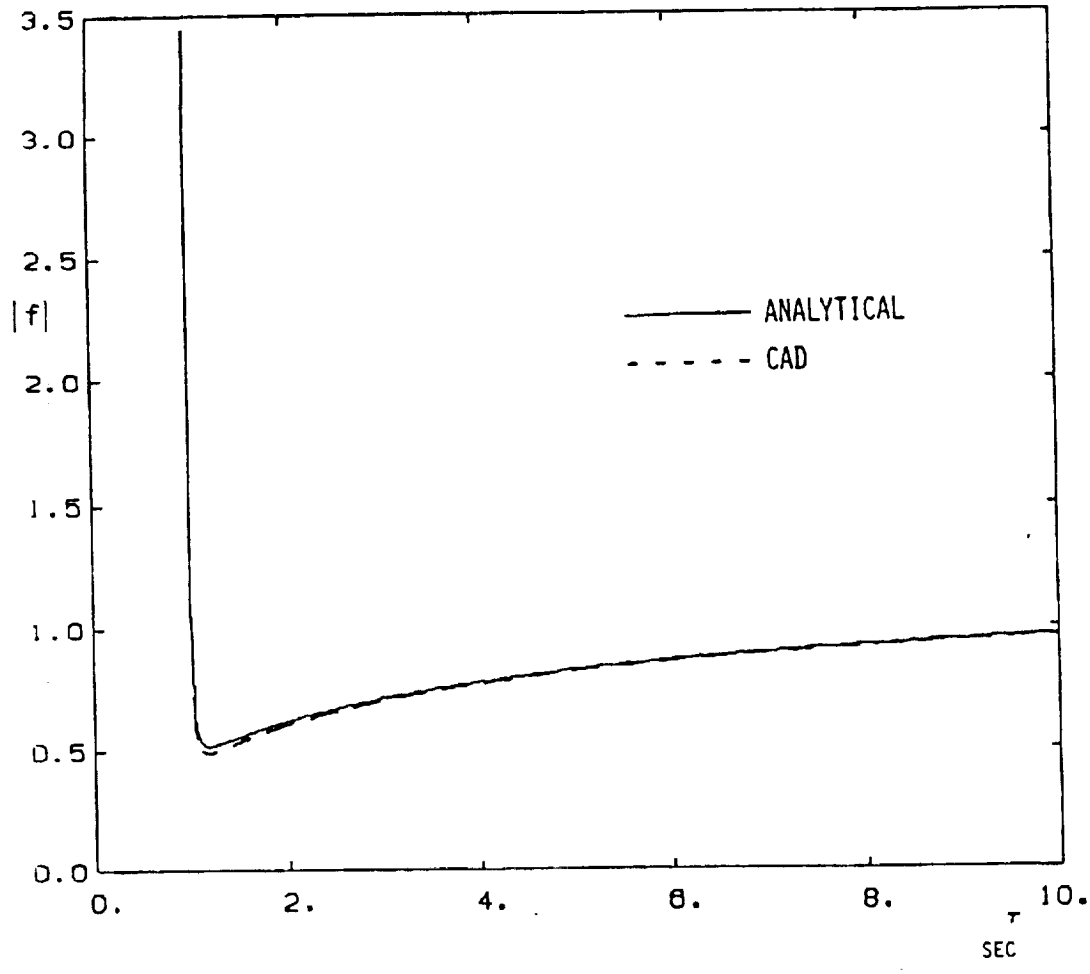

Figure 3.6 Threshold Selector for Example 3.1

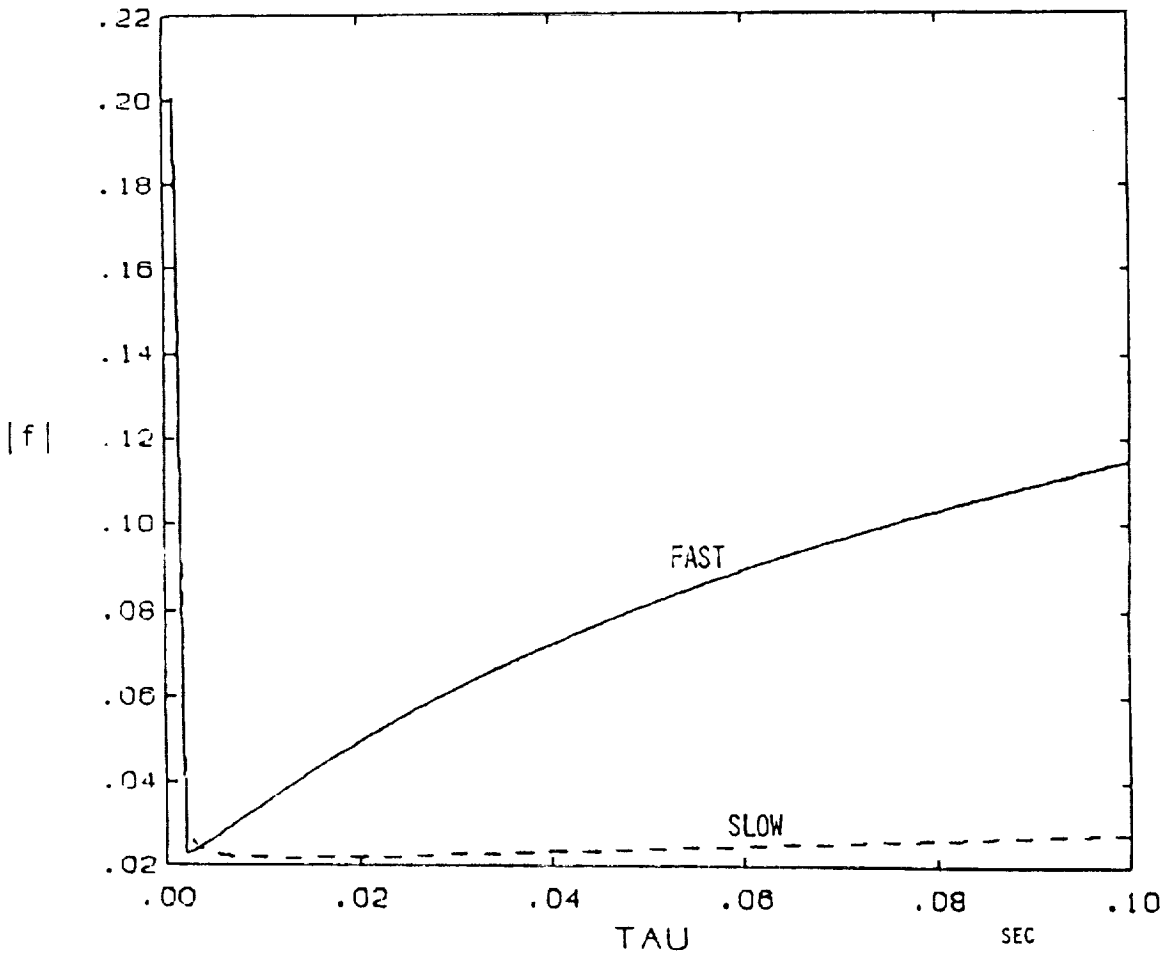

Figure 3.7 Threshold Selector for Example 3.1

U_3 = Fan Guide Vane Angle, FGV - deg

U_4 = Compressor Stator Vane Angle, SVA - deg

U_5 = Compressor Bleed Flow, BLC - %

and the engine outputs are

Y_1 = Fan Speed, SNFAN (N_1) - rpm

Y_2 = Compressor Speed, SNCOM (N_2) - rpm

Y_3 = Burner Pressure, PT4 - psia

Y_4 = Augmentor Pressure, PT6 - psia

Y_5 = Fan Turbine Inlet Temperature, FTIT - °R

The normalized system matrices for the example are shown in Table 3.1. The open loop poles are at -3.1616, -2.8807, -.7036 and -1.0865. There are two transmission zeros at -1.7294 and -.6456 and were computed using the algorithm in Ref. 22. It is interesting that one of the transmission zeros of the system is at -.6456 which indicates why it is not possible to move the slow temperature pole at -.7036 very far. The multivariable control law is proportional plus integral [6,7]

$$G_c(s) = C_p + \frac{1}{s} C_I \tag{3.78}$$

where the (normalized) proportional gain matrix (Cp) and the integral gain matrix (CI) are as shown in Table 3.2. The (normalized) filter gain matrix (K) is as shown in Table 3.2 and corresponds to filter poles at

-11.2034, -8.0777, -2.0051, -.6817

The transfer function matrices of interest are given by

Nominal Plant: $$P_o(s) = C(sI-A)^{-1} B + D \tag{3.79}$$

Controller: $$G_c(s) = C_p + \frac{1}{s} C_I \tag{3.80}$$

Table 3.1

System Matrices for the Example

A =

-3.9180D+00	4.1886D+00	-4.1148D-02	1.2279D-01
-1.8061D-01	-2.1480D+00	1.5853D-01	6.6994D-04
-1.3190D-01	-2.4056D-01	-6.6630D-01	2.3770D-04
-3.8191D-01	-1.0501D+00	-6.7400D-02	-2.0000D+00

B =

5.1991D-01	1.1942D+00	2.1974D-01	-2.4990D-02	-1.7226D-02
3.6266D-01	1.0836D-01	7.2562D-03	-1.2133D-02	-7.2114D-03
2.8427D-01	3.3231D-02	5.7770D-03	5.7672D-03	1.6319D-03
9.3743D-01	7.3072D-02	1.7417D-02	2.0418D-02	1.0634D-01

C =

2.2043D+01	0.0000D+00	0.0000D+00	0.0000D+00
0.0000D+00	2.7339D+01	0.0000D+00	0.0000D+00
3.7700D+00	1.0341D+01	-7.6298D-03	-4.3237D-03
8.0543D+00	3.1436D-01	-6.6634D-02	-3.7135D-02
-2.9070D+00	-7.9884D+00	-5.1265D-01	2.6855D-03

D =

0.0000D+00	0.0000D+00	0.0000D+00	0.0000D+00	0.0000D+00
0.0000D+00	0.0000D+00	0.0000D+00	0.0000D+00	0.0000D+00
1.0036D+00	-8.2350D-01	-1.5200D-01	-5.6233D-02	-5.8600D-02
9.7674D-01	-5.7450D+00	-3.8500D-01	9.5762D-03	-2.2963D-02
7.1316D+00	5.5560D-01	1.3247D-01	1.5533D-01	4.8290D-02

Table 3.2

Proportional Gain Matrix (Cp), Integral Gain Matrix (CI), Filter Gain Matrix (K)

K =

2.3692D-01	1.9395D-01	1.0177D-02	3.7510D-04	-1.6788D-02
6.8145D-02	2.8495D-01	5.1618D-03	3.6090D-05	-9.9733D-03
2.3950D-02	3.5780D-02	2.3172D-04	2.1026D-05	5.0178D-04
2.0241D-02	6.0917D-02	-5.0971D-04	-4.4286D-06	1.9605D-03

Cp =

-4.6597D-02	-2.2423D-01	-5.3984D-01	-2.5951D-02	0.0000D+00
-2.2281D-02	-4.5208D-07	0.0000D+00	3.5198D-02	0.0000D+00
-8.5667D-02	0.0000D+00	0.0000D+00	4.1154D-02	0.0000D+00
9.4676D-02	-2.9942D-01	0.0000D+00	5.4087D-02	0.0000D+00
8.0500D-01	2.3320D+00	7.5286D+00	0.0000D+00	0.0000D+00

CI =

-1.0062D+00	0.0000D+00	0.0000D+00	-1.7247D-02	0.0000D+00
-2.3333D-01	0.0000D+00	0.0000D+00	2.9998D-02	0.0000D+00
0.0000D+00	0.0000D+00	0.0000D+00	0.0000D+00	0.0000D+00
0.0000D+00	0.0000D+00	0.0000D+00	0.0000D+00	0.0000D+00
0.0000D+00	0.0000D+00	0.0000D+00	0.0000D+00	0.0000D+00

Filter: $$F(s) = C(sI-A)^{-1}K \tag{3.81}$$

From (2.26)

$$G(s) = P_o(s)\, G_c(s)$$

$$= [C(sI-A)^{-1}B + D][C_p + \frac{1}{s} C_I] \tag{3.82}$$

$$S(s) = [I + G(s)] \tag{3.83}$$

$$T(s) = [I + G(s)]^{-1}\, G(s) \tag{3.84}$$

$$L(s) = [I + C(sI-A)^{-1}K]^{-1} \tag{3.85}$$

$$M(s) = [I + C(sI-A)^{-1}K]^{-1}\, F(s) \tag{3.86}$$

and

$$\max_{\omega} \bar{\sigma}[L(j\omega)] = 11.9122 \tag{3.87}$$

Again it is relatively simple to obtain a minimal realization of $L(s)$. The state-space matrices are denoted by $(A_{r\ell}, B_{r\ell}, C_{r\ell}, D_{r\ell})$ and are as in Table 3.3. The poles are at

$$-11.2034,\ -8.077,\ -2.0051,\ -.6817$$

and the transmission zeros are at

$$-3.1616,\ -.7036,\ -2.8807,\ -1.9865$$

The block diagram of $L(s)T(s)$ is as shown in Figure 3.8. INTERC was used to obtain a non-minimal realization of the system. Note that for the purposes of defining the output to CTRL-C, it is necessary to introduce a fictitious block (6) in the diagram. The order of the non-minimal realization is $n_s = 27$. MINREAL was used to yield a minimal realization of order $n_s = 10$*. The final results for (A_r, B_r, C_r, D_r) are displayed in Table 3.4.

Table 3.3

Associated State-Space Matrices ($A_{r\ell}$, $B_{r\ell}$, $C_{r\ell}$, $D_{r\ell}$)

ARL =

-2.0003D+00	5.9409D-02	8.2386D-01	2.7009D+00
-7.2277D-03	-6.6573D-01	-6.5511D-01	-1.2030D+00
-1.2263D-01	-5.0294D-02	-9.2306D+00	-1.3534D+00
-1.5242D-03	1.5345D-01	-1.7314D+00	-1.0071D+01

BRL =

-2.0366D-02	-6.1104D-02	5.0848D-04	4.3184D-06	-1.9631D-03
2.3844D-02	3.5460D-02	2.3439D-04	2.1049D-05	4.9150D-04
2.3692D-01	1.9395D-01	1.0177D-02	3.7510D-04	-1.6788D-02
6.8145D-02	2.8495D-01	5.1618D-03	3.6090D-05	-9.9733D-03

CRL =

0.0000D+00	1.3878D-16	2.2043D+01	6.6613D-16
2.2204D-16	3.3307D-16	2.2204D-16	2.7339D+01
4.3636D-03	-7.6070D-03	3.7700D+00	1.0341D+01
3.7484D-02	-6.6438D-02	8.0543D+00	3.1436D-01
-8.3267D-17	-5.1265D-01	-2.9070D+00	-7.9884D+00

DRL =

-1.	0.	0.	0.	0.
0.	-1.	0.	0.	0.
0.	0.	-1.	0.	0.
0.	0.	0.	-1.	0.
0.	0.	0.	0.	-1.

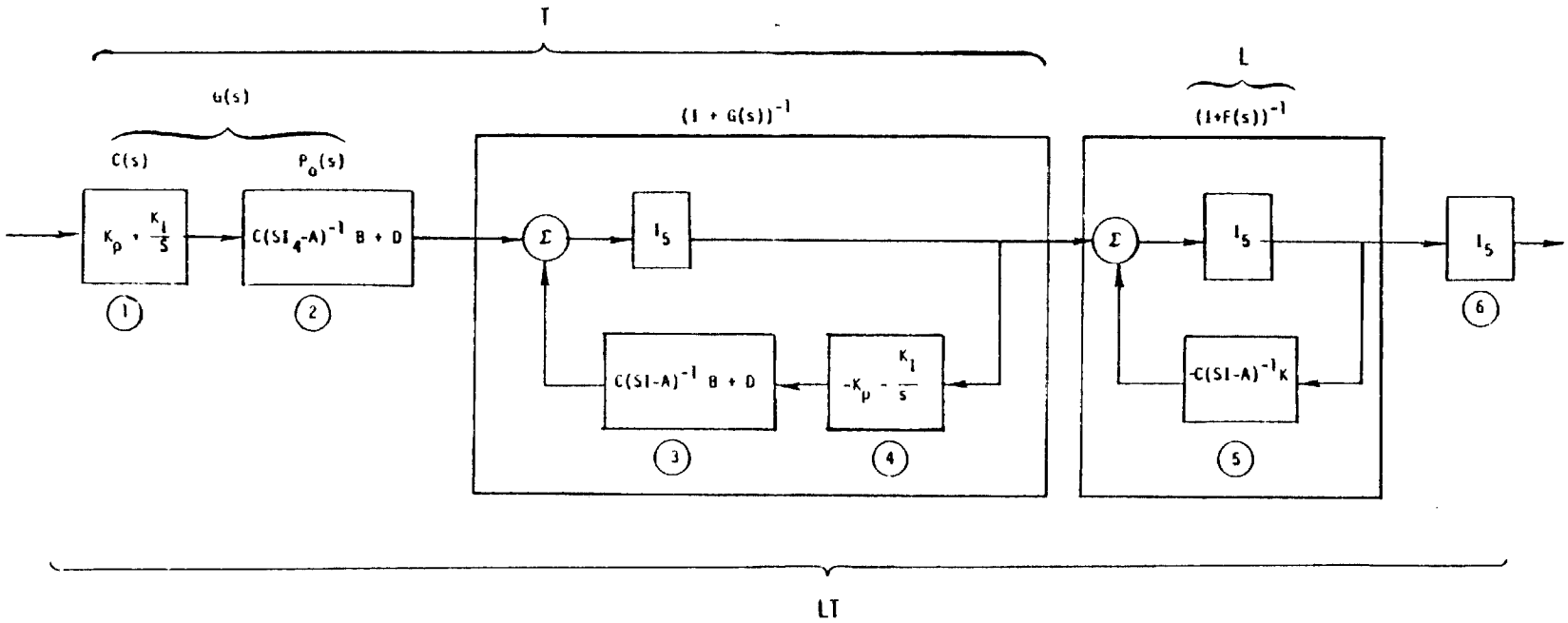

Figure 3.8 Block Diagram for MIMO Case: CAD Method

The poles of A_r are

$$\begin{array}{r} -11.2034 + 0.0000i \\ -8.0777 + 0.0000i \\ -4.7046 - 0.0000i \\ -2.6196 + 1.8997i \\ 2.7863 + 0.0000i \\ -2.0051 + 0.0000i \\ -0.7347 + 0.0000i \\ -0.6817 + 0.0000i \\ -0.1034 + 0.0000i \end{array}$$

and the transmission zeros are

$$-1.9865,\ -.7036,\ -3.1616,\ -2.8807$$

which are as expected.

The $(Q_{\tau 1})LT$ is then of the form

$$(Q_{\tau 1})LT(\tau) = \left(\frac{1}{\tau} \int_0^{\tau} [\int_0^t h(t_1)dt_1]^T [\int_0^t h(t_2)dt_2]dt \right)^{1/2} \qquad (3.88)$$

where $h(\cdot)$ is the impulse response matrix of the (A_r, B_r, C_r, D_r) system and its (i,j)-th element is the response of the i-th component of the output to an impulse applied at the j-th component of the input while all other components of the input are zero and the initial state is zero. Note that an expression such as:

$$\int_0^t h(t_1)\, dt_1 = \text{step response matrix} \qquad (3.89)$$

---

* This is a numerically delicate problem. The tolerance for MINREAL should be chosen to be $100 \left\| \begin{matrix} A & B \\ C & D \end{matrix} \right\|_2 \varepsilon$ where ε is the machine precision.

Table 3.4

Final Results for (A_r, B_r, C_r, D_r)

AR =

Starting at row 1 columns 1 thru 6

-1.8833D+00	2.2461D-02	4.1244D-01	-9.7421D-02	8.6466D-02	6.8098D-04
3.0702D-02	-1.9773D+00	5.3534D-02	-1.2298D-01	-1.4802D-01	4.3156D-02
3.0137D-01	1.1797D-02	-7.7122D-01	2.5823D-02	8.9131D-01	1.5985D-01
-1.6443D-01	-2.1904D-01	7.2472D-02	-6.8127D-01	1.8765D+00	3.0526D-01
-1.3275D-01	8.5894D-03	-5.1391D-02	3.4825D-04	4.0643D-01	-6.3688D-01
-3.1541D-02	-1.1947D-02	-3.1920D-02	-2.5310D-02	2.0529D+00	4.4477D-02
0.0000D+00	1.2095D-01	-1.6299D-02	-4.6428D-02	3.1668D-01	7.7116D-01
0.0000D+00	0.0000D+00	1.4931D-01	1.8504D-02	1.4743D+00	1.9028D-01
0.0000D+00	0.0000D+00	0.0000D+00	1.5650D-01	-7.9998D-01	1.4590D-01
0.0000D+00	0.0000D+00	0.0000D+00	0.0000D+00	1.1380D+01	2.1815D+00

Starting at row 1 columns 7 thru 10

4.7572D-01	1.7422D+00	2.1100D+00	4.8148D-01
6.1265D-01	-1.5215D+00	-9.1115D-01	1.1621D+00
-2.1959D+00	-1.3057D+00	-2.2261D+00	-5.5108D-01
-2.7577D+00	6.3804D-01	-2.9244D+00	-7.6130D-01
-1.1208D+01	1.9845D+00	-6.1734D+00	-1.0806D+00
-4.9271D+00	1.3970D+00	-1.6149D+00	-1.3658D+00
-9.4908D+00	4.9505D-02	-6.5492D+00	-3.6488D-01
-4.2548D+00	-8.4370D+00	-1.4728D+01	-6.2005D-01
6.6487D-01	-6.2387D-01	-6.3950D+00	1.2374D-01
-1.2398D+01	3.6584D+00	-1.6509D-01	-6.3510D+00

BR =

1.2913D-02	-3.5065D-03	6.7581D-02	-9.3985D-03	0.0000D+00
3.5216D-02	-3.5419D-03	9.7594D-02	-1.3254D-02	0.0000D+00
-6.2897D-02	5.7229D-03	-9.2170D-03	1.8487D-03	0.0000D+00
-1.1748D-01	-2.7295D-02	-2.5362D-02	-5.6664D-03	0.0000D+00
-2.6848D-01	1.7852D-02	5.2850D-02	-2.0758D-02	0.0000D+00
-1.8192D-01	-1.4634D-03	-1.2483D-03	1.4683D-02	0.0000D+00
-5.3986D-02	-4.5738D-02	-1.1493D-01	2.1870D-02	0.0000D+00
-1.3163D-01	-5.5903D-04	6.5713D-03	-4.2030D-03	0.0000D+00
5.2728D-02	-5.1607D-02	-1.2889D-01	8.8618D-03	0.0000D+00
-6.2446D-01	-7.4094D-03	-2.7436D-02	1.8488D-04	0.0000D+00

Table 3.4 (Continued)

CR =

Starting at row 1 columns 1 thru 6

1.9429D-16	-3.8858D-16	-1.1796D-16	-3.6082D-16	4.4409D-16	2.2204D-16
-5.0220D-16	-3.4001D-16	-1.9663D-15	-1.3704D-16	-9.0206D-16	-6.9389D-18
-6.8955D-17	-9.3675D-17	-2.6877D-16	-1.7781D-17	-5.8981D-17	1.0446D+00
1.4572D-16	-3.1919D-16	-2.2291D-16	-1.7347D-16	1.6653D-16	6.8199D+00
1.3878D-16	2.7756D-16	2.6472D-15	-4.7184D-16	6.1062D-16	-1.6653D-16

Starting at row 1 columns 7 thru 10

-3.7131D+01	-3.0531D-16	-8.8840D+00	0.0000D+00
9.5083D+00	-2.3928D+01	-3.9740D+01	1.5959D-16
-2.7291D+00	-1.0432D+01	-2.3954D+00	1.0780D+00
-1.5132D+01	-5.4949D-01	4.9940D+00	-2.7756D-17
-3.3307D-16	2.3384D-15	7.6032D+01	-6.9389D-17

DR =

0.0000D+00	0.0000D+00	0.0000D+00	0.0000D+00	0.0000D+00
0.0000D+00	0.0000D+00	0.0000D+00	0.0000D+00	0.0000D+00
3.7478D-02	1.6983D-01	4.8632D-01	2.6586D-02	0.0000D+00
-9.9875D-02	1.2594D-01	2.8937D-01	1.8044D-01	0.0000D+00
1.8695D-01	9.2186D-01	1.7470D+00	3.1605D-02	0.0000D+00

is a step response matrix, where the (i,j)-th element of it is the response at time t of the i-th component of the output when the j-th component of the input is a step function while all other components of the input are zero and the initial state is the zero state. In this case the step response matrix is a 5x5 matrix. Similar statements apply to $(Q_{\tau 1})L$ operator. We finally compute the multivariable threshold as

$$f(\tau) = \frac{2J_{th}(\tau)}{\beta(\tau)} \tag{3.90}$$

where

$$J_{th}(\tau) = (\max_{\omega} \bar{\sigma}[L(j\omega)])\bar{n} + \delta|r|\bar{\sigma}[(Q_{\tau 1}LT)(\tau)] \tag{3.91}$$

$$\beta(\tau) = \underline{\sigma}[(Q_{t1}L)(\tau - t_f)] \tag{3.92}$$

$$\|n\|_{\tau} < \bar{n} \tag{3.93}$$

$$\bar{\sigma}(\Delta(j\omega)) < \delta \tag{3.94}$$

The threshold selector results for the hard failure case are as shown in Figure 3.9. Note the similarity with the scalar case. The results for the soft failure case are as shown in Figure 3.10.

3.1.4 Summary

This chapter has discussed the effect of model error on detection. An innovative framework was developed to determine the effect of model error on sensor failure DIA algorithms analytically. A new concept called threshold selector was introduced. The threshold selector analysis allows determination of optimal threshold and size of smallest detectable failure as a function of model error bound, noise, variance, speed of the filter, class of reference

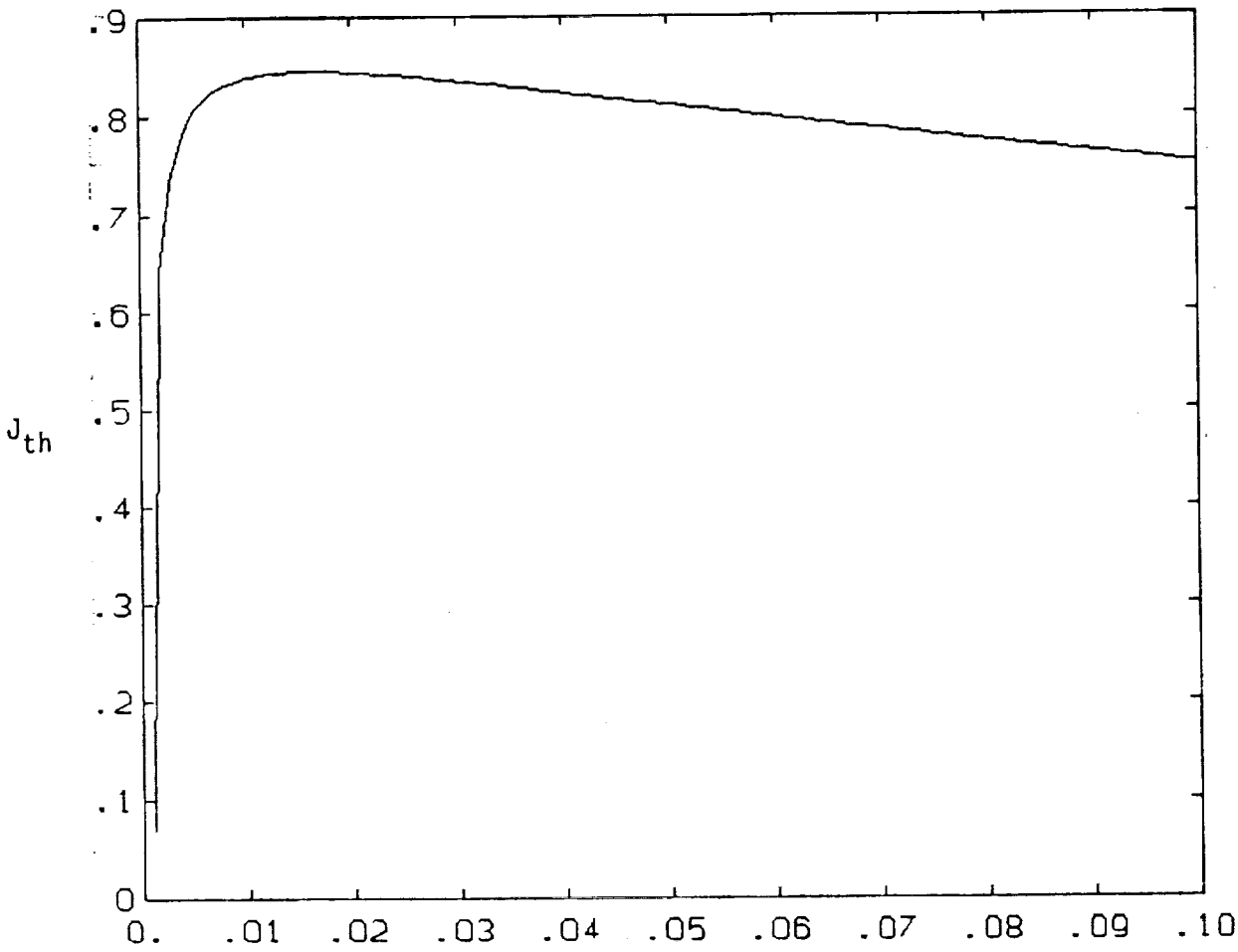

Figure 3.9a Threshold - Hard Failure Case, Example 3.2

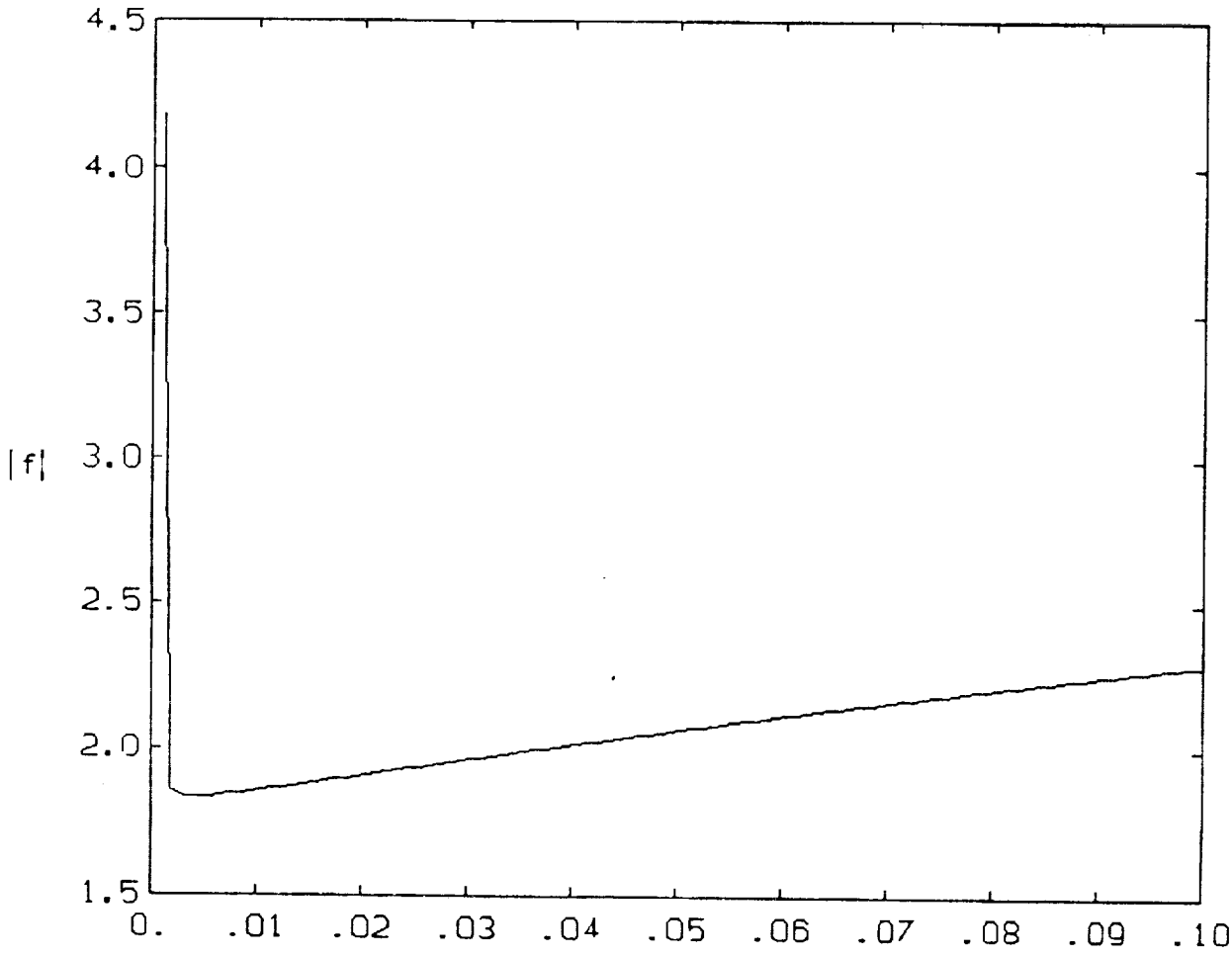

Figure 3.9b Minimum Detectable Failure - Hard Failure Case, Example 3.2

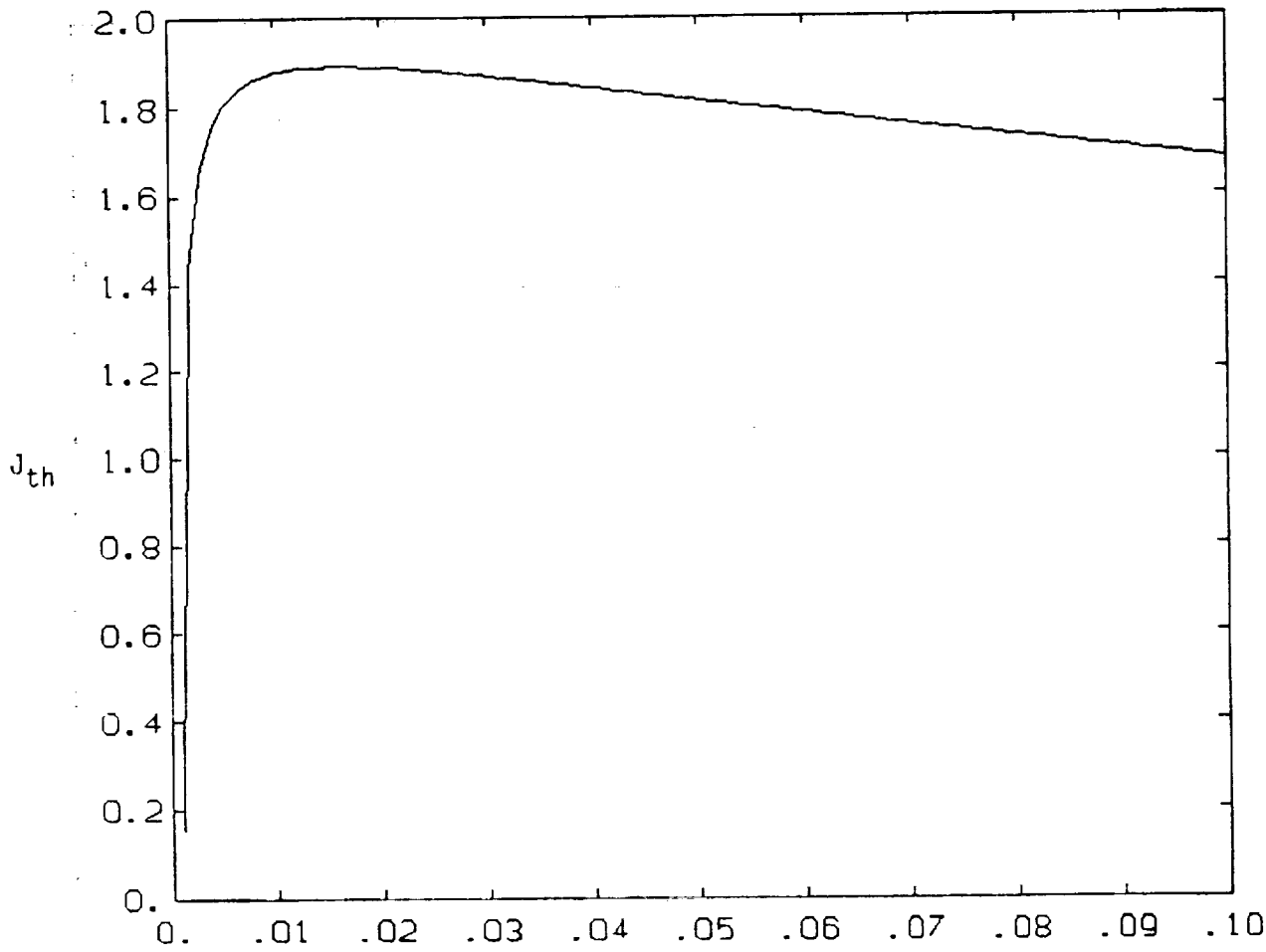

Figure 3.10a Threshold - Soft Failure Case, Example 3.2

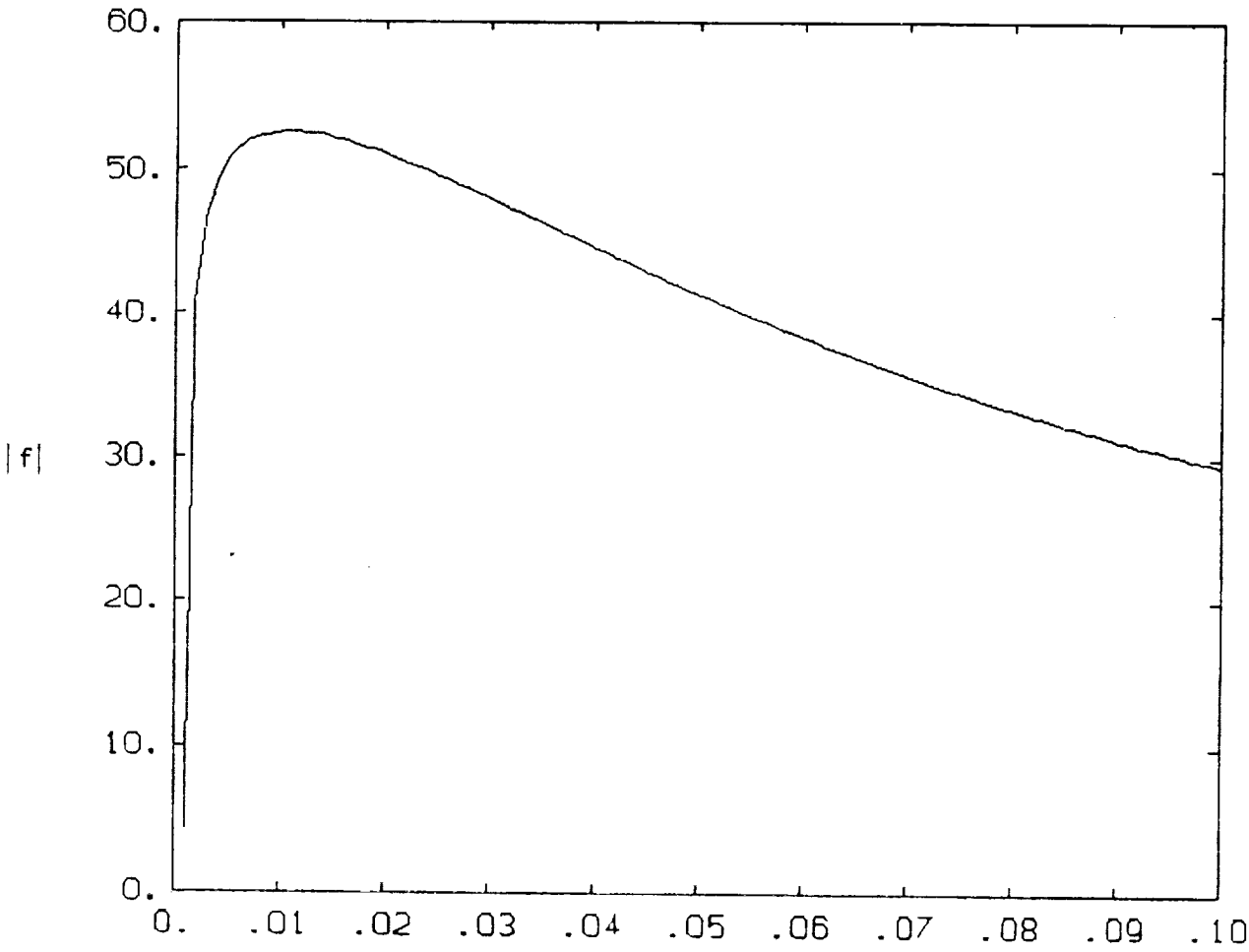

Figure 3.10b Size of Minimum Detectable Failure - Soft Failure Case, Example 3.2

input signal, and class of failure signal. The threshold selector constitutes a powerful design aid and allows one to arrive at a proper balance between robustness and DIA sensitivity. The analysis in this chapter can be extended to isolation and accommodation problems, as well as other DIA designs than those discussed here.

C-2

IV. ROBUST FILTER DESIGN FOR DIA

This chapter discusses the design of robust filters for use as part of a sensor failure DIA algorithm. The robustness of the filter is due to introduction of an internal model as well as frequency-shaping of the LQG cost functional. The necessity of the internal model was discussed in Chapter II (see Section 2.2.3). Recall that the presence of an internal model results in asymptotically unbiased filter estimates. The internal model also provides robustness with respect to parameter perturbations. However, since other sources of model uncertainty are present (see Chapters I and II), the filter may be made more robust by frequency shaping of the LQG cost functional. This is a result of taking the bound on model error into account. The concepts are applied to a multivariable turbofan engine example.

4.1 PROBLEM FORMULATION

A filter may be made robust by introduction of an internal model and by frequency shaping. The internal model provides robustness with respect to parameter perturbations and results in asymptotically unbiased estimates. The filter may be made more robust by adding dynamics to the filter to compensate for other types of modeling uncertainty. This can be done in a formal way by replacing the constant weighting matrices in a standard LQG cost functional with weighting matrices which are functions of frequency. This is referred to as frequency shaping. The weighting matrices are chosen to reflect model uncertainty. For example, if there is unmodeled high-frequency dynamics, the weighting matrices may be chosen to be constant over the frequency range where the system model is known accurately and increase as a function of frequency in the frequency range where the model is less accurate. This section discusses the design of robust filters for sensor failure DIA which employ both an internal model and frequency shaping.

4.1.1 Filter with Internal Model

The internal model principle and its application to robust filter design was discussed in Section 2.2.3. It was shown that the internal model is necessary to provide asymptotically unbiased estimates and robustness with respect to parameter perturbations. For a system with unknown constant measurement biases, an internal model (integrators) may be introduced by state augmentation:

$$\begin{bmatrix} \dot{\hat{x}} \\ \hline \dot{\hat{b}} \end{bmatrix} = \left[\begin{array}{c|c} A & 0 \\ \hline 0 & 0 \end{array}\right] \begin{bmatrix} \hat{x} \\ \hline \hat{b} \end{bmatrix} + \begin{bmatrix} B \\ \hline 0 \end{bmatrix} u + \begin{bmatrix} KP \\ \hline KI \end{bmatrix} (Z - \hat{Z}) \tag{4.1}$$

$$\hat{Z} = [C \quad I] \begin{bmatrix} \hat{x} \\ \hat{b} \end{bmatrix} + Du \tag{4.2}$$

where KP and KI are the proportional and integral estimator gains.

4.1.2 Filter Design with Frequency Shaping

Consider the system described by:

$$\text{state:} \qquad \dot{x} = Ax + Bu + B_1 w \tag{4.3}$$

$$\text{measurement:} \qquad z = Cx + Du + v \tag{4.4}$$

where w and v are independent, zero-mean, white Gaussian process and measurement noise processes. The standard Kalman filter for this system is of the form

$$\dot{\hat{x}} = A\hat{x} + Bu + K(z - Du - C\hat{x}) \tag{4.5}$$

where K is the Kalman filter gain. We desire to find a filter which minimizes the performance index,

$$\mathcal{J} = \frac{1}{2} \int_0^\infty \{(z - Cx)^T R^{-1}(z - Cx) + w^T Q^{-1} w\}\, dt$$

$$\mathcal{J} = \frac{1}{2}\int_0^\infty \{w^T Q^{-1} w + v^T R^{-1} v\}\, dt \tag{4.6}$$

In this cost function, Q and R are constant matrices independent of frequency. Using Parseval's theorem, the performance index in (4.4) can be transferred to the frequency domain

$$\mathcal{J} = \frac{1}{2\pi} \int_{-\infty}^{\infty} \{W^*(j\omega)\, Q^{-1} W(j\omega) + V^*(j\omega)\, R^{-1} V(j\omega)\}\, d\omega \tag{4.7}$$

Note that the two terms in the above integrand have the constant weighting at all frequencies. However, the model may be well known within a certain frequency range and not known accurately outside that frequency range. It would then seem desirable to have weighting matrices which are functions of frequency and be able to reduce the filter gain outside model bandwidth to reduce sensitivity and increase performance of the filter. It is possible to consider making Q and R functions of frequency

$$\mathcal{J} = \frac{1}{2\pi} \int_{-\infty}^{\infty} \{W^*(j\omega)\, Q^{-1}(\omega^2)\, W(j\omega) + V^*(j\omega)\, R^{-1}(\omega^2)\, V(j\omega)\}\, d\omega \tag{4.8}$$

A sufficient condition for the existence of a filter minimizing (4.8) is that $Q(j\omega)$ and $R(j\omega)$ be positive semi-definite matrices in ω^2.

The problem as posed in (4.8) can be converted to a standard LQG problem as shown below. One can treat w and v as colored noise sources generated by shaping filters of the form

$$W(j\omega) = Q^{1/2}(j\omega)\, W'(j\omega) \tag{4.9}$$

$$V(j\omega) = R^{1/2}(j\omega)\, V'(j\omega) \tag{4.10}$$

where W' and V' are white noise processes. $Q^{1/2}$ and $R^{1/2}$ are square roots of Q and R such that

$$Q(j\omega) = Q^{1/2}(j\omega)\,[Q^{1/2}(j\omega)]^{*} \tag{4.11}$$

$$R(j\omega) = R^{1/2}(j\omega)\,[R^{1/2}(j\omega)]^{*} \tag{4.12}$$

where $Q^{1/2}(j\omega)$ and $R^{1/2}(j\omega)$ are rational functions of $j\omega$.

In sensor failure DIA, the primary cause for the use of frequency-shaping is unmodeled dynamics. In our application to the engine problem, Q is taken to be constant (i.e., independent of frequency) and R is chosen as

$$R = \frac{r_2}{r_1}\,\frac{(\omega^2 + r_1)}{(\omega^2 + r_2)}\,, \qquad r_1 > r_2 \tag{4.13}$$

(see Example 4.1). Note that strictly proper transfer functions in $R^{-1/2}(j\omega)$ would cause $R(j\omega)$ to approach zero at high frequency. This implies perfect measurements. Therefore, in practice, one should choose $R^{-1/2}(j\omega)$ to be proper.

Next, the modified measurement z_1 is considered

$$z_1 = z - Du = Cx + v = y + v \tag{4.14}$$

If we define a shaped-measurement vector

$$Z_1'(j\omega) = R(j\omega)^{-1/2}\, Z_1(j\omega) \tag{4.15}$$

and the noise-free shaped output

$$Y'(j\omega) = R(j\omega)^{-1/2}\, Y(j\omega) \tag{4.16}$$

then a realization of the system with transfer function matrix $R(j\omega)^{-1/2}$ is

$$\dot{x}_v = A_v\, x_v + B_v\, Cx \tag{4.17}$$

$$y' = C_v x_v + D_v Cx \tag{4.18}$$

with the shaped-measurement equation

$$z_1' = C_v x_v + D_v Cx + v' \tag{4.19}$$

where v' is a white noise process as in (4.10).

The combination of equations (4.3) and (4.4), and (4.17), (4.18), and (4.19) defines a dynamic system driven by independent white noise sources and is a standard Kalman filtering problem:

$$\dot{\hat{x}} = A\hat{x} + Bu + K_e(z_1' - \hat{z}_1') \tag{4.20}$$

$$\dot{\hat{x}}_v = A_v \hat{x}_v + B_v C\hat{x} + K_v(z_1' - \hat{z}_1') \tag{4.21}$$

z_1' is obtained from z using the realization of $R^{-1/2}$:

$$\dot{x}_z = A_v x_z + B_v z_1 \tag{4.22}$$

$$z_1' = C_v x_z + D_v z_1 \tag{4.22}$$

Since equations (4.17) and (4.18), and (4.22) and (4.23) involve the same realization, the redundancy in the estimation equations can be eliminated by defining a new set of states [23]

$$\hat{x}' \triangleq x_z - \hat{x}_v \tag{4.24}$$

The overall frequency-shaped estimator equations are then given by

$$\begin{bmatrix} \dot{\hat{x}} \\ \dot{\hat{x}}_1 \end{bmatrix} = \underbrace{\left[\begin{array}{c|c} A - K_e D_v C & K_e C_v \\ \hline (K_v D_v - B_v) C & A_v - K_v C_v \end{array}\right]}_{A_s} \begin{bmatrix} \hat{x} \\ \hat{x}_1 \end{bmatrix}$$

$$+ \underbrace{\begin{bmatrix} K_e D_v \\ \hline (B_v - K_v D_v) \end{bmatrix}}_{B_{1s}} z + \underbrace{\begin{bmatrix} (B - K_e D_v D) \\ \hline (K_v D_v - B_v) D \end{bmatrix}}_{B_s} u \tag{4.25}$$

$$\hat{x} = \underbrace{[C \mid 0]}_{C_s} \begin{bmatrix} \hat{x} \\ \hline \hat{x}_1 \end{bmatrix} \tag{4.26}$$

The control law is then based on $\hat{x}$

$$u = K_R |\hat{x}| \tag{4.27}$$

where K_R is the regulator gain. A block diagram of the system showing the frequency-shaped optimal estimator is shown in Figure 4.1. The filter in Eqs. (4.22) and (4.23) acts as a prefilter on the measurements.

Theorem 4.1: The zeros of $R^{-1/2}$ are the transmission zeros of the frequency-shaped estimator whenever the sensors are frequency-shaped individually.

Proof: The transmission zeros of the estimator (with input z and output $\hat{x}$) are given by those frequencies such that the matrix pencil $S(\lambda)$ loses rank

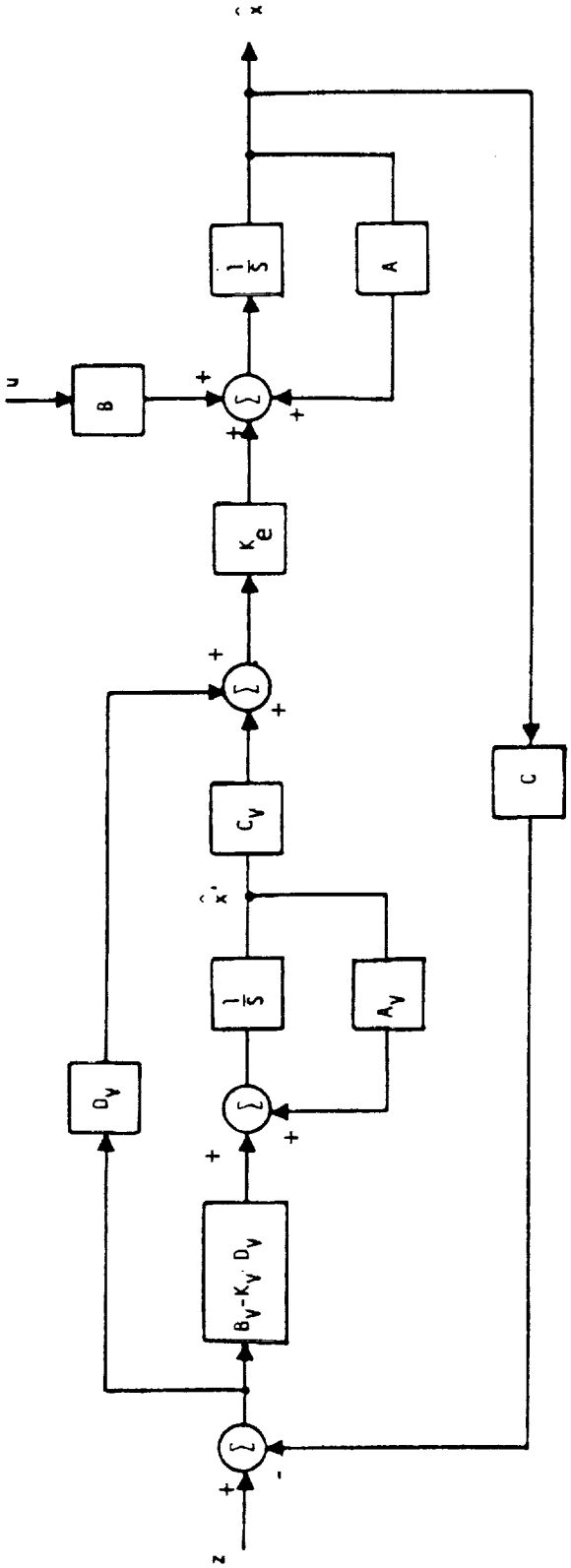

Figure 4.1 Block Diagram of Estimator (Eqs. 4.25 and 4.26)

$$S(\lambda) = \left[\begin{array}{c|c} sI - A_s & B_{ls} \\ \hline C_s & 0 \end{array}\right] \tag{4.28}$$

$$S(\lambda) = \left[\begin{array}{cc|c} sI - A + K_e D_v C & - K_e C_v & K_e D_v \\ - (K_v D_v - B_v) C & sI - A_v + K_v C_v & (B_v - K_v D_v) \\ \hline I & 0 & 0 \end{array}\right] \tag{4.29}$$

By performing elementary row and column operations, $S(\lambda)$ is equivalent to

$$S(\lambda) \sim \left[\begin{array}{c|c|c} sI - A & 0 & K_e D_v \\ \hline 0 & (sI - A_v + B_v D_v^{-1} C_v) & B_v - K_v D_v \\ \hline I & 0 & 0 \end{array}\right] \tag{4.30}$$

which loses rank at the location of the eigenvalues of $(A_v + B_v D_v^{-1} C_v)$ which are the zeros of $R^{-1/2}$ since it is diagonal, as are A_v, B_v, C_v, and D_v. Q.E.D

In the case of individually frequency-shaped sensors, $R^{-1/2}$ would be diagonal and, if a frequency shaping of first order is introduced in all sensors then

$$R_{ii}^{-1/2} = \frac{P_i(s + Z_i)}{Z_i(s + P_i)} \tag{4.31}$$

and hence

$$A_v = \text{diag } \{P_i\} \tag{4.32}$$

$$B_v = I \tag{4.33}$$

$$C_v = \text{diag } \left\{ \frac{P_i(Z_i - P_i)}{Z_i} \right\} \tag{4.34}$$

$$D_v = \text{diag}\left(\frac{P_i}{Z_i}\right) \tag{4.35}$$

Notice that R_{ii}'s have unity D.C. gain. These will introduce lag compensators into the measurement loops provided that

$$|Z_i| > |P_i| \tag{4.36}$$

which implies more noise at higher frequencies. Frequency shaping then improves the robustness properties of the system at higher frequencies, while maintaining performance at low frequencies. Notice that this is similar to introduction of first-order lags of classical control, but is inherently multivariable.

4.2 EXAMPLE 4.1

This example illustrates the ideas of internal model and frequency shaping presented in Sections 2.2.3 and 4.1, respectively. The internal model provides for asymptotically unbiased estimates in the presence of biases and parameter errors, i.e., the estimate of the engine outputs track the output measurements (i.e., $z - \hat{z} \to 0$). Frequency shaping provides for robustness with respect to unmodeled dynamic uncertainties. The combination of the internal model and frequency shaping results in the desirable robustness properties of the filter.

A turbofan engine model and its multivariable control law (the same as in Example 3.2) at sea level static condition and PLA=36° was chosen for design purposes. Figure 4.2a shows a steady-state run corresponding to Revision 2 of the previous program [9]. This figure shows that the estimate of N1, N2, PT4, PT6, and FTIT do not track the measurements (i.e., $z - \hat{z} \neq 0$ asymptotically). If an internal model (integrators) for biases is introduced, then the augmented system has the form of (4.1) and (4.2). The estimator gains were computed using CTRL-C [21] and are shown in Table 4.1. Figure 4.2b shows a steady-state run with the internal model present in the engine/control model.

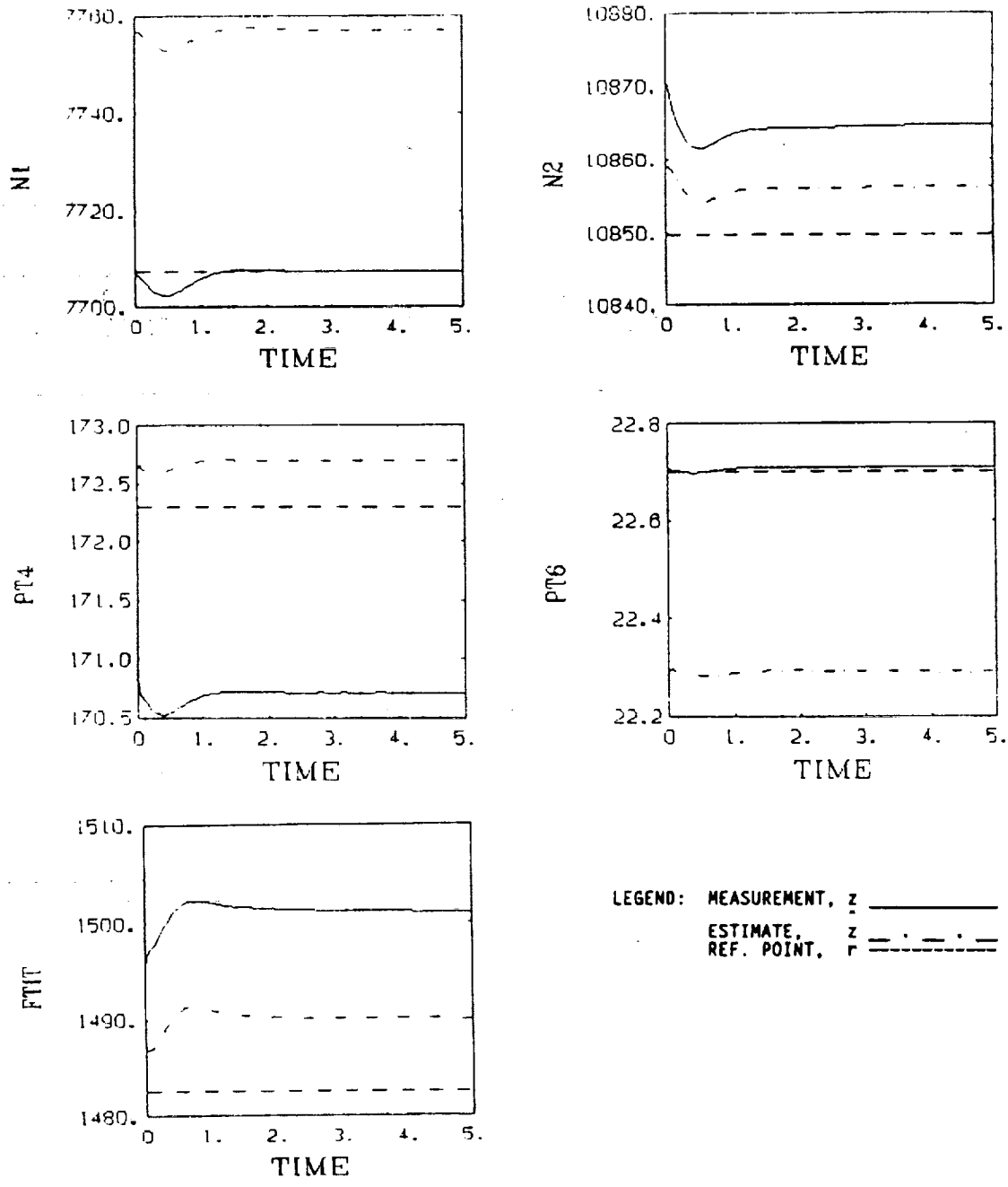

Figure 4.2a Engine Steady-State Response at Sea Level Static Condition and PLA = 36° with No Internal Model Present (Revision 2, Ref. 9)

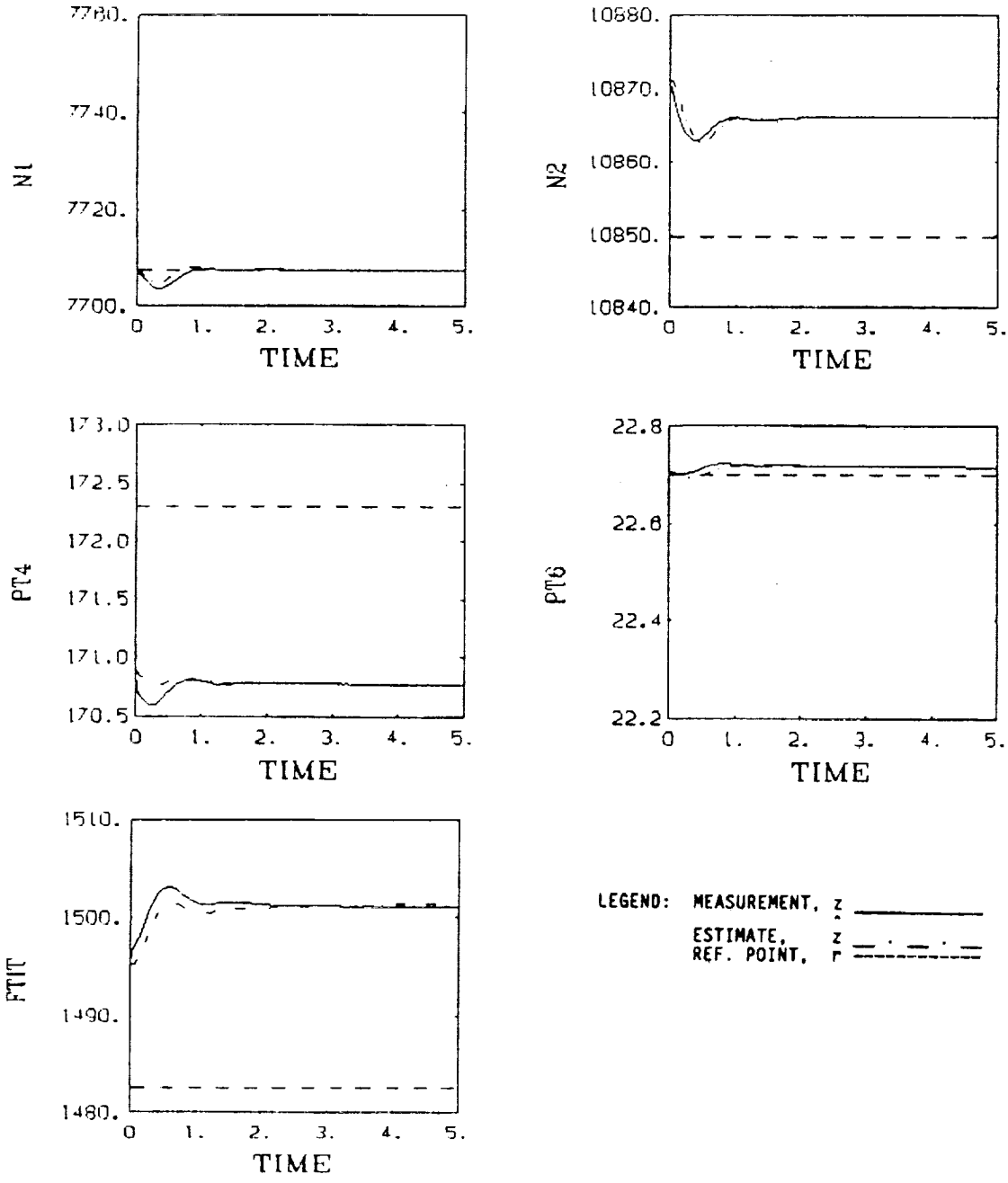

Figure 4.2b Engine Steady-State Response at Sea Level Static Condition and PLA = 36° with Internal Model

Table 4.1

Kalman Filter Gain Matrix

$$KK = \begin{bmatrix} 8.3760 & 3.1891 & 0.2311 & 0.0303 & -0.6314 \\ 4.5611 & 12.4951 & 0.4499 & 0.0173 & -1.2775 \\ 1.3178 & 2.0933 & 0.0836 & 0.0048 & -0.2963 \\ 0.0701 & -0.0033 & 0.0006 & 0.0001 & -0.0004 \\ 2.4511 & 1.0903 & 0.0253 & -0.0018 & -0.0429 \\ 0.0009 & 2.9770 & 0.0051 & -0.0014 & 0.0421 \\ 0.0121 & 0.0476 & 1.5822 & 0.0000 & -0.0013 \\ 0.0019 & 0.0036 & 0.0001 & 1.2247 & -0.0003 \\ -0.0945 & -0.1824 & -0.0054 & -0.0001 & 1.0077 \end{bmatrix}$$

$$= \begin{bmatrix} K_p \\ \hline K_I \end{bmatrix} \quad \begin{matrix} \} \text{ Filter} \\ \\ \} \text{ Internal Model} \end{matrix}$$

(This corresponds to Revision 3 of the previous program [9].) Figure 4.2b shows that the estimates now asymptotically track the measurements (i.e., $z - \hat{z} \to 0$) for all outputs. Note that there is a dip in Figures 4.2a and 4.2b, which is due to initialization transients of the engine simulation. Figures 4.3a and 4.3b are transient runs at sea level static condition and a PLA step from PLA=36° to 52°. Figure 4.3a shows transient responses with no internal model and Figure 4.3b illustrates the responses with the internal model present. It can be seen from Figure 4.3b that the estimates follow the measurements, i.e., $\hat{z} \to z \neq 0$, in steady state.

There are now two internal models in the closed-loop system (i.e., integrators both in the filter and controller. Figure 4.4 is a block diagram of the system showing the two internal models. The presence of the internal model in the filter ensures $z - \hat{z} \to 0$, and the presence of the internal model in the controller ensures $z - r \to 0$, which implies that $r - z \to 0$ in steady state. Note that the controller has a partial internal model, i.e. it only has integrators on N1 and PT6 outputs (see form of CI in Table 4.2). Therefore, even though all the estimates are unbiased, we can only guarantee zero steady-state tracking error in N_1 and PT_6 as seen in Figure 4.2b and 4.3b. Note that in Figure 4.2b and 4.3b for the PT6 output, $z - \hat{z}$ error has become zero whereas $z - r$ error has not. This is because the integrator (in the control law) associated with PT6 output has a small gain which explains why this error is slow in decaying to zero (for details, see Ref. 9).

We can now proceed to add frequency shaping in the filter. Based on the results of a bound on model error (Appendix A), we chose to frequency-shape all sensors using

$$R_{ii}^{-1/2}(s) = \frac{10\pi(s + 20\pi)}{20\pi(s + 10\pi)} \tag{4.37}$$

i.e., a first-order lag with breakpoint at 5 Hz. The frequency-shaped system matrices $\{A_v, B_v, C_v, D_v\}$ are shown in Table 4.3, and Table 4.4 shows the

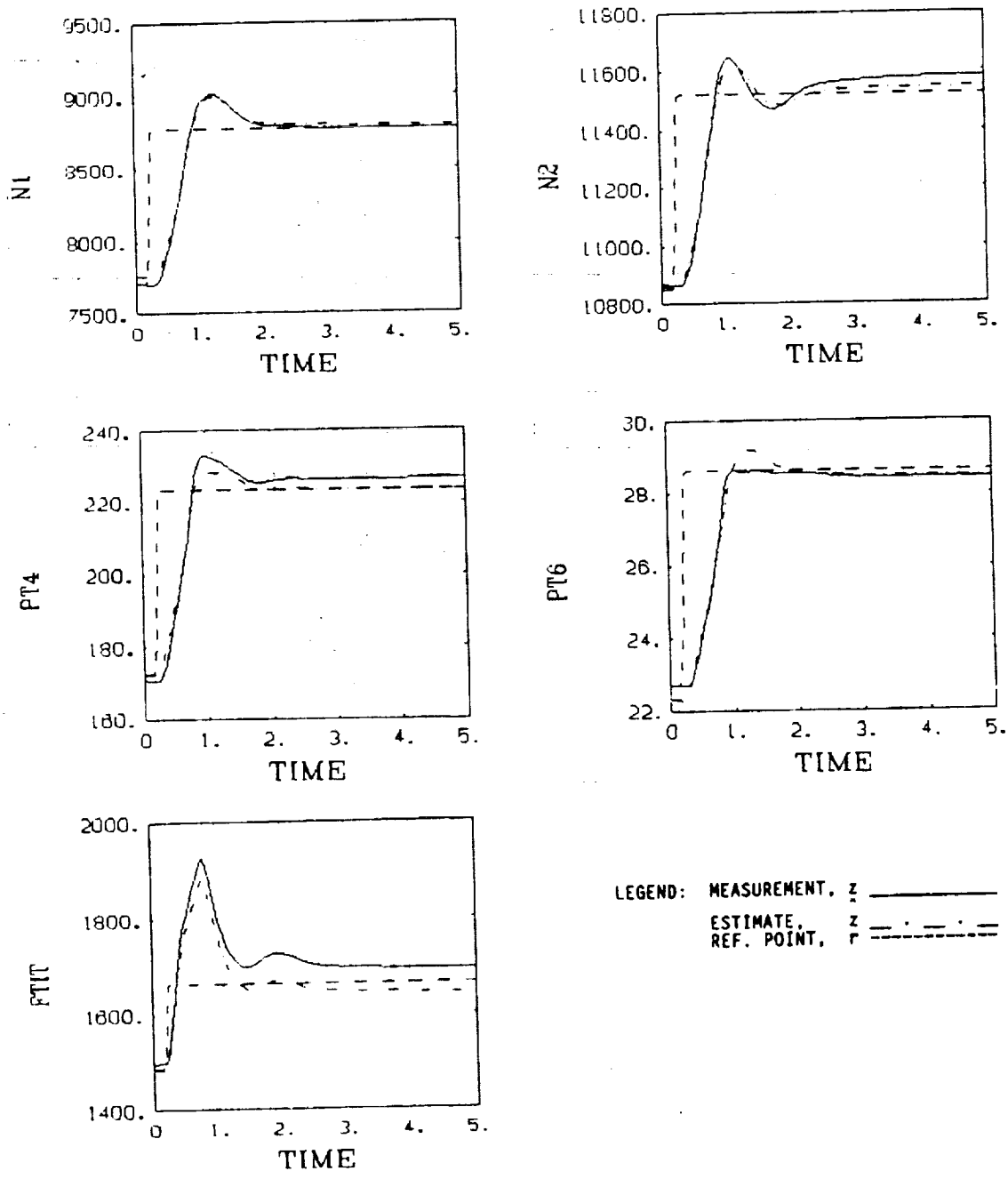

Figure 4.3a Engine Transient Response at Sea Level Static Condition and PLA Step Input from 36° to 52° at 0.2 Seconds, and with No Internal Model Present (Revision 2, Ref. 9)

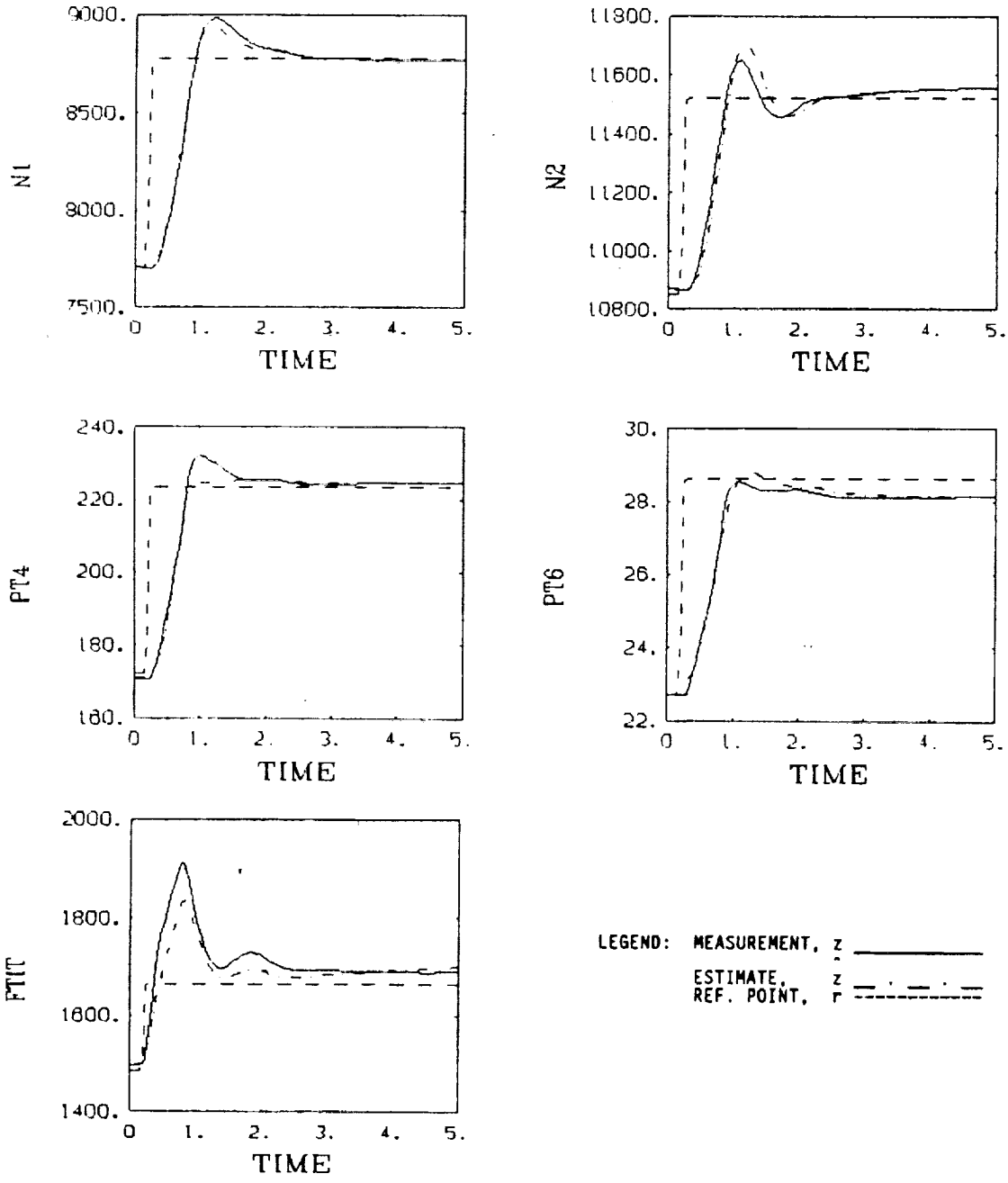

Figure 4.3b Engine Transient Response at Sea Level Static Condition and PLA Step Input from 36° to 52° at 0.2 Seconds, and with Internal Model Present

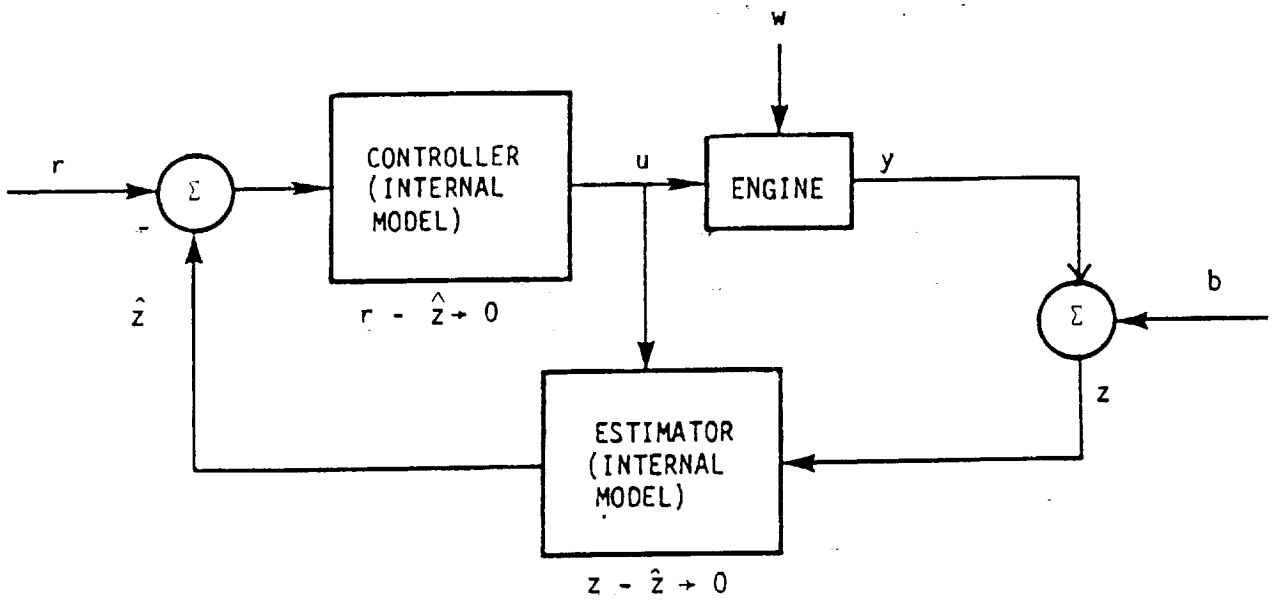

Figure 4.4 Overall Robust Servomechanism with Internal Models

Table 4.2

Proportional and Integral Gain Matrices

CP =

-0.4632	-1.9502	-62.6000	-30.0927	0.0000
-0.0002	0.0000	0.0000	0.0352	0.0000
0.0061	0.0000	0.0000	-0.3429	0.0000
-0.0025	0.0068	0.0000	-0.1640	0.0000
0.0000	0.0001	0.0025	0.0000	0.0000

CI =

-10.0012	0.0000	0.0000	-20.0000	0.0000
-0.0020	0.0000	0.0000	0.0300	0.0000
0.0000	0.0000	0.0000	0.0000	0.0000
0.0000	0.0000	0.0000	0.0000	0.0000
0.0000	0.0000	0.0000	0.0000	0.0000

Table 4.3
Frequency-Shaped System Matrices

AV =

-31.4159	0.0000	0.0000	0.0000	0.0000
0.0000	-31.4159	0.0000	0.0000	0.0000
0.0000	0.0000	-31.4159	0.0000	0.0000
0.0000	0.0000	0.0000	-31.4159	0.0000
0.0000	0.0000	0.0000	0.0000	-31.4159

BV =

1	0	0	0	0
0	1	0	0	0
0	0	1	0	0
0	0	0	1	0
0	0	0	0	1

CV =

15.7080	0.0000	0.0000	0.0000	0.0000
0.0000	15.7080	0.0000	0.0000	0.0000
0.0000	0.0000	15.7080	0.0000	0.0000
0.0000	0.0000	0.0000	15.7080	0.0000
0.0000	0.0000	0.0000	0.0000	15.7080

DV =

0.5000	0.0000	0.0000	0.0000	0.0000
0.0000	0.5000	0.0000	0.0000	0.0000
0.0000	0.0000	0.5000	0.0000	0.0000
0.0000	0.0000	0.0000	0.5000	0.0000
0.0000	0.0000	0.0000	0.0000	0.5000

Table 4.4
Frequency-Shaped Filter Gain

KK =

8.3760	3.1891	0.2311	0.0303	-0.6314
4.5611	12.4951	0.4499	0.0173	-1.2775
1.3178	2.0933	0.0836	0.0048	-0.2963
0.0701	-0.0033	0.0006	0.0001	-0.0004
2.4511	1.0903	0.0253	-0.0018	-0.0429
0.0009	2.9770	0.0051	-0.0014	0.0421
0.0121	0.0476	1.5822	0.0000	-0.0013
0.0019	0.0036	0.0001	1.2247	-0.0003
-0.0945	-0.1824	-0.0054	-0.0001	1.0077
0.2647	0.0778	0.0054	0.0007	-0.0142
0.0980	0.3518	0.0099	0.0003	-0.0272
0.0059	0.0095	0.0489	0.0000	-0.0010
0.0006	0.0002	0.0000	0.0379	0.0000
-0.0242	-0.0374	-0.0015	-0.0001	0.0357

$$\begin{bmatrix} K \\ \hline K_I \\ \hline K_V \end{bmatrix} \begin{matrix} \text{Filter} \\ \text{Internal Model} \\ \text{Frequency Shaping} \end{matrix}$$

frequency-shaped Kalman filter gain matrix. The closed-loop filter poles are shown in Table 4.5. Figure 4.5 shows the transient engine response corresponding to the closed-loop system with both internal models and frequency shaping. Figure 4.5 shows the effects of the frequency shaping in this case, i.e., the engine transient response has been slowed down slightly.

4.3 SUMMARY

In this chapter, we have discussed the design of robust filters for DIA. The robustness properties of the filters are twofold. First, the filter is made robust with respect to parameter perturbations, using an internal model. This is an extension to internal model principle of multivariable robust servomechanism theory. The robustness property achieved is due to creation of certain structurally robust blocking zeros. Second, the filter was made robust with respect to other sources of uncertainty via frequency shaping. This robustness property is achieved also through creation of certain transmission zeros. The results were applied to a multivariable turbofan engine example.

Table 4.5

Closed-Loop Filter Poles

-23.4786 + 4.9215i
-23.4786 - 4.9215i
-13.1757 - 0.0000i
-29.4962 + 0.0000i
-0.1160 + 0.0000i
-2.0722 - 0.0000i
-1.8294 - 0.0000i
-0.9693 + 0.0146i
-0.9693 - 0.0146i
-1.5835 + 0.0000i
-1.2255 + 0.0000i
-31.4027 + 0.0000i
-31.3980 + 0.0000i
-31.3860 + 0.0000i

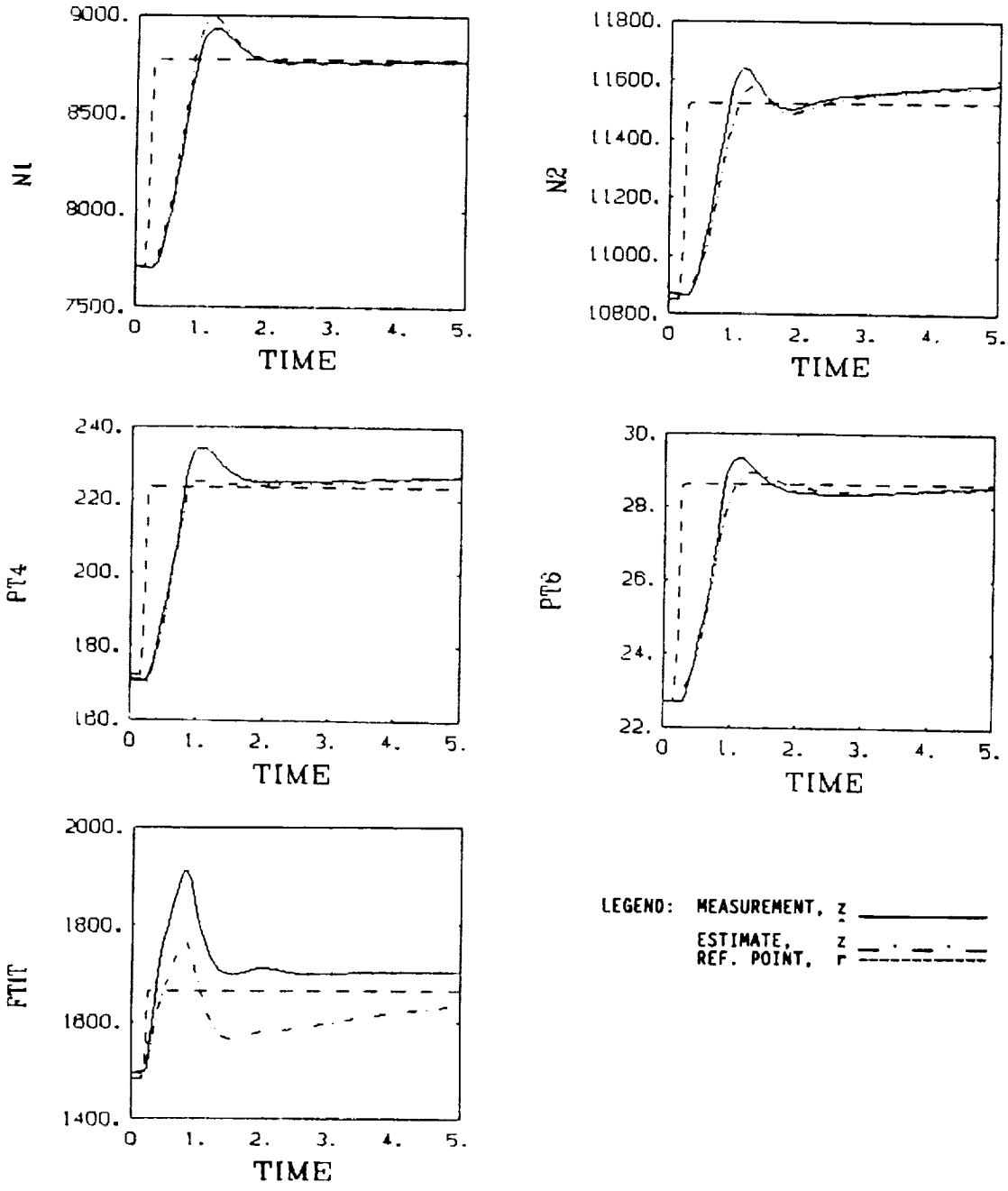

Figure 4.5 Transient Response at Sea Level Static Condition and PLA Step Input from 36° to 52° at 0.2 Seconds, and with Internal Model and Frequency Shaping

V. EVALUATION RESULTS

5.1 INTRODUCTION

This chapter evaluates the results of this program through the validation of the threshold selector results of Chapter III. Before the actual validation, it is useful to summarize the results of the report and put the evaluation results into perspective.

This report has presented the results of recent research in the development of robust fault detection, isolation, and accommodation (DIA) algorithms for sensor failures. Specifically, tools and procedures have been developed that allow a designer to use information about model uncertainty when designing a sensor DIA logic. This is a major step in developing an ability to design and implement a practical fault-tolerant control system.

A DIA system, as treated in this report, consists of three main components:

(1) a filter that compares measurements to predictions (based on a model) to produce an innovations sequence;

(2) a norm computation that reduces the innovations to a single measure useful for comparing against a threshold; and

(3) a threshold.

The goal of the design process described in Figure 1.9 is to select a combination of these three components to produce a system that has adequate performance (smallest magnitude of failure detectable, speed of detection, and minimum false alarm rate) without being excessively complex.

The emphasis of this reported effort has been to provide tools and procedures that allow the design process of Figure 1.9 to be carried out. Specifically produced have been techniques that

(1) permit the performance of filter innovations measure combination to be computed analytically using an estimate of the model uncertainty in the system; and

(2) permit a filter's performance to be improved by incorporating a knowledge of the modeling error bounds in its design.

The first was addressed in Chapter III under the heading of the Threshold Selector; the second was addressed in Chapter IV.

Selecting the best filter/innovations measure combination is a multistep and iterative process (Figure 1.9). The filters used to generate the innovations sequences can vary in complexity from constant gain types to ones that include frequency shaping and internal models to a fully adaptive design.

As a general rule, increased complexity is required to improve the filter performance. The study reported in Ref. 9 dealt with constant gain filters. This report described the use of frequency shaping and internal models to improve filter performance in the presence of modeling errors. Adaptive filter designs are left for future studies.

Many measures of the size of innovations sequence are also possible for consideration. Examples include weighted sum squared residual (WSSR), likelihood ratio, and generalized likelihood ratio. The performance of each in combination with the different filters could be different and should be investigated before a final system is designed. Note, however, that the only measure of the innovations sequence dealt with in this effort in the WSSR norm. This is the same as that used in Ref. 9.

While the filter and size of innovations measure selections are clearly critical to designing a successful DIA system, it is the ability to evaluate analytically the performance of the combination that makes the design process of Figure 1.9 feasible. This capability is what is provided by the Threshold Selector described in Chapter III. It produces an estimate of the sizes of the smallest failures that can be detected and a measure (i.e., threshold) against which the norm of the innovations sequence can be compared to determine the presence of a failure.

As an example, the threshold selector can be used to predict the performance of the robust filter designed in Chapter IV. Figure 5.1 shows the threshold selector results for a soft failure using the robust filter with internal model and frequency shaping designed in Example 4.1. This figure shows that the robust filter is capable of detecting failures of smaller size compared to the constant gain filter developed in Ref. 9 (compare Figures 5.1 and 3.10).

5.2 VALIDATION OF THE THRESHOLD SELECTOR

Because of its critical role in the design process, the ability of the Threshold Selector to predict realistic thresholds has been validated experimentally. The goal was to demonstrate the fact that induced failures are detected and that false alarms are avoided.

The filter/norm chosen for this demonstration is the same as that developed in Ref. 9 for a multivariable turbofan engine. Specifically, the filters are constant gain filters with no frequency shaping or internal models. The norm is a WSSR. The flight condition is sea level static at 36° PLA.

The reason for this filter/norm choice is that it allows direct evaluation of the Threshold Selector only. Reasonable thresholds were determined empirically for this combination and a full evaluation was performed in a previous program [9]. Consequently, there is a data base against which to compare the results obtained with a new threshold implemented.

Compared in Table 5.1 are the thresholds determined empirically in the previous program [9] and the thresholds computed with the Threshold Selector. Note that while the results are of similar magnitudes, the Threshold Selector computed values are smaller. This indicates that failures of smaller magnitude can be detected (and faster) with the filter/norm combination than were previously expected. Required to be validated experimentally is that false alarms are not induced as a result of decreasing the thresholds.

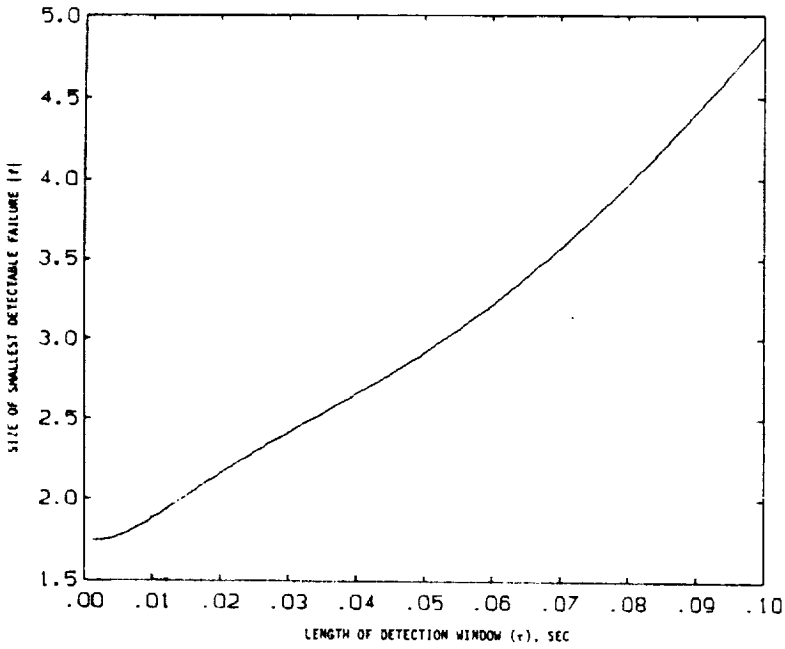

(a)

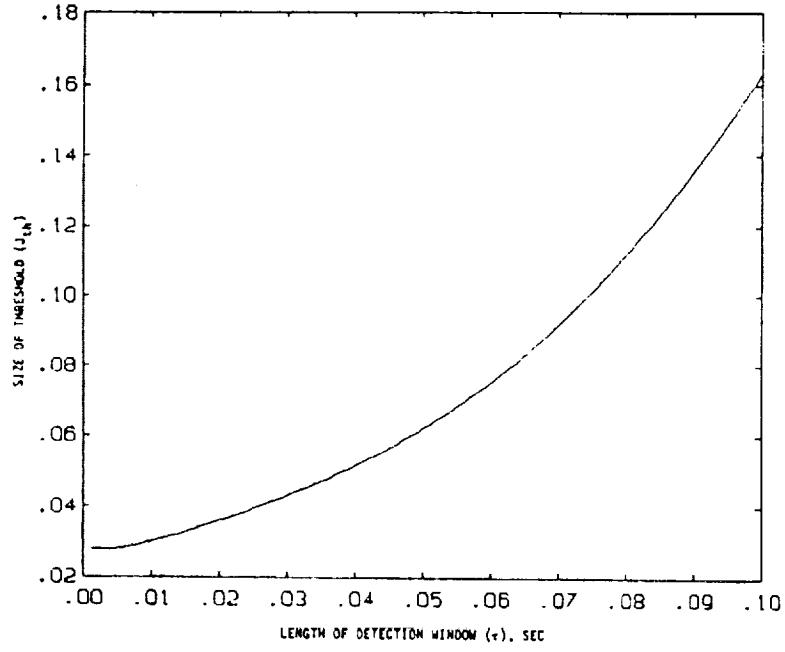

(b)

Figure 5.1 Threshold Selector Results for Robust Filter with Internal Model and Frequency-Shaping

Table 5.1

Comparison of Sizes of Thresholds

TYPE OF FAILURE	SIZE OF THRESHOLD USED IN REVISION 2 OF REF. 9	SIZE OF THRESHOLD COMPUTED BY THRESHOLD SELECTOR
HARD	2.0	.62
SOFT	1.43	.62

Our evaluation consisted of the comparison of failure detection times for various failures using the thresholds in Ref. 9 and the thresholds computed using the threshold selector. A turbofan engine dynamic model (the same one as in Examples 3.2 and 4.1) at sea level static condition and PLA = 36° was used for this evaluation. Figures 5.2 through 5.4 compare the response of the same DIA algorithm (i.e., the same filter/norm combination) for the two threshold levels presented in Table 5.1. Figures 5.2 and 5.3 present selected responses to a hard failure in N1 for the DIA scheme using the empirical threshold and the Threshold Selector computed threshold, respectively. Figures 5.4 and 5.5 present the results for a hard failure in N2. Figures 5.6 and 5.7 present the results of a drift failure in N1. Figures 5.8 and 5.9 present the results of a drift failure in PT4. Note that key events characteristic of all the plots are indicated in Figure 5.2.

The results are as expected and are summarized in Table 5.2. Large step failures create a WSSR norm of the innovations sequence larger than the threshold in both cases and trigger a failure indication within one window width of the WSSR norm. The size of the norm has no effect on the performance. For drift failures, however, the smaller threshold does permit more rapid detection of the failure.

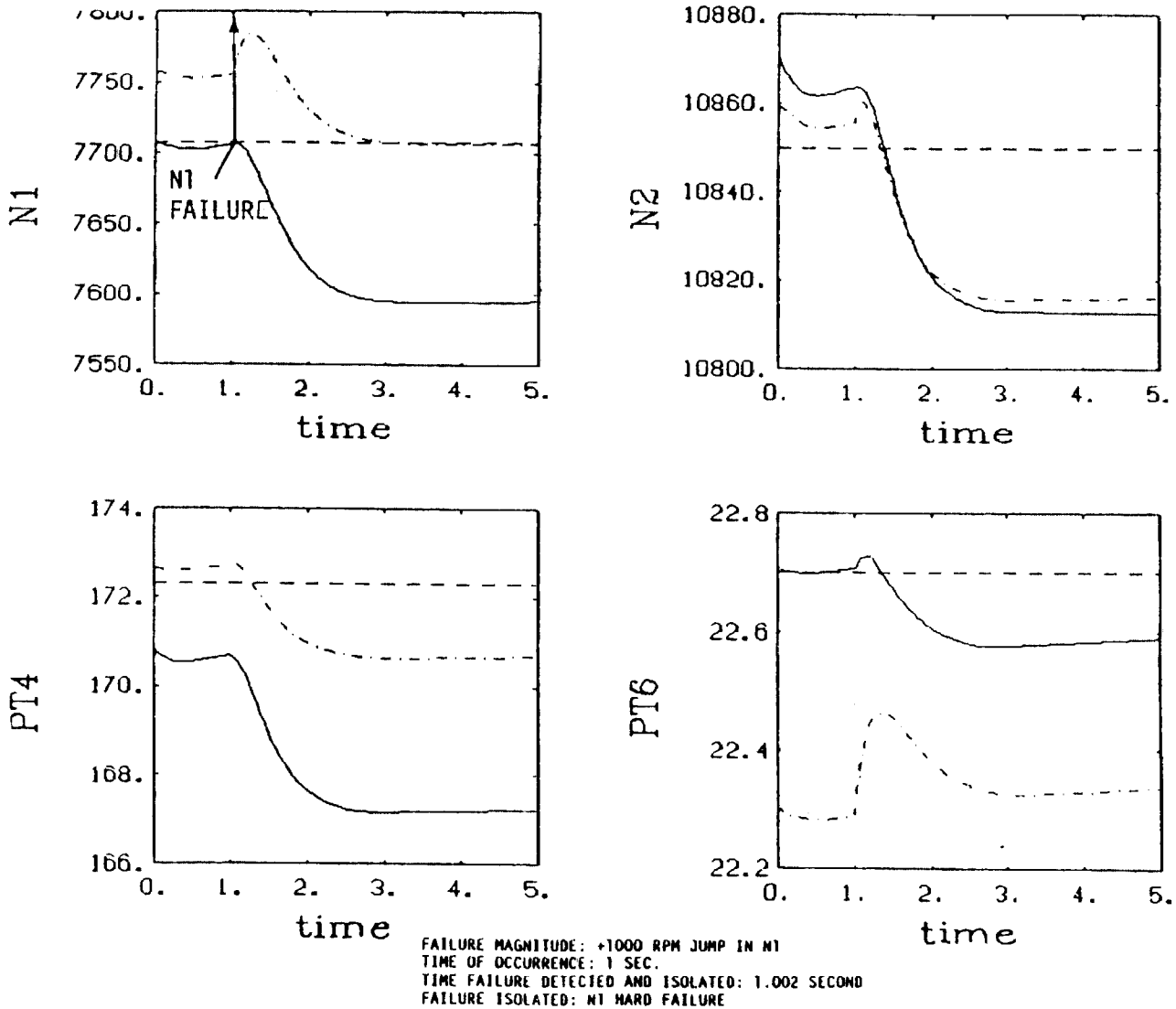

Figure 5.2 N2 Hard Failure Transients Using Method (Revision 2) of Ref. 9

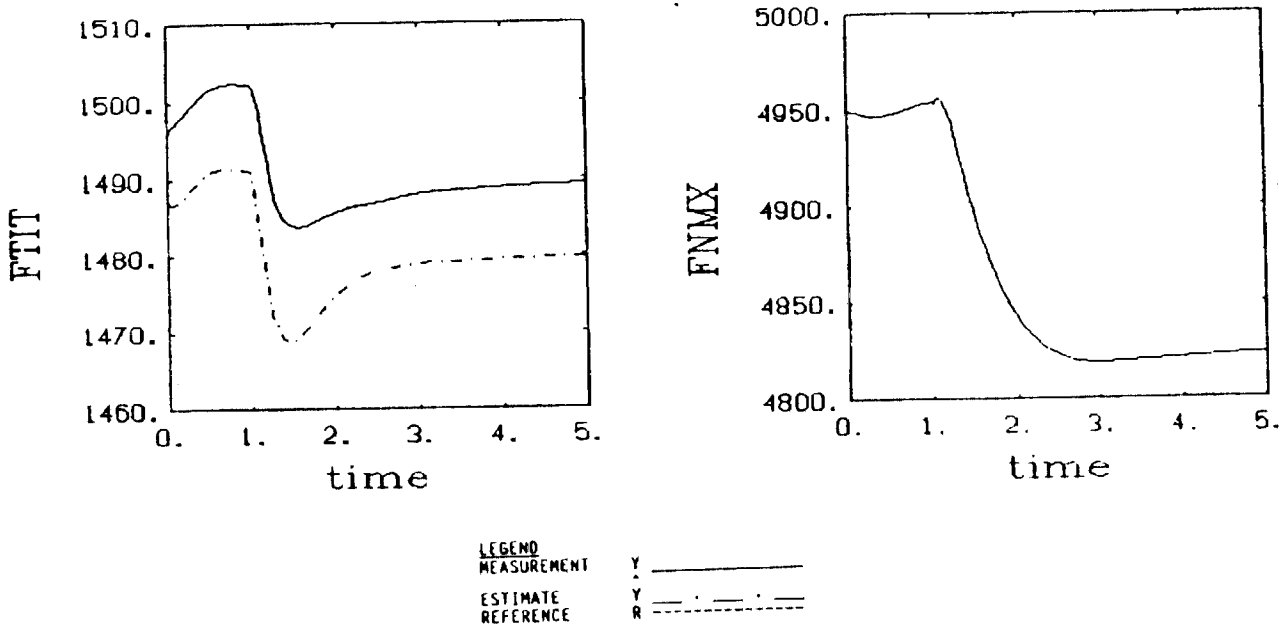

Figure 5.2 (Continued)

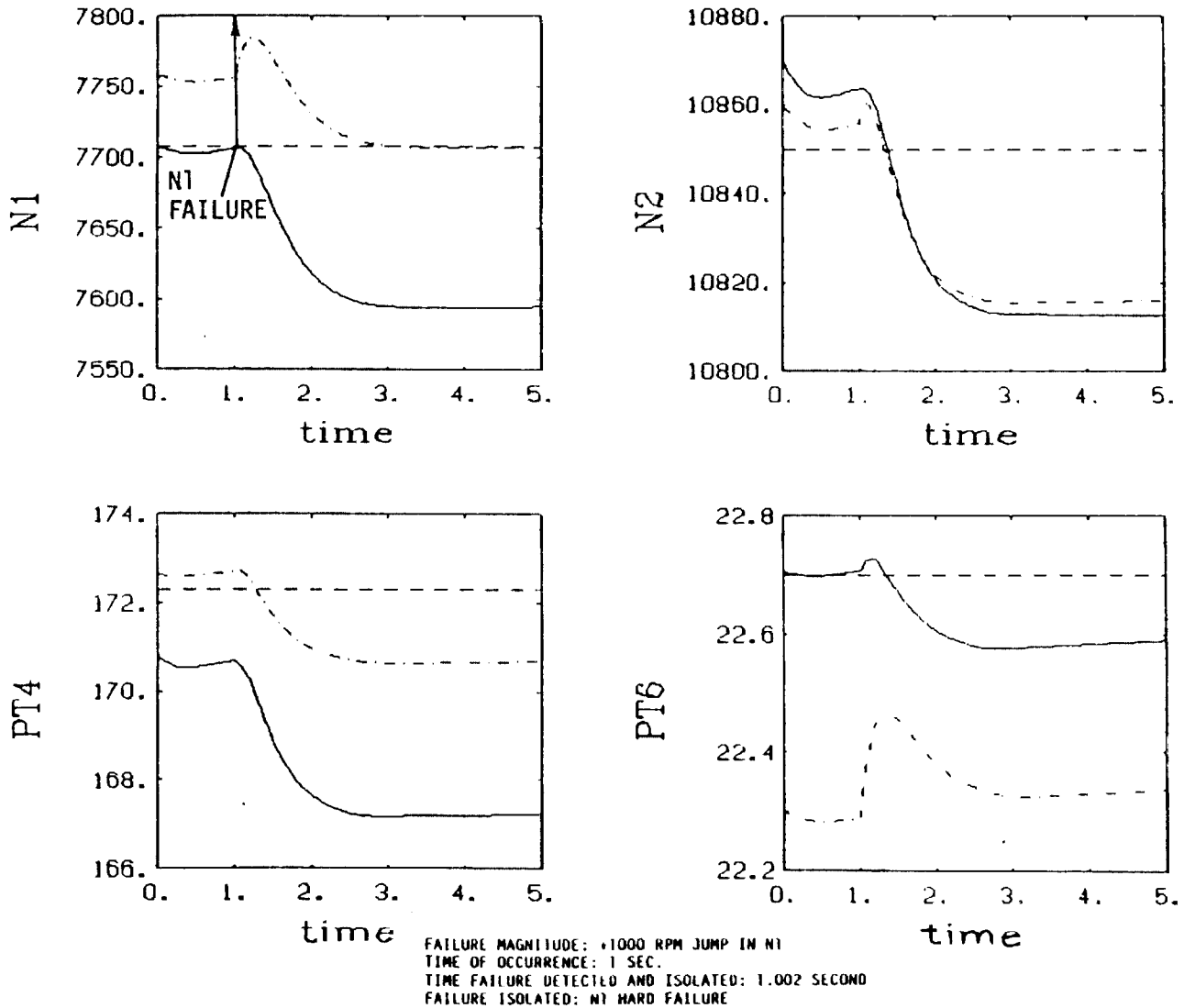

Figure 5.3 N1 Hard Failure Transients Using Threshold Selector

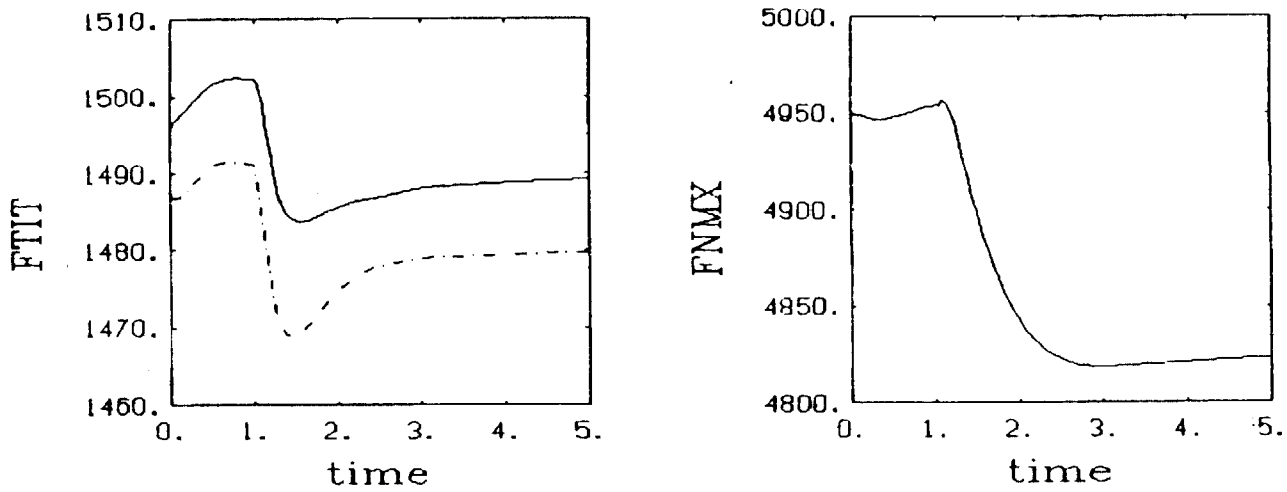

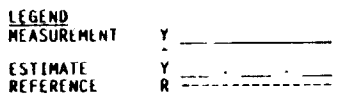

Figure 5.3 (Continued)

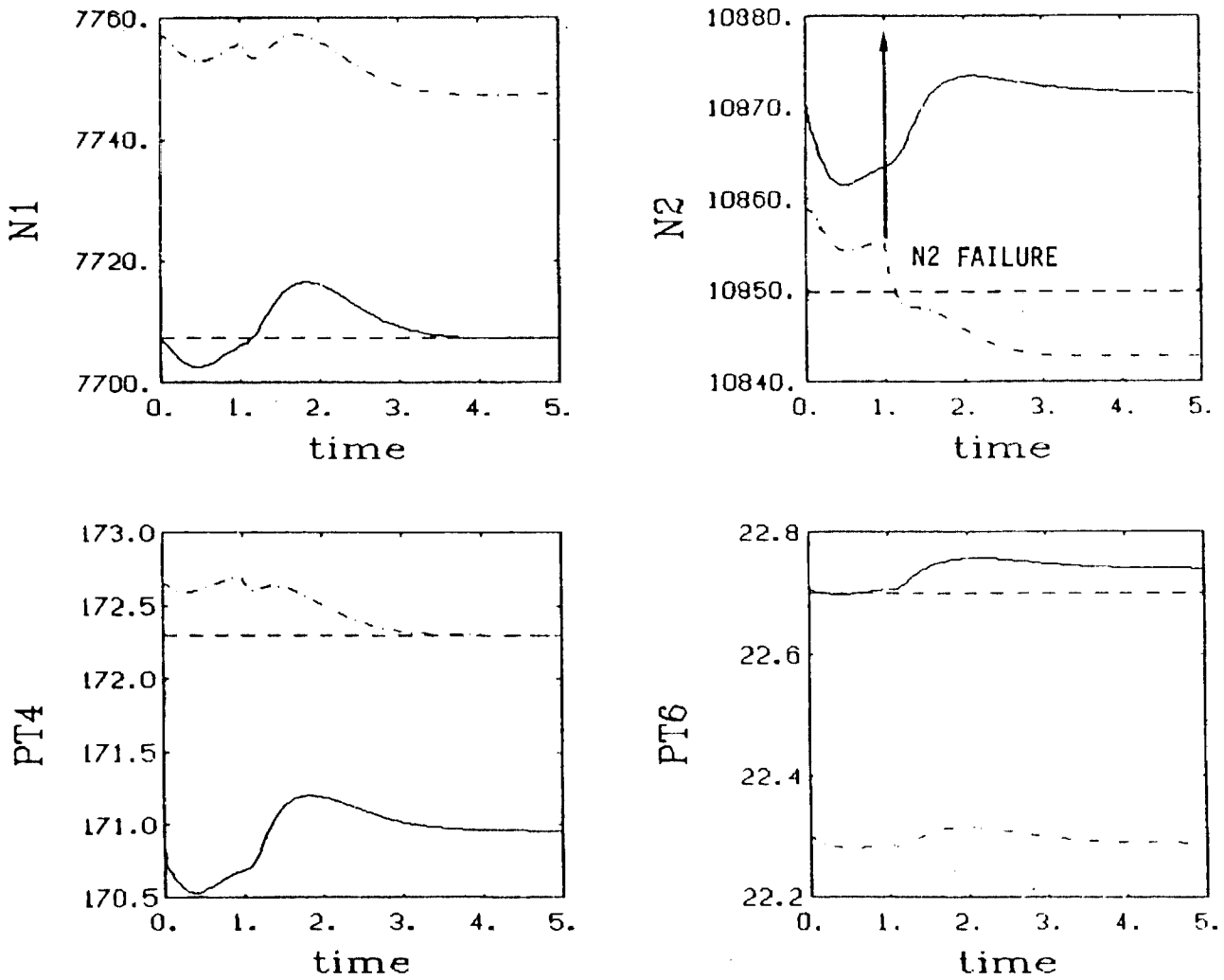

FAILURE MAGNITUDE: +1000 RPM JUMP IN N1
TIME OF OCCURRENCE: 1 SEC.
TIME FAILURE DETECTED AND ISOLATED: 1.002 SECOND
FAILURE ISOLATED: N2 HARD FAILURE

Figure 5.4 N2 Hard Failure Transients Using Method (Revision 2) of Ref. 9

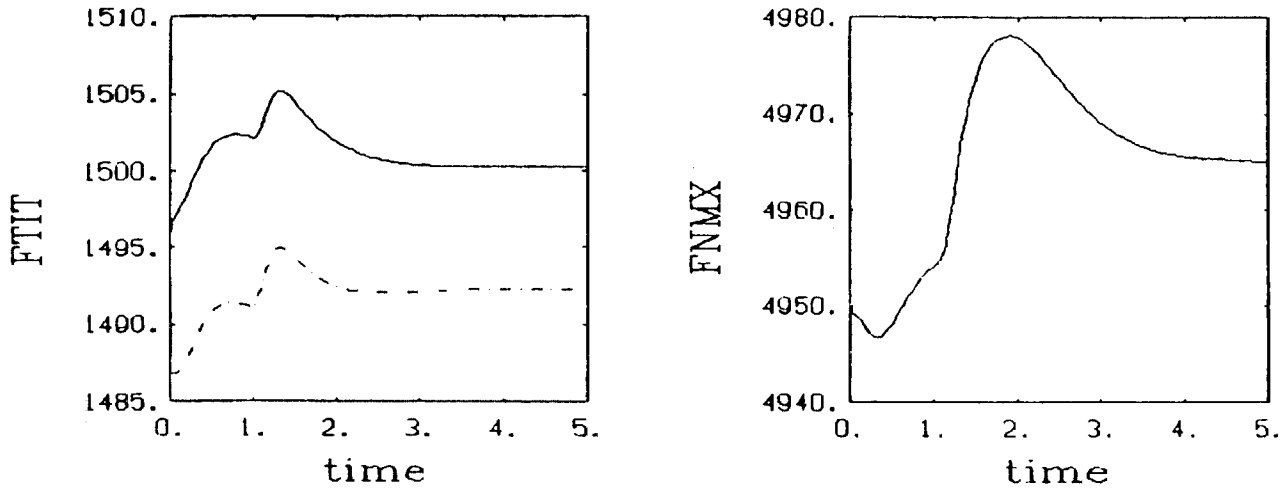

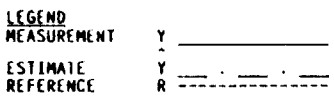

Figure 5.4 (Continued)

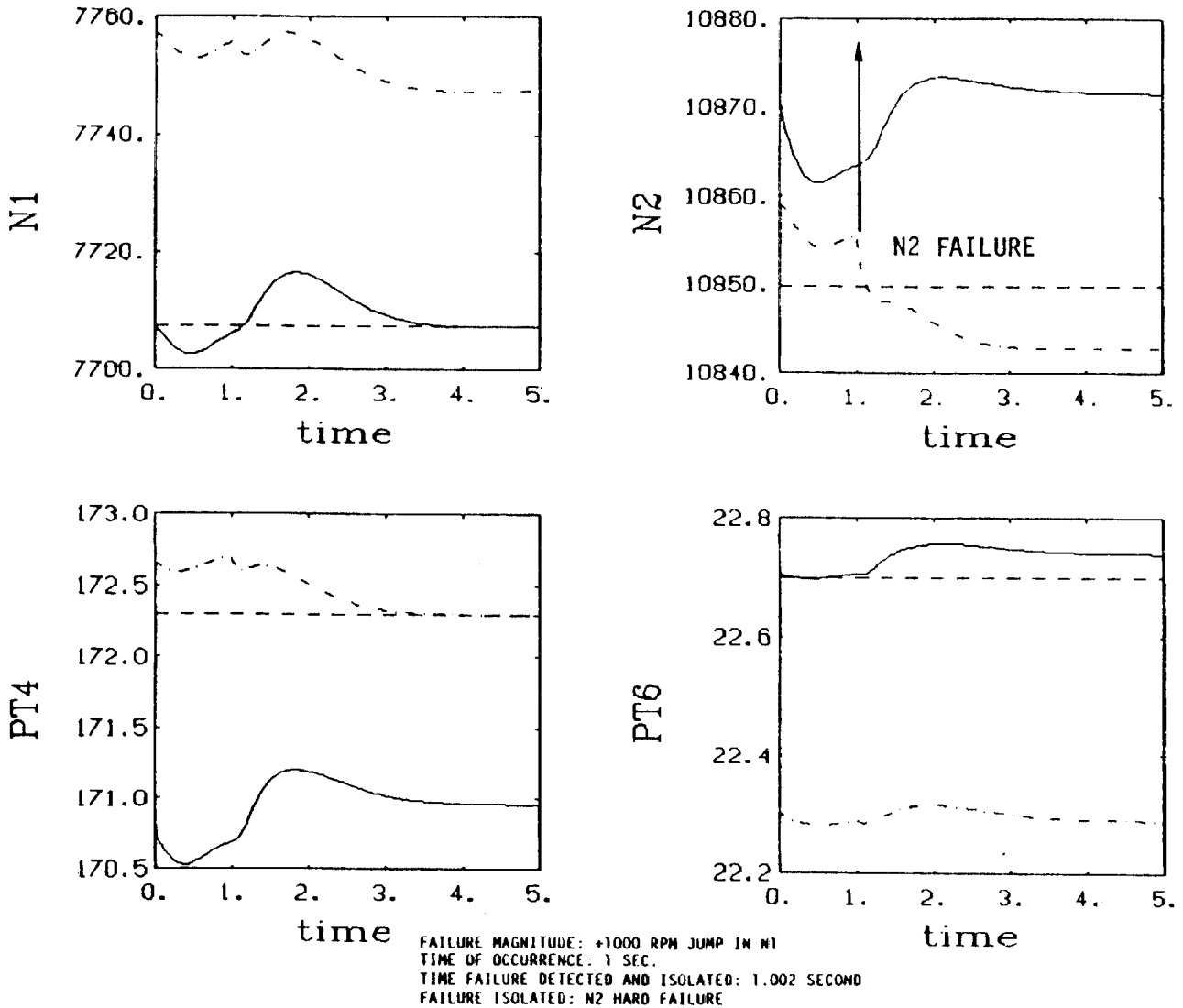

Figure 5.5 N2 Hard Failure Transients Using Threshold Selector

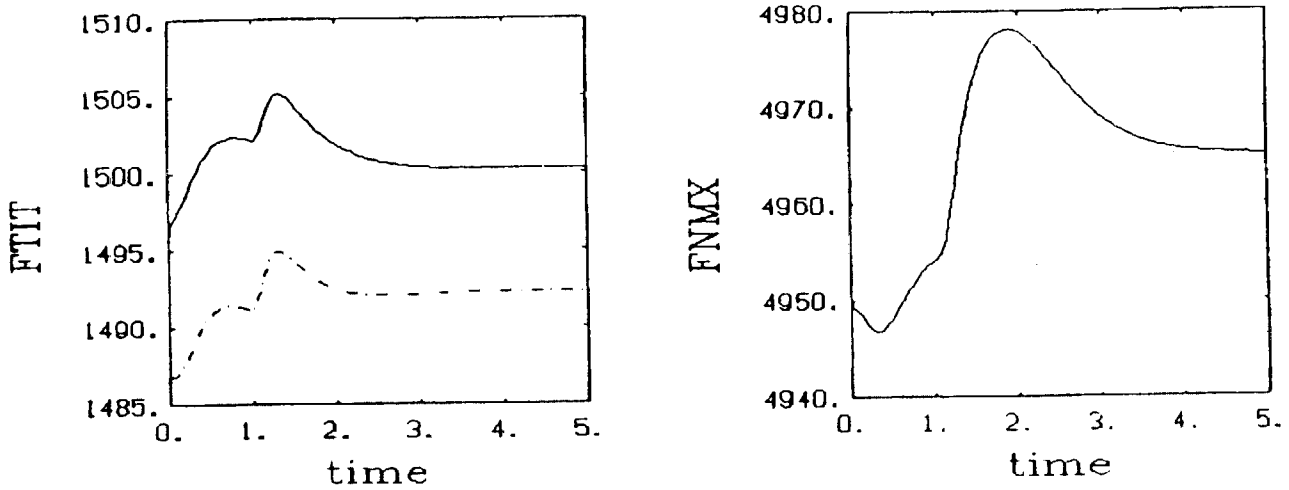

LEGEND
MEASUREMENT Y _____
ESTIMATE Y _ . _ . _
REFERENCE R - - - - - -

Figure 5.5 (Continued)

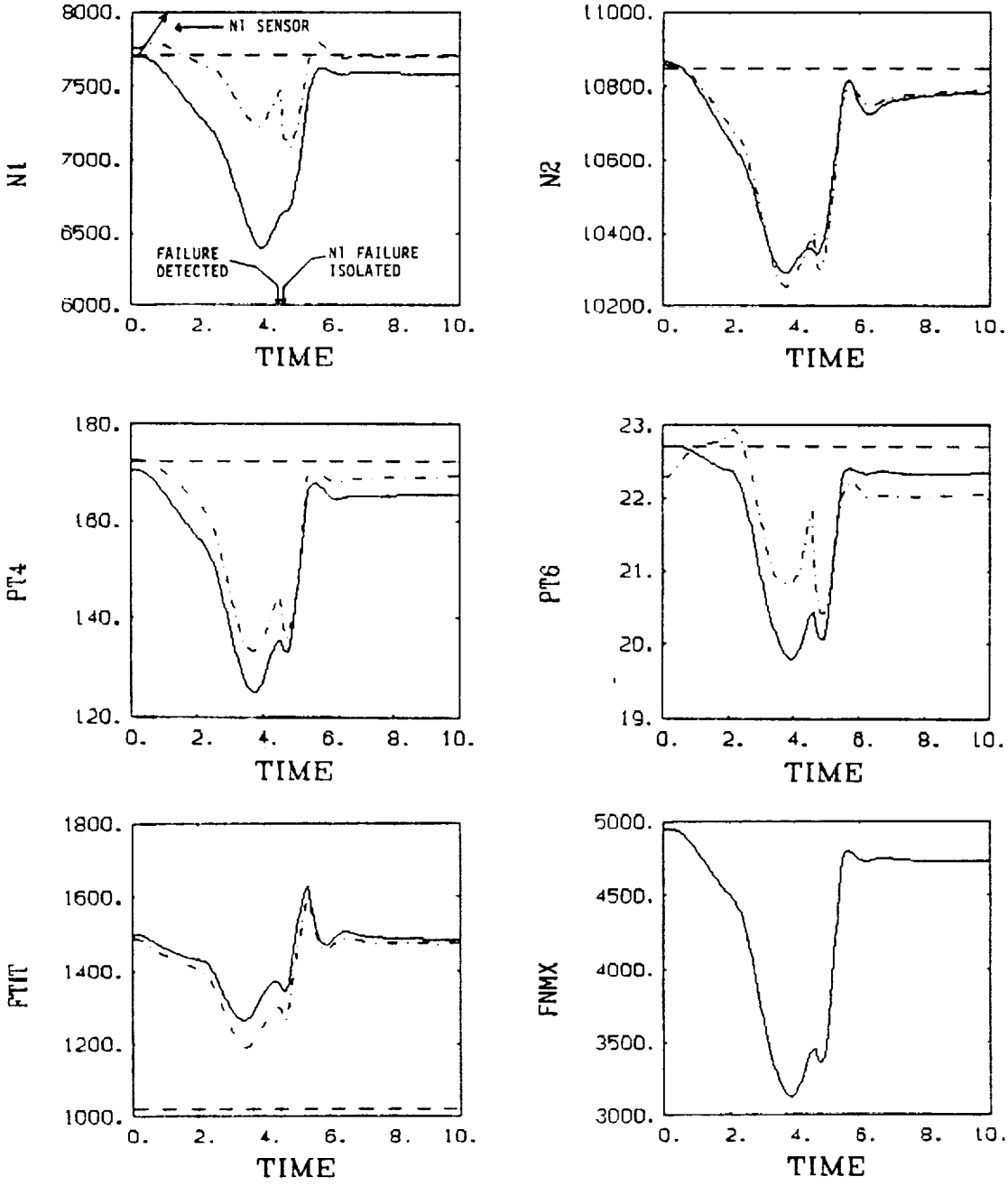

Figure 5.6 Failure Transients for N1 Sensor Drift Rate of 300 RPM/second at Sea Level Static Condition and PLA = 36° using Method [9] (see Table 5.2)

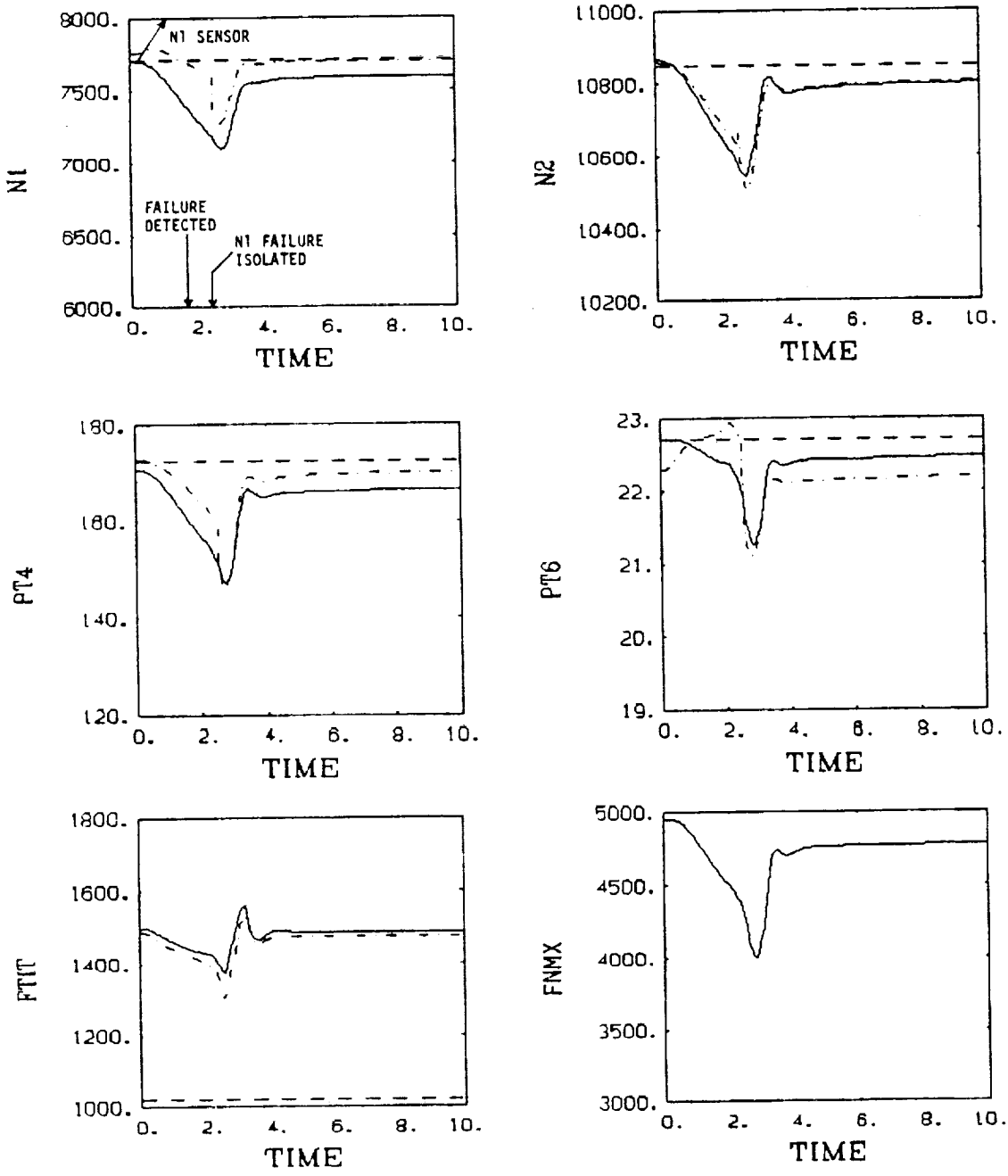

Figure 5.7 Failure Transients for N1 Sensor Drift Rate of 300 RPM/sec at Sea Level Static Condition and PLA = 36 using Modified Thresholds (Table 5.1) Computed from the Threshold Selector (see Table 5.2)

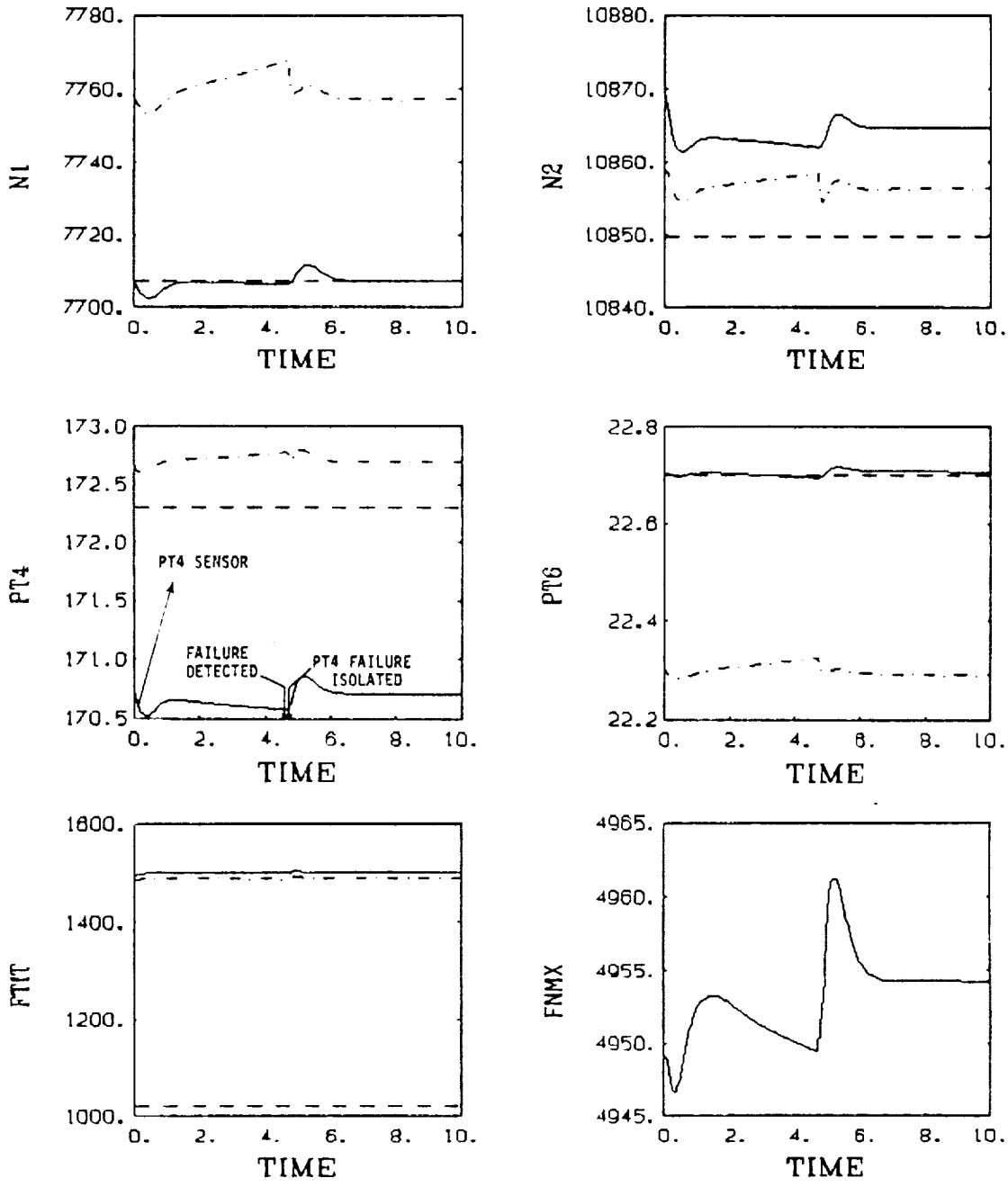

Figure 5.8 Failure Transients for PT4 Sensor Drift Rate of 10 PSI/sec at Sea Level Static Condition and PLA = 36 using Method [9] (see Table 5.2)

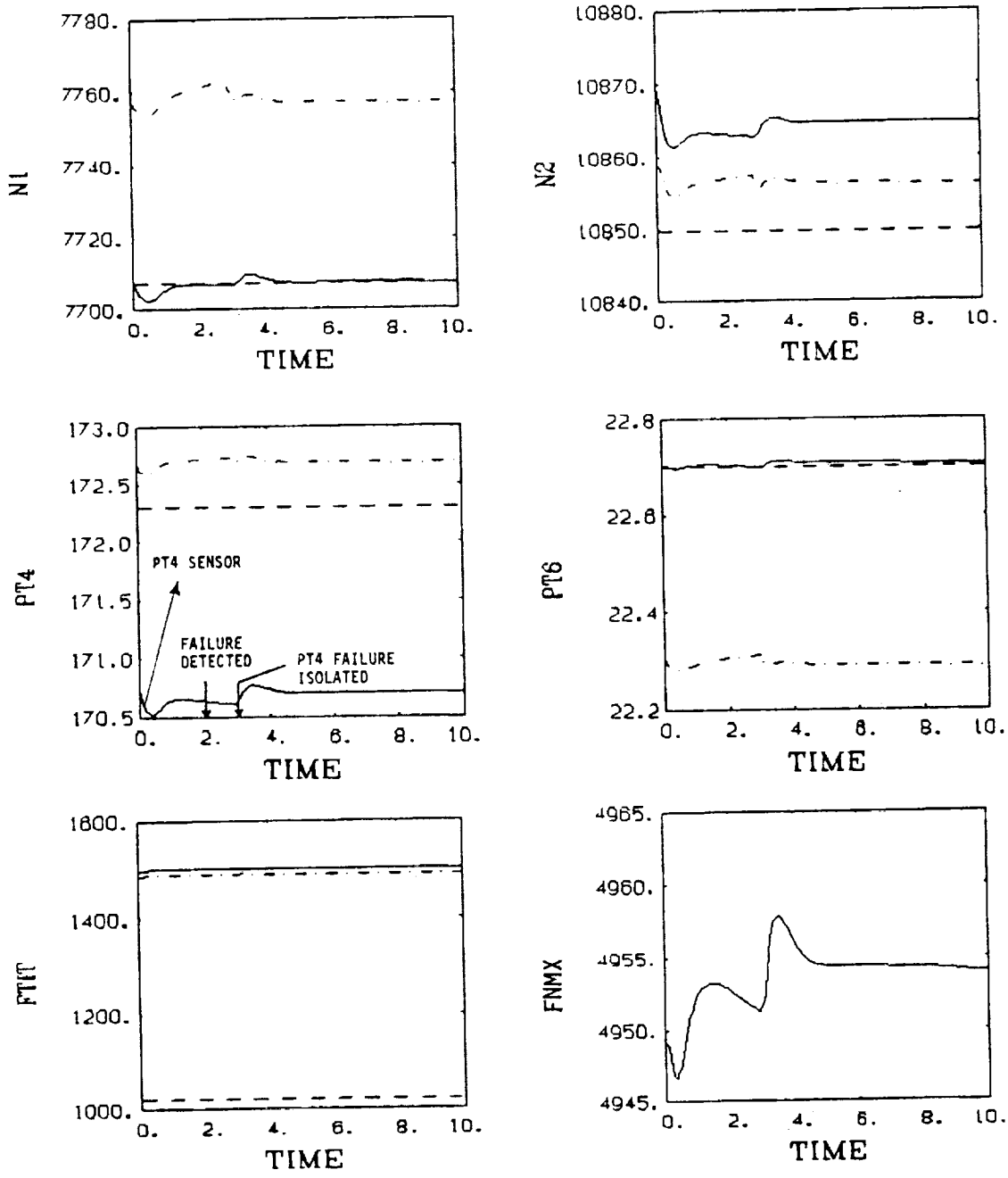

Figure 5.9 Failure Transients for PT4 Sensor Drift Rate of 10 PSI/sec at Sea Level Static Condition and PLA = 36 using Modified Thresholds (Table 5.1) Computed from the Threshold Selector (see Table 5.2)

Table 5.2

Comparison of Detection Times

TYPE OF FAILURE	DETECTION TIME (SEC) USING METHOD (REVISION 2) [9]	DETECTION TIME (SEC) USING THRESHOLD SELECTOR
N1 HARD FAILURE +1000 RPM STEP	0.002	0.002
N2 HARD FAILURE +1000 RPM STEP	0.002	0.002
N1 DRIFT RATE OF +300 RPM/SEC	4.466	1.734
PT4 DRIFT RATE OF +10 PSI/SEC	4.584	2.042

Of primary importance in this comparison is that this increase in performance was gained without a penalty of false alarms. This verifies that the Threshold Selector does produce a useful estimate of the threshold and can replace the previously required empirical approach to threshold calculations to accommodate modeling errors in addition to noise considerations.

5.3 SUMMARY

This chapter has presented evaluation results for this research effort. The results of this study were summarized at the beginning of this chapter. The evaluation validated the threshold selector results. It was verified that the generally lower thresholds, predicted by the threshold selector analysis, results in improvements for soft failure detection. This is done without triggering false alarms. The detection time was lowered by at least a factor of two for soft failures compared to previous techniques.

VI. CONCLUSIONS

This report contains the results of recent research in the area of robust fault detection, isolation, and accommodation for sensor failures. The results have been illustrated by application to sensor DIA for an aircraft turbine engine. At the center of attention is model uncertainty. Model uncertainty has been singled out as the main source of problems with previous DIA algorithms as it affects performance. Various sources of model uncertainty were discussed. The effects of model uncertainty are represented by a bound as a function of frequency. This is consistent with recent approaches in robust control theory. The effects of model uncertainty on stability, asymptotic tracking, and tracking performance was studied and new performance robustness measures were derived. The effects of model uncertainty on failure detection were also studied. The main machinery used was robust multivariable control theory. Fundamental results were derived for selection of optimal thresholds in innovations-based DIA algorithms. The estimator logic used in the DIA technique was made robust by providing robustness both at low and high frequencies. Evaluation results show improvements compared to previous techniques.

The general contribution of this research has been the extension of recent advances in robust control system design to sensor DIA and estimator design. The specific contributions are:

- analysis tools with which to quantify the trade-off between performance robustness and DIA sensitivity;
- design methods which allow higher levels of performance robustness to be achieved for given levels of DIA sensitivity;
- demonstration of the applicability of these tools using an aircraft turbine jet engine multivariable control example.

A powerful synthesis tool has been developed for DIA algorithms. This would allow for optimal achievable levels of performance. In particular:

- a "threshold selector" has been created which quantifies the effects of uncertainty on DIA performance;

- measures have been derived to quantify the uncertainty and the performance robustness.

The advances to robust estimator design to achieve higher levels of performance robustness include

- the development of estimators using the "internal model principle" to achieve asymptotic convergence despite model error;

- the incorporation of frequency weighting in an LQG cost functional to modify an estimator design for DIA.

The results were demonstrated on a dynamic simulation of a multivariable turbofan jet engine example and showed improvements over previous techniques.

The results of this research can be pursued in other directions. It is possible that even higher levels of performance are achievable in some cases by an adaptive technique (see Figure 1.9). It would also be interesting to pursue the idea of this research in a decentralized control strategy. This is important as integration of flight and propulsion control systems is being considered [25].

APPENDIX A
GENERATION OF BOUND ON MODEL UNCERTAINTY

A.1 SYSTEM UNCERTAINTIES

All nominal design models of a system (plant) contain some degree of modeling errors. High fidelity models represent a plant more accurately than others. These errors are called "model uncertainties." There are, in general, two types of uncertainties: structured and unstructured. For example, the former refers to model parameter uncertainties, whereas unmodeled dynamics lies in the latter category. Reduced order modeling, linearization about operating points, neglecting nonlinearities, all result in contributions to either structured or unstructured uncertainty.

The model uncertainties can be broadly grouped into two categories:

(1) uncertain external inputs

- reference commands
- environmental disturbances
- biases or drifts in a failed sensor

(2) uncertain internal dynamics

- plant model errors
- sensor failures
- controller or estimator reconfigurations from DIA

The representations of the model uncertainty vary according to how well its structure is known. For a highly structured representation, e.g., aerodynamic coefficients in flight control, engine model parameters in engine control, the uncertainty can be represented by defining a range of variation in the parameter space. For less structured uncertainties, bounds on errors can be defined. The model uncertainties can in general be classified as additive or multiplicative. The additive type of model uncertainty is defined as follows

$$P(s) = P_0(s, c^*) + \Delta(s)$$

with

$$\bar{\sigma}[\Delta(s)] < \delta_\alpha(\omega) \qquad \forall\, \omega \geq 0 \tag{A.1}$$

where $P(s)$ is the transfer function of the plant, $P_0(s, c^*)$ is the nominal parameterized model of the plant, with structured uncertainty c^*. In other words, $P_0(s, c^*)$ is a known function of c^*, but the values of c^* are uncertain. The function $\Delta(s)$ is the variation in the nominal model, P_0, and is an unstructured uncertainty. It is unknown but limited to be some function bounded by $\delta_\alpha(\omega)$, where $\delta_\alpha(\omega)$ is a positive scalar function which defines a bound on P_0 in the neighborhood of P. It can be viewed as a frequency dependent "radius" of uncertainty of the true plant, $P(s)$, about some model $P_0(s, c^*)$ for all c^*. Figure A.1a illustrates the additive type of uncertainty. In general a good model will be well known at low frequencies where $\delta_\alpha(\omega)$ will be small, and less well known at high frequencies where $\delta_\alpha(\omega)$ will be large. This type of curve is characteristic of unmodeled, uncertain, high-frequency phenomena. Note that in equation (A.1), the structure of $\Delta(s)$ is not defined, and may be caused by a variety of mechanisms (for example, parameter changes, unmodeled dynamics, etc.). The two types of multiplicative uncertainties are the input multiplicative and the output multiplicative and are given by the following equations.

Input multiplicative:

$$P(s) = P_0(s, c^*)\,[I + \Delta(s)]$$

with

$$\sigma[\Delta(s)] < \delta_m(\omega) \qquad \forall\, \omega \geq 0 \tag{A.2}$$

Output multiplicative:

$$P(s) = [I + \Delta(s)]\, P_0(s, c^*)$$

with

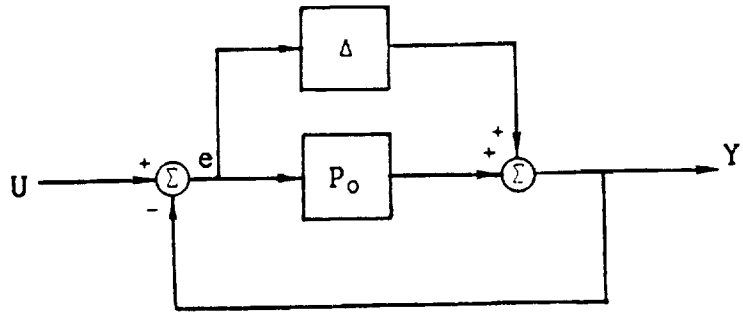

Figure A.1a Additive Perturbation

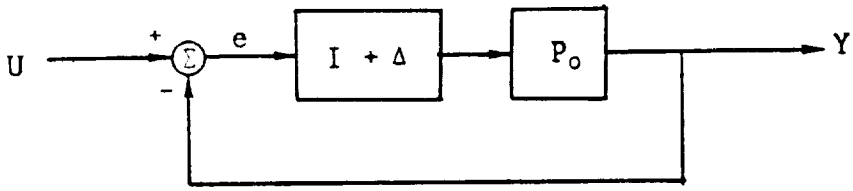

Figure A.1b Input Multiplicative Perturbation

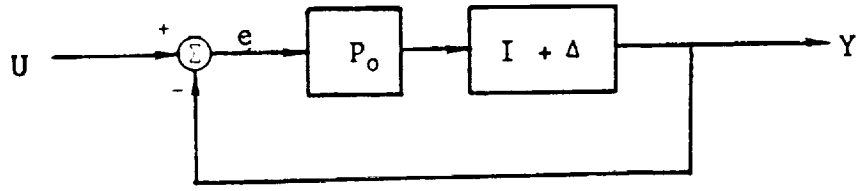

Figure A.1c Output Multiplicative Perturbation

$$\bar{\sigma}[\Delta(s)] < \delta_m(\omega) \qquad \forall\, \omega \geq 0 \tag{A.3}$$

Figure A.1b and A.1c shows the representations of the multiplicative type of uncertainties.

For the multivariable jet engine example [12], an output multiplicative bound was determined. This bound takes into account both the structured and unstructured uncertainties. This will represent a bound on such model uncertainties as, unmodeled dynamics, parameter variation in system matrices (A, B, C, and D), unmodeled nonlinearities, reduced-order modeling, and linearization.

A.1.1 Why Determine Bounds on Model Errors?

Under the NASA contracts NAS3-22481 and NAS3-23282, the feasibility of the DIA concept for application to the multivariable jet engine was demonstrated. However, several problem areas were identified which are stated below:

(1) steady-state and dynamic mismatch of the simplified nonlinear models of the engine;

(2) steady-state estimator errors, with no sensor failures;

(3) instabilities when accommodating failures;

(4) accommodation inaccuracies; and

(5) missed detections and false alarms.

These problems arise from system uncertainties.

The fundamental control design problem is to establish the relationship between performance, robustness, and system uncertainty. The first two are conflicting requirements and need trade-off or design compromises to meet the system requirements. A unified method of approach is to:

(1) establish quantitative relationships between performance, robustness, and system uncertainty;

(2) recognize that the plant model error, sensor failures, and DIA reconfigurations all belong to the same class of system uncertainty.

Figure A.2 illustrates how the system uncertainties can be isolated. The dynamic uncertainties such as model errors, sensor failures, and DIA reconfigurations, are "inside" the system and function as a feedback loop around the "interconnection" system. This system maps the external and internal uncertainties into the outputs, i.e., tracking error and filter residuals. The dynamic uncertainties propagate in a specific way so as to cause a quantifiable uncertainty about the map from the input into the outputs, provided bounds can be found for the dynamic uncertainties. These bounds are obtainable from simple input/output system tests, and are to be used in robustifying the filter/s and determining the thresholds.

A.1.2 Model Error Bound for Output Multiplicative Error

A bound for model uncertainties can be obtained experimentally as shown in Figure A.2. In Figure A.2a, P represents a high-fidelity simulation of the plant whereas P_o is a simplified low-order linearized model of the plant. A sinusoidal test input is applied to the plant and the model. The error is defined as

$$\begin{aligned} e &= P(s)\ \delta u - P_o(s, c^*)\ \delta u \\ &= (I + \Delta)P_o(s, c^*)\ \delta u - P_o(s, c^*)\ \delta u \\ &= \Delta P_o(s, c^*)\ \delta u \end{aligned} \tag{A.4}$$

The normalized error, $\delta(\omega)$, provides a worst-case frequency-dependent bound, and is given by

$$\delta(\omega) = \max_u \frac{\| e \|_2}{\| P_o(s, c^*)\ \delta u \|_2} \tag{A.5}$$

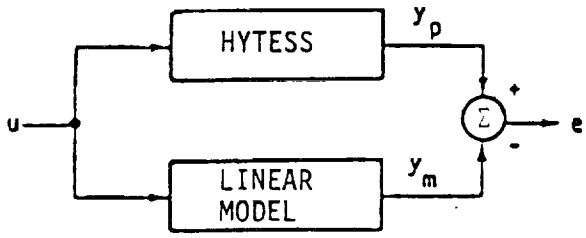

Figure A.2a Experiment to Determine Model Error Uncertainty

$$\delta(\omega) = ||e|| / ||y_m|| \text{ with } u = u_o + a \sin \omega t$$

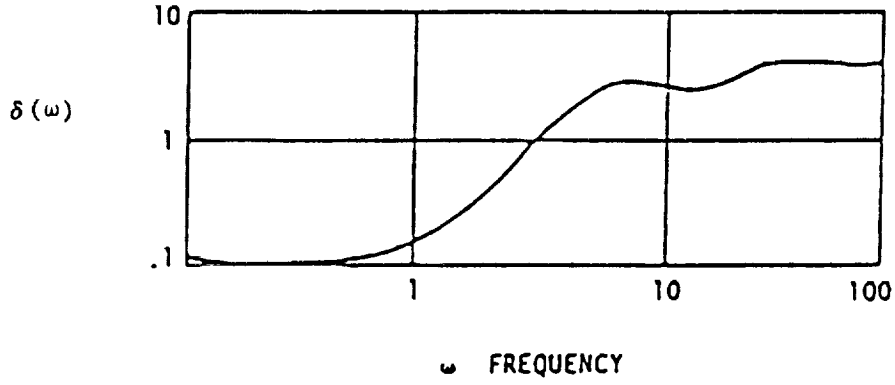

Figure A.2b Frequency-Dependent Uncertainty

where $\|\cdot\|_2$ is the norm, and $\delta(\omega)$ is the bound on model uncertainty. Figure A.2b shows a typical bound on the model error uncertainties, which includes structured and unstructured uncertainties.

A.2 QUANTIFICATION OF MODEL ERROR UNCERTAINTIES

This section describes a method to quantify the model error uncertainties using the experimental procedure given in Section A.1.2. The error bound was determined for a jet engine model [12]. A description of this model is also included in this section.

A.2.1 Computation of Model Error Bound using the Turbofan Model

An experimental procedure to determine a bound on model error was discussed in Section A.1.2. A nonlinear fourth-order engine model (HYTESS - A Hypothetical Turbofan Engine Simplified Simulation [12]) was used to represent the physical plant, i.e., the turbofan engine (see Figure A.2a). The model P_o was represented by a linear model of the engine at sea level static flight condition and PLA at 36° (0/0/36). By applying the same sinusoidal input to P and P_o, an error signal between the outputs is computed using Eq. (A.4). A frequency-dependent error bound is determined using Eq. (A.5).

The procedure for determining the error bounds is shown in Figure A.2. A step-by-step discussion follows.

The states of the system are:

x1 = Fan Speed, SNFAN (N1) - RPM

x2 = Compressor Speed, SNCOM (N2) - RPM

x3 = Burner Exit Slow Response Temperature, Tt41o - °R

x4 = Fan Turbine Inlet Slow Response Temperature, Tt4.51o - °R

The engine inputs are:

u1 = Main Burner Fuel Flow, WFMB - lb/hr

u2 = Nozzle Jet Area, Aj - ft^2

u3 = Fan Guide Vane Angle, FGV - deg

u4 = Compressor Stator Vane Angle, SVA - deg

u5 = Compressor Bleed Flow, BLC - %

The engine outputs are:

y1 = Fan Speed, SNFAN (N1) - RPM

y2 = Compressor Speed, SNCOM (N2) - RPM

y3 = Burner Pressure, PT4 - psia

y4 = Augmentor Pressure, PT6 - psia

y5 = Fan Turbine Inlet Temperature, FTIT - °R

The system matrices for the linear model and HYTESS are shown in Tables A.1 and A.2, respectively.

A.2.2 Description of the Engine Models

Two models of a jet engine are discussed in Section A.2.1, namely, HYTESS and a linear model at 0/0/36. Both models are fourth-order state space models. HYTESS is a nonlinear model generated by scheduling linear model matrices (A, $A^{-1}B$, C and D) over the flight envelope using normalized variables (such as δ, θ, P/8, T/θ, N/$\sqrt{\theta}$) as scheduling parameters. The linear model was extracted from HYTESS at the flight condition of altitude = 0 feet, Mach No. = 0, and PLA = 36°.

The linear fourth-order state space models are of the form

$$\dot{x} = Ax + Bu$$

$$y = Cx + Du$$

where

$$x^T = [x_1 \quad x_2 \quad x_3 \quad x_4]$$

Table A.1

Jet Engine System Matrices

A =

-3.9180	2.9550	-1.5450	6.2260
-0.2560	-2.1480	8.4370	0.0482
-0.0035	-0.0045	-0.6663	0.0003
-0.0075	-0.0146	-0.0499	-2.0000

B =

1.0D+04 *

0.0001	0.3071	-0.0068	0.0021	-1.3290
0.0001	0.0395	-0.0003	0.0015	-0.7886
0.0000	0.0002	0.0000	0.0000	0.0034
0.0000	0.0004	0.0000	0.0000	0.1618

C =

1.0000	0.0000	0.0000	0.0000
0.0000	1.0000	0.0000	0.0000
0.0147	0.0284	-0.0011	-0.0009
0.0031	0.0001	-0.0010	-0.0007
-0.0377	-0.0731	-0.2495	0.0018

D =

0.0000	0.0000	0.0000	0.0000	0.0000
0.0000	0.0000	0.0000	0.0000	0.0000
0.0087	-8.2350	0.1824	0.1855	-175.8000
0.0008	-5.7450	0.0462	-0.0032	-6.8890
0.2050	18.5200	-0.5299	-1.7080	482.9000

Table A.2

Simplified Nonlinear Model Matrices

FULL ENVELOPE MODEL OF A MATRIX

```
F(1,1) = -0.9683E-1/DL1-0.1886E-2*XPT6**2-2.463
F(2,1) = -0.1820E-3*XN1+0.2768E-9*XPT6*XN1**2+0.7721
F(3,1) = -0.2201E-2*XPT6+0.8295E-4*XTT45-0.8207E-1
F(4,1) =  0.6353E-2/DL1+0.1038E-8*XPT4**3-0.2724E-1
F(1,2) = -0.2596E+1*TH1+0.8159E-1/DL1+5.78
F(2,2) = -0.2381E+1/TH1-0.2348E-7*XN1**2+1.549
F(3,2) = -0.4095E-2*DL1-0.8174E-2/DL1+0.1212E-1
F(4,2) = -0.1010E-1*DL1-0.2312E-1/DL1+0.2996E-1
F(1,3) = -1.597
F(2,3) = -0.1569/DL1+0.2382E-1*XPT4+4.2890
F(3,3) = -0.6377/DL1+0.5218/TH1-0.5229
F(4,3) = -0.1156
F(1,4) = -0.1143/DL1+0.8349E-7*XN1**2+1.074
F(2,4) =  0.6013E-1
F(3,4) =  0.2632E-2
F(4,4) = -0.1914E+1/DL1+0.1564E+1/TH1-1.568
```

FULL ENVELOPE MODEL OF $A^{-1}B$ MATRIX

```
FIG(1,1) =  0.9327E-3*XN1-0.3145E-11*XN1**3-6.56
FIG(2,1) = -0.3616*TH1-0.3850E+8/XN1**2+0.4541
FIG(3,1) =  0.1183E-3*XPT4-0.363E-9*XPT4**3-0.372E-1
FIG(4,1) =  0.9333E-3*XPT6-0.9744E-9*XN1*XPT6**2-0.306E-1
FIG(1,2) = -0.2971E+2*XPT6+0.2182E+2/(TH1*DL1)-260.4
FIG(2,2) =  0.1121*XN1-0.1545E-2*XPT4*XPT6**2-721.8
FIG(3,2) =  0.5845E-1*XPT4-0.7198E-4*XPT4*XPT6**2-1.568
FIG(4,2) =  0.3761*XPT6-0.5675E-4*XPT4*XPT6**2-1.418
FIG(1,3) =  0.1627*XPT4-0.4133E-4*XPT4*XPT6**2-2.104
FIG(2,3) = 0.275*XPT6-6.304
FIG(3,3) =  0.1306E-1*XPT6-0.2379
FIG(4,3) =  0.1068E-1*XPT6-0.1881
FIG(1,4) =  0.8670E+1/TH1+0.5090E-1*XPT4-26.19
FIG(2,4) =  0.1168E+3*TH1+0.1092E+3/TH1-220.7
FIG(3,4) =  0.2010*TH1-0.1262E-2*XPT4+0.2459
FIG(4,4) =  0.9386E-1*TH1-0.1157E-2*XPT4+0.2951
FIG(1,5) =  0.5357E+4/(DL1*RTH1)-75.87
FIG(2,5) =  0.3754E+4/(DL1*RTH1)+157.9
FIG(3,5) = -0.9392E+2*(RTH1/DL1)-0.7399E+1*(TH1/DL1**2)+8.53
FIG(4,5) = -0.8524E+2*(RTH1/DL1)-0.5902E+1*(TH1/DL1**2)+9.7
```

Table A.2 (Continued)

FULL ENVELOPE MODEL OF C MATRIX

```
H(1,1) =  1.
H(2,1) =  0.
H(3,1) = -0.2814E+1/XPT4-0.2378E-3*XPT4*XPT6+0.4341E-1
H(4,1) = -0.5318/XPT4-0.4950E-10*XN1**2+0.9636E-2
H(5,1) =  0.8714E-3*XPT4+0.1784E+2/XPT4-0.2067
H(6,1) =  0.9184/TH1-0.3491E+4/XPT4**2+0.1318
H(7,1) =  0.3119E-2/XPT6-0.2978E-1/XPT6**2-0.7264E-4
H(1,2) =  0.
H(2,2) =  1.
H(3,2) =  0.2913E-1/TH1+0.4644E-3*XPT6-0.1333E-1
H(4,2) = -0.9080E-7*XN1-0.6644E-1/XPT4-0.1132E-2
H(5,2) = -0.1327E-3*XTT45-0.1907E-4/XN1-0.4014
H(6,2) =  0.3287E-1
H(7,2) =  0.2899E-3/DL1+0.6102/XPT4**2-0.3523E-4
H(1,3) =  0.
H(2,3) =  0.
H(3,3) = -0.7570E-7*XPT6**3-0.4867E-3
H(4,3) = -0.3204E-6*XN2+0.2399E-2
H(5,3) =  0.3111E-1*TH1+0.5486E-4*XTT45-0.3612
H(6,3) =  0.1445E-1/DL1-0.1271E-3*XN1+0.3134
H(7,3) = -0.1322E-5
H(1,4) =  0.
H(2,4) =  0.
H(3,4) = -0.1980E-3*XPT6+0.3175E-2
H(4,4) = -0.4300E-5*XPT4-0.5102E-4
H(5,4) =  0.8484E-2
H(6,4) =  0.1140E-1/DL1-0.1300E-3*XN1+0.5192
H(7,4) = -0.1324E-5
```

FULL ENVELOPE MODEL OF D MATRIX

```
D(1,1) = 0.
D(2,1) = 0.
D(3,1) = -0.4135E-14*XN1**3+0.1983E-5*XPT6**2+0.9972E-2
D(4,1) = -0.9442E-7*XN1-0.2207E-5/XN1**2+0.2096E-2
D(5,1) = -0.3541E-1*TH1+0.3135E-2/XPT4+0.4914E-1
D(6,1) = -0.6850E+4/XN1+0.1326E+9/XN2**2+0.3303
D(7,1) = -0.8329E-2/XPT4+0.1035E-4
D(1,2) = 0.
D(2,2) = 0.
D(3,2) = -0.7192E-3*XPT6**3+1.255
D(4,2) = -0.4047*XPT6+2.908
D(5,2) =  0.2658E-2*XPT6**3-7.119
D(6,2) = -0.2704E+4/TH1+0.8536E+7/XN1+131.6
D(7,2) = -0.3962E-6*XPT6**3+0.2829E-3
D(1,3) = 0.
D(2,3) = 0.
D(3,3) =  0.5336E-2*XPT4-0.1670E-5*XPT4*XPT6**2-0.4101
D(4,3) =  0.8815E-3*XPT4-0.2836E-8*XPT4**3-0.6458E-1
D(5,3) =  0.1110E-4*XPT4**3-0.1789E-5*XN1*XPT4+0.5499
D(6,3) =  0.1347E+1*XPT6-12.67
D(7,3) =  0.2049E-3
D(1,4) = 0.
D(2,4) = 0.
D(3,4) =  0.7838*TH1-0.4444
D(4,4) = -0.3430E-2
D(5,4) = -0.2147E+1*TH1+0.2716E-7*XN1**2-1.36
D(6,4) = 1.073
D(7,4) =  0.5327E-2*TH1-0.8434E-2
D(1,5) = 0.
D(2,5) = 0.
D(3,5) = -0.3143E+3/DL1-0.1685E+1*XPT4+425.9
D(4,5) = -0.1446E+2*(RTH1/DL1)-0.9268E-1*XPT4+24.09
D(5,5) =  0.1183E+4/DL1-431.2
D(6,5) = -0.7482E+4/DL1+1454.0
D(7,5) =  0.9854/DL1+0.3580E-1
```

$$u^T = [u_1 \quad u_2 \quad u_3 \quad u_4]$$

$$y^T = [y_1 \quad y_2 \quad y_3 \quad y_4]$$

A.3 DETERMINATION OF MODEL ERROR BOUND

The procedure for computation of the error bound on modeling error is shown in Figure A.3, and a step by step discussion follows.

Step 1: The input to the system is a sinusoidal signal superimposed on a constant signal. This input is of a specific frequency and of high amplitude, i.e., the amplitude of the sinusoid should be carefully selected so that the region of operation of the simplified model remains linear. The amplitudes of the sinusoid for each input were determined from Ref. 24. These input amplitudes give the best overall match between the linear and the nonlinear models of the engine. These amplitudes are as follows:

u(1) = WFMBH	3 %
u(2) = AJ	3 %
u(3) = CIVV	5 degrees
u(4) = RCVV	1 degree
u(5) = BLC	0.2 %

The inputs were excited one at a time according to the procedure. The outputs of P and P_0 are sinusoids superimposed over a transient (system transient), as shown in Figure A.4. Once the transient dies out, the outputs are sinusoids of constant amplitude. The magnitude of the outputs are determined by computing the amplitude of the sine waves. The error, e, is determined by subtracting the output of the plant, y, from the output of the model, ym, and then computing the magnitude.

Step 2: The bound, $\delta(\omega)$, on the model error is given by

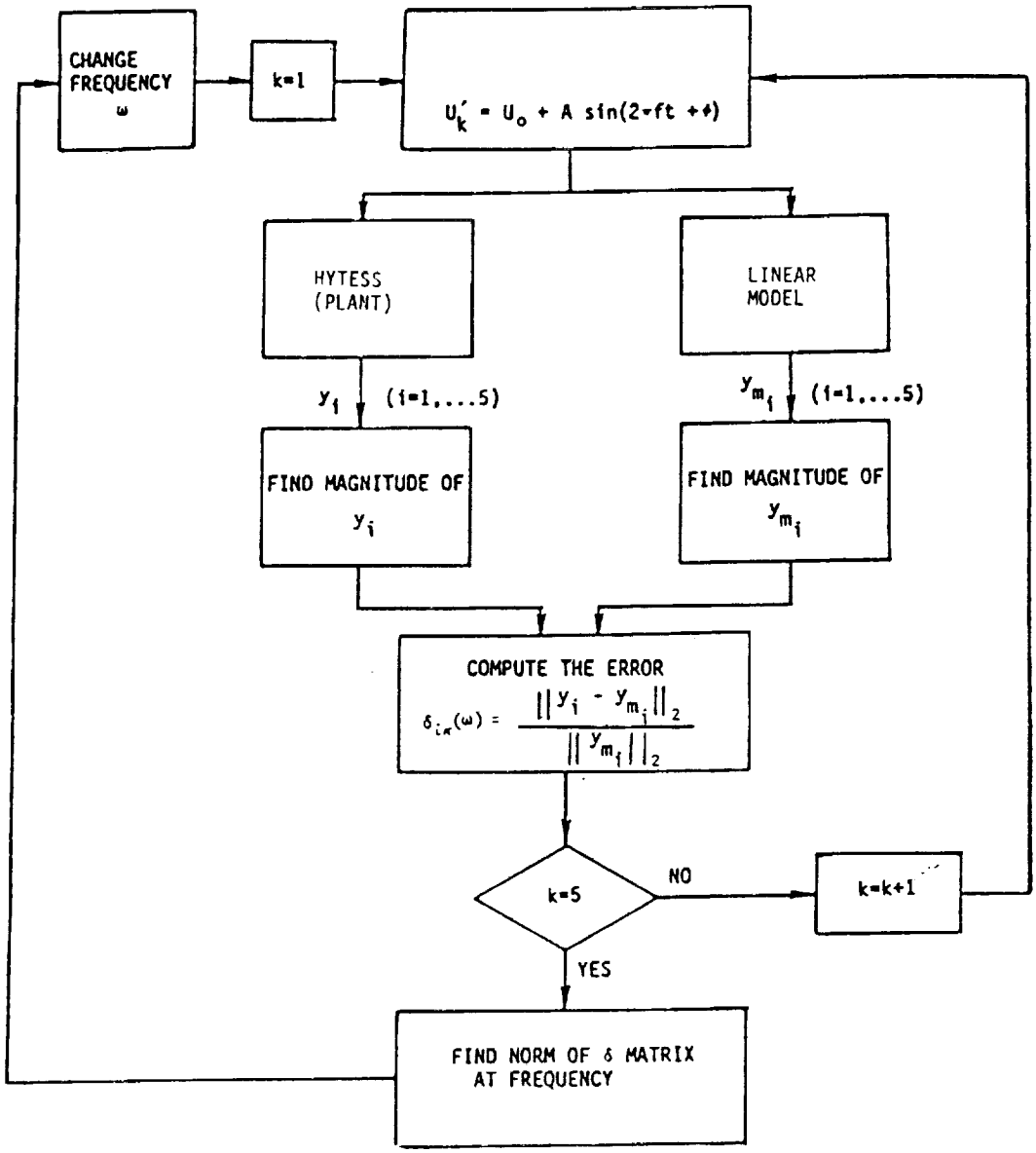

Figure A.3 Procedure for Computing Error Bound, $\delta(\omega)$

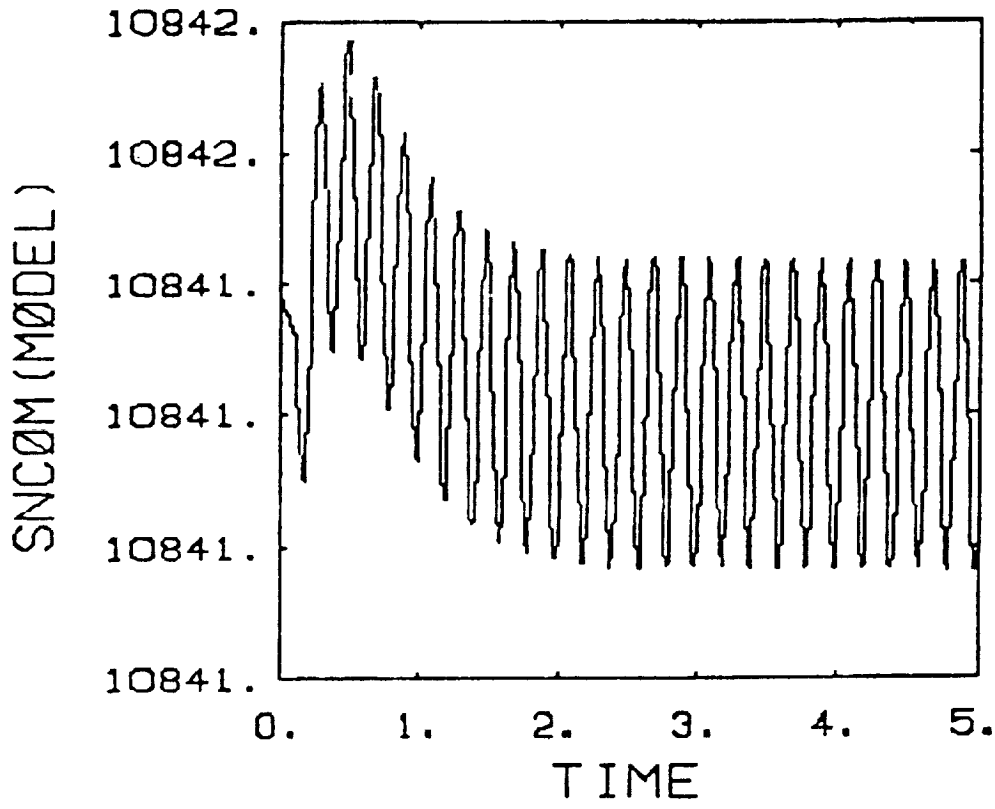

Figure A.4 Compressor Speed Response when CIVV is Modulated with Sine Wave at 5 Hz

$$\delta(\omega) = \begin{vmatrix} \delta_{11} & \cdots & \delta_{15} \\ \vdots & & \vdots \\ \delta_{51} & \cdots & \delta_{55} \end{vmatrix} \qquad (A.6)$$

Each input when excited, produces errors in all the five outputs, which determines one column of the δ matrix. For example, if u_1 is modulated with a sinusoid, it produces

$$\delta_{11} = \|y_1 - ym_1\| \,/\, \|ym_1\|, \quad \delta_{21} = \|y_2 - ym_2\| \,/\, \|ym_2\|, \ \ldots$$

$$\delta_{51} = \|y_5 - ym_5\| \,/\, \|ym_5\|.$$

This gives the first column of the δ matrix. Similarly, other four inputs are excited one at a time to determine the other four columns of the δ matrix. To determine the bound at a given frequency, 25 elements of the δ matrix have to be computed.

Step 3: The simplified model has a bandwidth of about 5 hz. A range of frequencies from 0 hz (DC) to 9 hz was chosen for computation of the δ matrix. The discrete frequencies at which δ was computed are 0.1, 0.3, 0.5, 0.7, 0.8, 1., 2., 3., 4., 5., 7., 9. hz.

Step 4: At each frequency, the maximum singular value of the $\delta(\omega)$ matrix is computed. This is denoted by $\bar{\sigma}[\delta(\omega)]$, and is the worst case bound at that frequency. Figure A.4 illustrates a plot of $\bar{\sigma}$ against frequency.

A.4 DISCUSSION

The bound on the model errors determined in this procedure has some limitations. The plant is represented by a simplified nonlinear simulation and the model is linearized at one flight point. This limits the validity of the model error bound to only one flight condition. This also does not

include the errors which arise from the unmodeled nonlinearities and the linearization of $P(s)$ to produce simplified model $P_0(s)$. For a more general error bound, the plant should be represented by the cycle deck, and the bound δ should be determined at all the representative flight points in the flight envelope. However, cost is an important consideration in such an exercise.

There are marked differences between the theoretical curves of Figure A.2 and Figure A.5. The error bound is expected to grow at high frequencies (Figure A.2b), but as seen in Figure A.4, it is constant. This is attributed to the fact that the plant and the model are of the same order and have approximately the same A, B, C, and D matrices at 0/0/36. The difference in the system matrices is that the model is represented by the constant A, B, C, and D matrices (Table A.1), whereas the plant $P_0(s, c^*)$ is represented by the A, B, C, and D matrices which are polynomial functions. The error bound in this case is a constant. This can be shown using equation A.3 as follows,

$$P(s) = [I + \Delta(s)]\, P_0(s, c^*) \tag{A.7}$$

where $P(s)$ and $P_0(s, c^*)$ are of the same order. In reality, $\Delta(s)$ would be a complicated transfer function of order different from the order of $P(s)$ or $P_0(s, c^*)$. In this case it is simply a constant and therefore the error bound $\bar{\sigma}(\omega)$ is a constant in Figure A.5 as shown by the following equation,

$$\lim_{s \to \infty} \frac{\|P(s) - P_0(s, c^*)\|}{\|P_0(s)\|} = \|\Delta(s)\| = \text{constant} \tag{A.8}$$

It is expected that if high-frequency dynamics is added to the plant $P(s)$, the high frequency response of $\bar{\sigma}$ in Figure A.5 will follow the pattern of Figure A.2b.

The difference between the two models $P(s)$ and $P_0(s, c^*)$, causes the peak at low frequency in Figure A.5. This difference gives rise to different

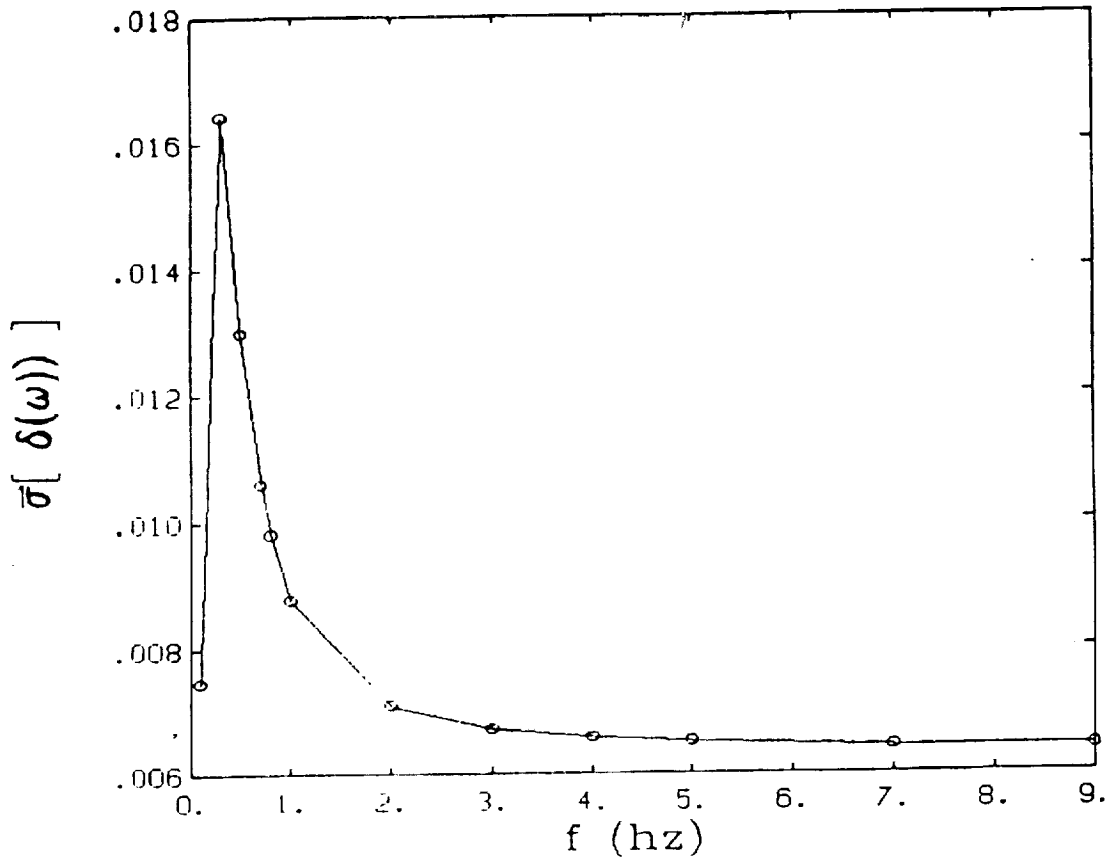

Figure A.5 Maximum Singular Value Plotted Against Frequency

dynamic responses. It is expected that if the two models are exactly the same (no modeling errors), the plot of $\bar{\sigma}$ should be a constant, i.e., $\bar{\sigma}(\omega) = \bar{\sigma}$ (constant) = 0.

A.5 SUMMARY

A procedure to compute the bound on the modeling errors is developed and demonstrated on an engine example. The bound is limited to only one flight condition. For a more general bound, a comprehensive experiment will have to be run where the plant is represented by the cycle deck and the experiment conducted at a number of operating points on the flight envelope, with particular emphasis on the choice of the amplitude of the input signals.

REFERENCES

1. Willsky, A.S., "A Survey of Several Failure Detection Methods," Automatica, pp.601-611, November 1976.

2. Clark, R.N., "The Dedicated Observer Approach to Instrument Failure Detection," in Proc. IEEE Conf. Dec. Contr., pp.237-241, December 1979.

3. Isermann, R., "Process Fault Detection Based on Modeling and Estimation Methods -- A Survey," Automatica, Vol. 20, No. 4, pp.387-404, 1984.

4. Leininger, G.G., "Model Degradation Effects on Sensor Failure Detection," in Proc. JACC, 1981.

5. Sidar, M., "Design of Analytical Failure - Detection Systems Using Secondary Observers," NASA TM-84284, August 1982.

6. DeHoff, R.L., et al., "F100 Multivariable Control Synthesis Program -- Volume I, Development of F100 Control System," AFAPLTR-77-35, 1977.

7. DeHoff, R.L., et al. "F100 Multivariable Control Synthesis Program -- Volume II, Appendices A through K," AFAPL-TR-77-35, 1977.

8. Beattie, E.C., LaPrad, R.F., McGlone, M.E., Rock, S.M., Akhter, M.M., "Sensor Failure Detection System," NASA CR-165515, August 1981.

9. Beattie, E.C., LaPrad, R.F., Akhter, M.M., Rock, S.M., "Sensor Failure Detection for Jet Engines," NASA CR-168190, May 1983.

10. DeLaat, J.C., "A Real-Time FORTRAN Implementation of a Sensor Failure Detection, Isolation, and Accommodation Algorithm," Proc. American Contr. Conf., pp.572-573, 1984.

11. DeLaat, J.C. and W.C. Merrill, "A Real-Time Implementation of an Advanced Sensor Failure Detection, Isolation, and Accommodation Algorithm," NASA TM-83553, January 1984.

12. Merrill, W.C., E.C. Beattie, LaPrad, R.F., Rock, S.M., and Akhter, M.M., "HYTESS -- A Hypothetical Turbofan Engine Simplified Simulation," NASA TM-83561, January 1984.

13. Doyle, J.C. and Stein, G., "Multivariable Feedback Design: Concepts for a Classical/Modern Synthesis," IEEE Trans. Auto. Control, Vol. AC-26, No. 1, pp.4-16, February 1981.

14. "Special Issue on Linear Multivariable Control Systems," IEEE Trans. Auto. Control, Vol. AC-26, No. 1, February 1981.

15. Safonov, M.G., "Tight Bounds on the Response of Multivariable Systems with Component Uncertainty," Proc. Allerton Conf. on Comm., Contr., and Compute., Monticello, ILL, October 4-6, 1978.

16. Zames, G., "On the Input/Output Stability of Time/Varying Nonlinear Feedback Systems; Part I: Conditions Using Concepts of Loop Gain Conicity and Positivity," IEEE Trans. on Auto. Control, Vol. AC-11, No. 2, pp.228-238, April 1966.

17. Zames, G., "On the Input/Output Stability of Time/Varying Nonlinear Feedback Systems; Part II: Conditions Involving Circles in the Frequency Plane and Sector Nonlinearities," IEEE Trans. on Auto. Control, Vol. AC-11, No. 3, pp.465-476, July 1966.

18. Francis, B.A., and Wonham, W.M., "The Internal Model Principle of Control Theory," Automatica, Vol. 12, 1976, pp.457-465.

19. Emami-Naeini, A., "Application of the Generalized Eigenstructure Problem to Multivariable Systems and the Robust Servomechanism for a Plant which Contains an Implicit Internal Model," Ph.D. Dissertation, Dept. of Elect. Engr., Stanford University, April 1981.

20. Franklin, G.F. and Emami-Naeini, A., "A New Formulation of the Multivariable Robust Servomechanism Problem," Internal Report, Stanford University, ISL, July 1983.

21. Little, J.N., A. Emami-Naeini, and S.N. Bangert, "CTRL-C and Matrix Environments for the Computer-Aided Design of Control Systems," Proc. Sixth International Conf. on Analysis and Optimization of Systems, pp.191-205, June 1984.

22. Emami-Naeini, A. and P. Van Dooren, "Computation of Zeros of Linear Multivariable Systems," Automatica, Vol. 18, No. 4, pp.415-430, July 1982.

23. Bossi, J.A., "Robust Compensator Synthesis by Frequency-Shaped Estimation," Proc. AIAA Guidance and Contr. Conf., pp.529-534, August 1984.

24. "F100 Multivariable Control System Engine Models/Design Criteria," Technical Report AFAPL-TR-76-74, November 1976.

25. Emami-Naeini, A., R.P. Anex, S.M. Rock, "Integrated Control: A Decentralized Approach," Proc. IEEE Conf. Decision and Contr., December 1985.

26. Gupta, N.K., "Frequency-Shaped Cost Functionals: Extensions of Linear-Quadratic-Gaussian Design Methods," J. Guidance and Control, Vol. 3, No. 6, pp.529-535, November-December 1980.

27. Merrill, W.C., "Sensor Failure Detection for Jet Engines Using Analytical Redundancy," J. Guidance and Control, Vol. 8, No. 6, pp.673-682, November-December 1985.

28. Desoer, C.A. and M. Vidyasagar, Feedback Systems: Input-Output Properties, Academic Press, 1975.

1. Report No.	2. Government Accession No.	3. Recipient's Catalog No.
NASA CR-174825		

4. Title and Subtitle	5. Report Date
Robust Detection, Isolation, and Accommodation for Sensor Failures	July 1986
	6. Performing Organization Code

7. Author(s)	8. Performing Organization Report No.
Abbas Emami-Naeini, Muhammad M. Akhter, and Stephen M. Rock	SCT-85-5449
	10. Work Unit No.

9. Performing Organization Name and Address	11. Contract or Grant No.
Systems Control Technology, Inc. 1801 Page Mill Rd.; P.O. Box 10180 Palo Alto, California 94303	NAS3-24079
	13. Type of Report and Period Covered
	Contractor Report

12. Sponsoring Agency Name and Address	14. Sponsoring Agency Code
National Aeronautics and Space Administration Washington, D.C. 20546	505-34-02

15. Supplementary Notes

Final report. Project Manager, Walter C. Merrill, Instrumentation and Control Technology Office, NASA Lewis Research Center, Cleveland, Ohio 44135

16. Abstract

The objective of this research program is to extend the recent advances in robust control system design of multivariable systems to sensor failure detection, isolation, and accommodation (DIA), and estimator design. This effort provides analysis tools to quantify the trade-off between performance robustness and DIA sensitivity, which are to be used to achieve higher levels of performance robustness for given levels of DIA sensitivity. An innovations-based DIA scheme is used. Estimators, which depend upon a model of the process and process inputs and outputs, are used to generate these innovations. Thresholds used to determine failure detection are computed based on bounds on modeling errors, noise properties, and the class of failures. The applicability of the newly developed tools are demonstrated on a multivariable aircraft turbojet engine example. A new concept called the threshold selector was developed under this program. It represents a significant and innovative tool for the analysis and synthesis of DIA algorithms. Analytical results were obtained for the SISO case to compute optimal thresholds and to determine the size of minimum detectable failures, and a computer-aided technique was developed for the multivariable case. The estimators were made robust by introduction of an internal model and by frequency shaping. The internal model provides asymptotically unbiased filter estimates. The incorporation of frequency shaping of the LQG cost functional modifies the estimator design to make it suitable for sensor failure DIA. The results are compared with previous studies which used thresholds that were selected empirically. Comparison of these two techniques on a nonlinear dynamic engine simulation shows improved performance of the new method compared to previous techniques.

17. Key Words (Suggested by Author(s))	18. Distribution Statement
Analytical redundancy; Robust detection; Sensor failure; Jet engines	Unclassified - unlimited STAR Category 07

19. Security Classif. (of this report)	20. Security Classif. (of this page)	21. No. of pages	22. Price*
Unclassified	Unclassified	159	A08

*For sale by the National Technical Information Service, Springfield, Virginia 22161